

POLITECNICO DI TORINO

FACOLTÀ DI INGEGNERIA

Ingegneria per l'ambiente e il territorio

Anno accademico 2017/2018



Tesi di Laurea Magistrale

THE GROUND PENETRATING RADAR AS A TOOL FOR PLANNING THE EXPLOITATION OF THE CANDOGLIA MARBLE QUARRY

Candidata:

Veronica Janeth Rumbos Ruedas

Matricola: 239014

Relatori

Prof. Ing. Luigi Sambuelli

Prof. Ing. Claudio Oggeri

Prof. Ing. Pierpaolo Oreste

Table of Contents

Chapter 1 Presentation.....	8
1.1 Abstract.....	8
1.2 Introduction.....	8
1.3 Objective.....	9
Chapter 2 The Candoglia quarry.	10
2.1 History	10
2.2 Location	11
2.3 Geometrical characteristics.....	12
2.4 Geology.....	13
Chapter 3 Terms and definitions	15
3.1 Basic concepts about the electromagnetic properties of the soils.....	15
3.1.1 Ground Penetrating Radar.....	15
3.1.2 Electric permittivity (ϵ):	15
3.1.3 Electric conductivity (σ).....	16
3.1.4 Magnetic permeability (μ).....	16
3.2 Theoretical basis of EM, EM waves and propagation.	17
3.2.1 Electromagnetic waves.....	17
3.2.2 Generation of electromagnetic waves	17
3.2.3 Fundamentals of Electromagnetism	18
3.2.4 Constitutive equations	19
3.2.5 Propagation Velocity.....	21
3.2.6 Energy losses: absorption, dispersion and spherical divergence.....	22
3.2.7 Reflection, refraction and transmission in the interfaces.	23

3.2.8 Electromagnetic impedance	24
3.2.9 Vertical and horizontal resolution	26
Chapter 4 Data acquisition	27
4.1 Equipment and tools	27
4.2 Acquisition parameters for each survey.....	30
Chapter 5 Processing	36
5.1 Data import	36
5.2 Graphical modifications.....	37
5.2.1 South inner and outer wall	38
5.2.2 South base and north base	39
5.2.3 North base and west base	41
5.3 Processing on the signal using Reflex-Win	45
5.3.1 Subtract mean Dewow	46
5.3.2 Move start time.....	47
5.3.3 Time cutting	48
5.3.4 Divergence compensation	49
5.3.5 Gain function.....	51
5.3.6 Spectral Whitening.....	52
5.3.7 Band-Pass Butterworth.....	53
5.4 3D Assembling	54
Chapter 6 Test on Matlab: Mixing of GPR data acquired with different frequencies....	56
6.1 Data import	57
6.2 Dewow	59
6.3 Resampling on time	60
6.4 Remove initial delay	61
6.5 Equal dimensions	62

6.6 Mixing in frequency.....	64
6.7 Energy filter	65
6.8 Mean trace.....	67
6.9 Band pass filter	69
6.10 Energy recovery	70
Chapter 7 Results and interpretation	72
Chapter 8 Conclusions and future works.....	80
8.1 Conclusions.....	80
8.2 Future works	81
Appreciations	82
Chapter 9 Bibliography	83
Appendix 1. Main code for the mixing of two frequency signals	85
Appendix 2. Functions that conform the code.....	93
1) Dewow function	93
2) Resampling function.....	93
3) Remove initial delay function.....	94
4) Equal size function	95
5) Energy filter function.....	96
6) Mean trace function.....	97
7) BandPass filters function	97
8) Energy recovery function	99

Table of figures

Figure 2.1. The Cathedral of Milan	10
Figure 2.2. Reconstruction of a part of the Cathedral	11
Figure 2.3. Location of the quarry	12
Figure 2.4. The Candoglia Quarry	13
Figure 2.5. General view of the zone with principal geological composition [3]	14
Figure 2.6. Virtual view illustrating the most prominent geologic unit. [3]	14
Figure 3.1. Some dielectric constant values of rocks [6]	16
Figure 3.2. Electromagnetic Wave propagation	18
Figure 3.3. Dispersive attenuation (for scattering) [11]	22
Figure 3.4. Energy losses scheme.....	23
Figure 3.5. Reflection of electromagnetic waves	24
Figure 4.1. Equipment: at the left, the 900MHz antenna with the wheel odometer, in the center the computer, in the right the GPR Unit and the 200MHz antenna.....	28
Figure 4.2. Survey in the points 19-20-21-22 with the 200MHz antenna.....	28
Figure 4.3. Survey in the points 15-16-17-18 with the 200MHz antenna.....	29
Figure 4.4. Survey in the points 1-2-3-4 with the 200MHz antenna.....	29
Figure 4.5 Modification from the image provided by studio bertinotti.....	30
Figure 4.6. Points 1-2-3-4-5-6 from the image provided by studio Bertinottii	31
Figure 4.7. South wall: points 7-8-9-10 from the image provided by studio bertinotti .	32
Figure 4.8. Points 1-2-3-4' from the image provided by studio bertinotti.....	33
Figure 4.9. Points 15-16-17-18 from the image provided by studio bertinotti.....	33
Figure 4.10. Points 19-20-21-22 from the image provided by studio bertinotti.....	34
Figure 4.11. North wall, points 23-24-25-26 from the image provided by studio bertinotti	34
Figure 4.12. South wall: points 7-8-9-10 from the image provided by studio bertinotti	35
Figure 5.1. Data import table.....	36
Figure 5.2. X Y coordinates data table	37
Figure 5.3. South inner and outer wall 900MHz	38
Figure 5.4. South inner and outer wall 900 MHz coordinate table	39
Figure 5.5. South and north base 200 MHz coordinate table	39

Figure 5.6. South base (on the left side) and north base (on the right side)	40
Figure 5.7. South and north base profiles	40
Figure 5.8. North base and west base 200 MHz coordinate table	41
Figure 5.9. North base and west base profiles	41
Figure 5.10. North base and west base radargram.....	42
Figure 5.11. 4 bases merging coordinate table, part one (west base+ first north base)..	43
Figure 5.12. Four bases merging coordinate table, part two (north base+south base) ...	43
Figure 5.13. The 4 acquisitions made on the floor.	44
Figure 5.14. Raw radargram	45
Figure 5.15. Radargram after dewow	46
Figure 5.16. Radargram after moving start time	47
Figure 5.17. Radargram after time cutting	48
Figure 5.18. Radargram with divergence recovery	49
Figure 5.19. Radargram with divergence recovery and trace normalization.....	50
Figure 5.20. Radargram with divergence recovery and plotscale modification	50
Figure 5.21. Radargram with Manual Gain (y)	51
Figure 5.22. Radargram with spectral whitening	52
Figure 5.23. Radargram with bandpass butterworth.....	53
Figure 5.24. 3D data import table.....	54
Figure 5.25. 3D Cube result	55
Figure 6.1. Processing flow of the matlab program	56
Figure 6.2. High frequency radargram	57
Figure 6.3. Parameters imported for the High frequency antenna.....	57
Figure 6.4. Low frequency radargram	58
Figure 6.5. Parameters imported for the low frequency antenna.....	58
Figure 6.6. Dewow effect in one trace of the low frequency radargram.....	59
Figure 6.7. Dewow effect in one trace of the high frequency radargram.....	59
Figure 6.8. Adjustment of the resampled trace.....	60
Figure 6.9. Tool for the selection of the time for the removing of the initial delay	61
Figure 6.10. Result after removing of the initial delay.....	62
Figure 6.11. Low frequency signal with equal dimensions.....	63
Figure 6.12. High frequency signal with equal dimensions	63

Figure 6.13. Mixed in frequency radargram.....	64
Figure 6.14. At the left, the low frequency amplitude spectrum, at the right, the high frequency amplitude spectrum.....	64
Figure 6.15. Amplitude spectrum of the mixed signal	65
Figure 6.16. 2D Amplitude spectrum before filter	66
Figure 6.17. Amplitude histogram.....	66
Figure 6.18. 2D amplitude spectrum after the filter	67
Figure 6.19. Trace with mean removed.....	68
Figure 6.20. Radargram with mean trace removed	68
Figure 6.21. Trace amplitude spectra	69
Figure 6.22. Bandpass filter fixed at 1.5 high frequency antenna.....	70
Figure 6.23. Radargram with Divergence recovery	71
Figure 7.1. 3D cube containing the acquisitions made in the floor, with a X,Y,Z cut showing the main fractures found. Radar acquisition plane: y.....	72
Figure 7.2. Interpretation of the figure 7.1 showing the main fracture plains found. Radar acquisition plane: y.....	73
Figure 7.3. Lateral cut positioned north the amphibolite vein, showing the attenuation effect of this material, and the continuity of the fracture plain. Radar acquisition plane: y	74
Figure 7.4. View of the continuity of the fracture identified earlier with a green plane, radar acquisition plane: y.....	75
Figure 7.5. Lateral cut positioned south the amphibolite vein, radar acquisition plane: y	75
Figure 7.6. Visualization of the main fracture found, radar acquisition plane: y.....	76
Figure 7.7. North wall, scale enhancing the visibility of the bigger fracture at 4,2m, radar acquisition plane: x.....	77
Figure 7.8. North wall, scale trying to improve the visualization of the deeper fracture, radar acquisition plane: x.....	78
Figure 7.9. Profile 07 of the inner and outer wall acquisition with the 200Mhz antenna	78
Figure 7.10. Profile 07 of the inner and outer wall acquisition with the 900 MHz antenna	79

Chapter 1 Presentation

1.1 Abstract

In the geophysics world, the Ground Penetrating Radar is an instrument every day more known and used, due to its easy implementation and methodology, short acquisition times and good results; the main application fields are archeology, the construction industry, geology, mining, among others. The present thesis work mainly consisted in the acquisition, processing and interpretation of GPR data in the Pink Marble Quarry of Candoglia, which is the main source of marble for the reconstruction of the Cathedral of Milan, the main historic structure of the mentioned city.

The data acquisition process consisted in 7 different surveys in 5 areas, both on the floor and on the walls of the quarry, with 200MHz and 900MHz antennas, with the aim of finding contacts between the marble and the adjacent rock and/or fractures that could compromise the excavation that will be carried out in the future. Regarding the adjacent rock, the information obtained in the lateral wall was not very useful, because the minimum contact distance for structural reasons should be 5m, and the radargrams show very superficial information, between 1m and 2m. A Matlab code was made with the aim of being able to handle the data more freely, hoping to retrieve information in depth, obtaining unpleasant results. The main and useful information obtained consist in different 3D cubes, which were constructed from the interpolation of the 2D lines, showing some possible dip-slope direction fractures at a moderate depth, which would be of interest to the next excavation stage.

1.2 Introduction

The Ground Penetrating Radar (GPR) technique is a geophysical prospection method based on the emission of electromagnetic pulses of short duration, those pulses travel through the soil, when they find a variation of electromagnetic properties, reflections, refraction and diffraction of the waves can be generated. The receiver detects those wave responses and a 2D image, called radargram, is generated. Usually the vertical axis is the two-way travel time of the pulses and the horizontal one represents the distance along the acquisition line.

The use of the GPR has increased its popularity and acceptance as a non-invasive method due to its effectiveness to characterize the presence of buried elements, like pipelines for example, determine stratigraphic and geologic conditions: faults, sediments, geologic contacts, lake bed shapes, archaeological applications, among others.

The Candoglia pink marble is a very important ornamental stone, used in the construction of the Cathedral of Milan, currently it is still used for maintenance and reparation works in the cathedral. Being exploited for a very long time, a lot of stability works has been done in the quarry, because the void left after the extraction activity grow in time.

For the future mark downs, projected to be done in 2025, many studies are currently being done, such as numerical modelling, new geological surveys, new geomechanical characterizations, and geophysical prospection including seismic and GPR, this last method will be the central topic developed on this thesis work.

1.3 Objective

The following study has the aim of identifying fracture planes, discontinuities, heterogeneities and contacts between the marble and the adjacent rocks, to contribute to the correct future planning of the mine. In the following chapters the acquisition, processing and interpretation of the georadar data recently acquired in the lowest area of the quarry, from which the lowering works will start, will be presented.

Chapter 2 The Candoglia quarry.

2.1 History

The Candoglia quarry is the main source of the pink marble that was used in the construction of the cathedral of Milan (Figure 2.1) one of the greatest examples of gothic art in Italy. During the XV-XVI centuries it was also used in other monuments, like the Certosa di Pavia church and the Colleoni Chapel in Bergamo, however, from 24 October 1387, on the basis of a privilege of Gian Galeazzo Visconti, it was reserved exclusively for the Milan Cathedral Factory.



Figure 2.1. The Cathedral of Milan

Nowadays, the action of natural phenomena such as sunlight, rain, wind and pollution generate damages on the structure because of the weathering of the marble, especially in the more elaborated, decorative parts. For safety purposes, these parts are periodically replaced (Figure 2.2), and it is necessary to use the same marble for this maintenance works, both for structural and aesthetic reasons. For this reason, although the cathedral construction is completed, the fabric is steel on production.



Figure 2.2. Reconstruction of a part of the Cathedral

In the same space that belongs to the quarry the restoration workshop is located, and is constantly in function to restore all the necessary parts of the cathedral, that are transported directly from Milan to there. In this way is easy to work on the new marble, because almost no transportation is needed.

2.2 Location

The quarry is located in the Ossola Valley, more specifically in Mergozzo at the North of Italy at an altitude of 580 m.s.l.m over the locality of Candoglia (Figure 2.3), near to the Toce river quoted at 210 m.s.l.m. The river in those times was the key to allow the construction of the cathedral, in the XVIII century this facilitated the transportation of the big and heavy marble blocks from the locality of Candoglia to Milan. This quarry is one of the oldest quarries that are still in production, of which there is certain information from 1814.

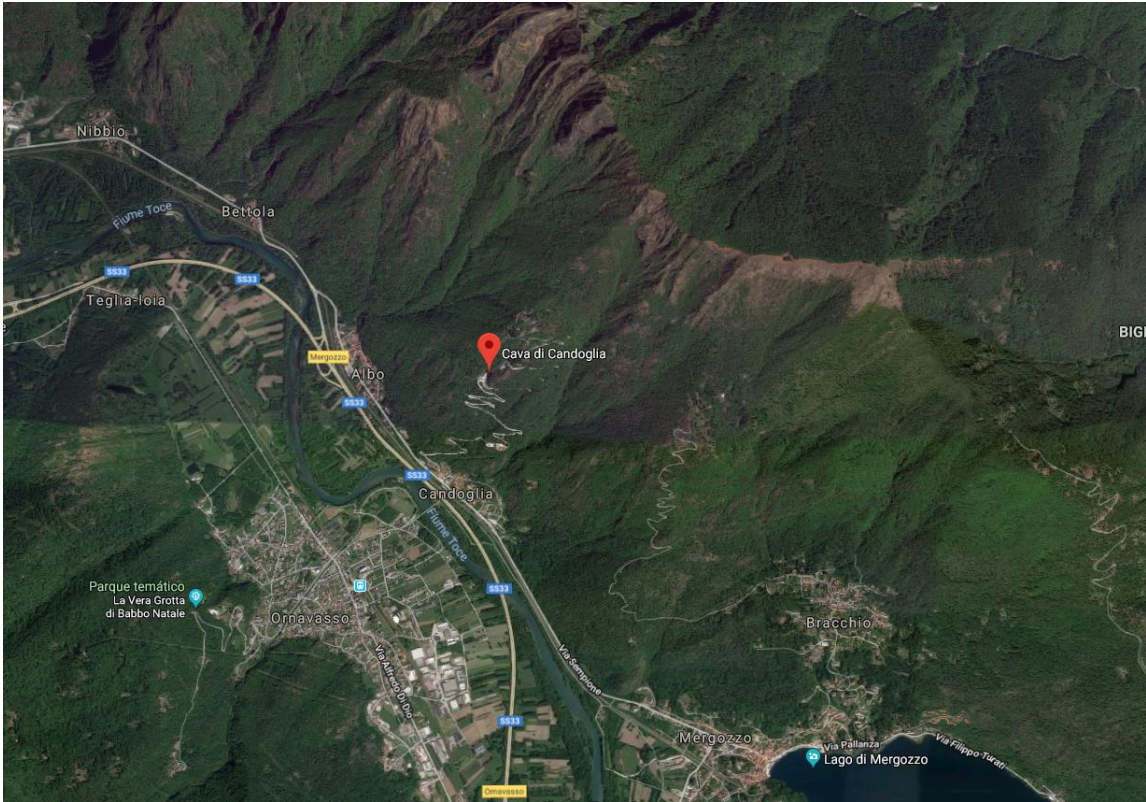


Figure 2.3. Location of the quarry

2.3 Geometrical characteristics

The quote of the cave has been time to time lower, currently is 605m s.l.m at the top of the cavity, where the marble has been already extracted. The lower part is situated at 565m.s.l.m, after the future works the expected quote is 550 m.s.l.m considering 2 lowering of 5m each, for which numeric modelling is still been made to find the best option to reach the objectives proposed. In the upper part, a concrete structure has been constructed for stability and logistic purposes; attached to this structure there is a derrick, installed to lift the heavy blocks and facilitate the transportation process.

As the excavation has more than 100 years the dimensions of the cave had also changed: in the 1950's were 50m long, 22m wide and 32m high [1], later in the 2000's this dimensions has reached approximately 80m long, 22 wide and 48m high [2] (Figure 2.4), nowadays the dimensions are even higher. Due to the size of the cave several stability works have been performed to maintain the safety of the workers in the cave.



Figure 2.4. The Candoglia Quarry

2.4 Geology

The area in which is located the quarry, is part of an extension on where several marble caves exist, the basin of extraction is constituted by 5 different quarries: “Cava Mergozzoni”, “Cava Cornovo Ovest”, “Cava Cornovo est”, “Cava del Carrettone” and the “Cava Madre di Candoglia”, the last one is the only that is still active, its extension is in NE direction [3]. The area is represented in the page 15 “Domodossola” of the Geologic Map of Italy.

The marble excavated at Candoglia is part of thin layers of marble-calc-silicate and quartzite that form very narrow two-phase near isoclinal folds that accompany the amphibolite-facies rocks of the Ivrea-Verbano zone.

Some of these marble layers can be traced for considerable distances along strike. The surrounding ‘kinzignite gneisses’ (biotite-feldspat-gneisses with quartz, fibrolitic silimanite, etc) are veined by deformed acidic (granitic) partial melting products (migmatites). [3]

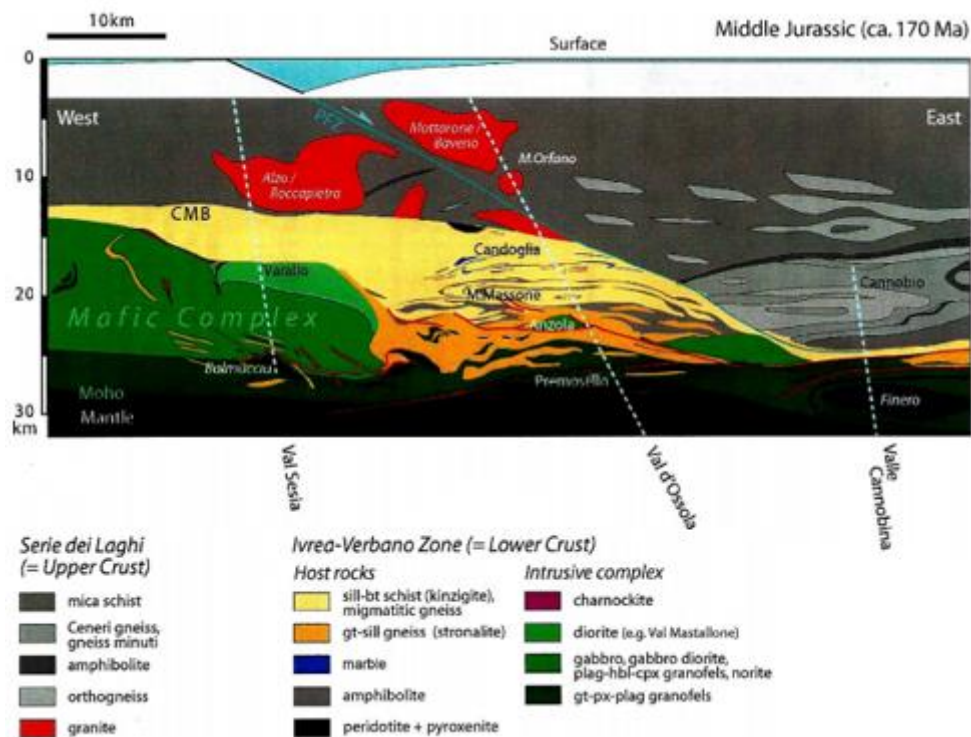


Figure 2.5. General view of the zone with principal geological composition [3]

In the Candoglia cave, the marble is disposed in a vertical block with an almost constant thickness. The fractures are disposed mainly with dip slope direction [3]. The marble is medium grain, white or pink with parallel dark streaks, according to studies at the polytechnic of Torino, the composition: mainly calcite, rare quartz, muscovite and pyrite. In the south part of the mine, it is in contact with altered shales, gneiss or quartzite, while on the north side quartzite and compact schists are found.

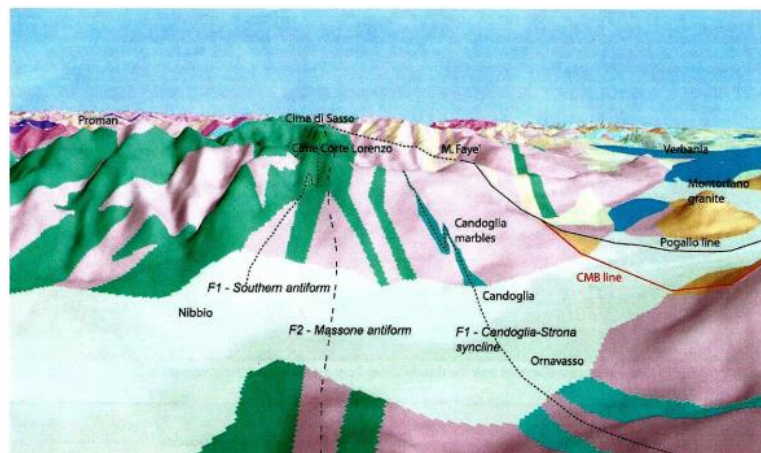


Figure 2.6. Virtual view illustrating the most prominent geologic unit. [3]

Chapter 3 Terms and definitions

The present chapter will treat the concepts related with the electromagnetic waves propagation, electric and magnetic properties of the soils and physical laws for the understanding the performance and logic behind the Georadar method.

In a structural way, this chapter has 2 sections: the first deals with the concepts related to the electromagnetic properties of the media and the second exposes the theoretical foundations of electromagnetism and propagation of electromagnetic waves.

3.1 Basic concepts about the electromagnetic properties of the soils.

3.1.1 Ground Penetrating Radar

The Ground-penetrating radar (also referred to as ground-probing radar, surface-penetrating radar, subsurface radar, georadar or impulse radar) is a noninvasive geophysical technique that detects electromagnetical discontinuities in the shallow subsurface (<50 m). It does this by generating discrete pulses of high frequency (MHz) electromagnetic energy, which propagate into the ground and after, reflections, refractions and diffractions are received at the ground surface. During the 1980s radar systems became commercially available, but it was not until the mid-1990s that sedimentary geologists and others began to widely exploit the technique. [4]

The basic methodology of the GPR technique consists in moving the receiving / transmitting antenna over the surface of the area of interest, while sending electromagnetic pulses and measuring the reflected signal. This signal will have changes in its amplitude and energy, because of the propagation through a material that has heterogeneities, objects, subsurface structures or discontinuities. The response is exposed in a radargram, which shows the space-time relation of the emitted waves.

3.1.2 Electric permittivity (ϵ):

The electric permittivity [F/m] describes the ability of a material to store or release electromagnetic energy in the form of electric charge and is classically related to the storage capacity of a capacitor. Alternatively, this can be described as the ability of a

material to restrict the flow of free charges or the degree of polarization exhibited by a material under the influence of an electric field [5]

Rock	Source, mineral composition in %	ϵ	Frequency, cps	Water content, %
Gneiss		8.0–15.0		
Granite gneiss		8.0–9.0	$5 \cdot 10^2 - 5 \cdot 10^7$	
Quartzite	Sholshinskoe	4.36	$5 \cdot 10^5$	dry
"	Ridderskoe	4.85	$5 \cdot 10^5$	"
"		6.6		
"		7.0		
Marble		8.22		dry
"		8.37		0.002
"		8.9–9.0	$10^3 - 10^7$	dry
Talc slate		7.5–34.0	$5 \cdot 10 - 5 \cdot 10^7$	"
Micaceous slate		9.0–10.0	$5 \cdot 10 - 5 \cdot 10^7$	"
Roofing slate	Georgian SSR	6.71		"
"	"	7.74		0.1
Phyllite		13.0		
Igneous rocks, acid				
Biotite-granite aplite	quartz, 40 microcline, 32 plagioclase, 20 other, 8	4.8		dry
Granite	Altai	5.42	$5 \cdot 10^5$	"
"	Leznikovskoe	4.74	$5 \cdot 10^5$	"
Granite	Garm	5.06	$5 \cdot 10^5$	"
"	Valaamskoe	4.5	$5 \cdot 10^5$	"
"		7.0–9.0		combined moisture
Volcanic tuff		3.8–4.5		dry
Igneous rocks, intermediate				
Diorite	Kola Peninsula	5.9–6.3	$10^5 - 10^7$	dry

Figure 3.1. Some dielectric constant values of rocks [6]

3.1.3 Electric conductivity (σ)

The electrical conductivity [S/m] in a material characterizes the free movement of charges under the influence of an electric field. It is the inverse of the electric resistivity ρ [Ωm], it depends mainly on the atomic and molecular structure and on the temperature. In metals, for example, the electric conductivity is high because of electrons with weak links, allowing easy movement, while in fluids the electrical conductivity is related to the dissolved cations and anions. Resistance to charge flow leads to energy dissipation in form of heat. [5]

3.1.4 Magnetic permeability (μ)

The magnetic permeability [H/m] is the ability of a material to attract and let pass a magnetic field through it. It can also be defined as the parameter that relates the magnetic induction and the intensity of the magnetic field. It is denoted with the symbol μ and can be described as follows:

$$\mu = \mu_r \mu_0 = \frac{B}{H} \quad \text{Equation 3.1}$$

Where B and H are the magnetic and electric field, and μ_0 is the permeability constant, or permeability of free space ($4\pi \cdot 10^{-9} \text{ Hm}^{-1}$) the relative magnetic permeability μ_r in most materials is very close to 1 (unless they are ferromagnetic, in this case is higher than 1) [7].

Similarly to the electric permittivity and conductivity, the magnetic permeability is a complex parameter, where the real component represents the stored energy and the imaginary component represents the magnetic energy losses.

In the majority of cases the magnetism has a very small effect in the propagation of the GPR wave (for diamagnetic and paramagnetic materials), so it is usually approximated to its value in the void. Nevertheless, for ferromagnetic materials it has a considerable effect on the wave velocity and attenuation of the signal [5].

3.2 Theoretical basis of EM, EM waves and propagation.

3.2.1 Electromagnetic waves

They are variations of the electric and magnetic field that propagate in the same direction, both electric and magnetic fields are orthogonal to each other (Figure 3.2). Unlike other types of waves, electromagnetic waves can propagate in a vacuum at the speed of light. [7]

3.2.2 Generation of electromagnetic waves

An electric charge generates an electric field, the intensity of electric field will be given by the magnitude of the charge. If this charge also begins to move, it will generate an electric current, which in turn will generate a magnetic field. If the electric charge begins to vary its speed of displacement, a variable current and a variable magnetic field will be generated, this variable magnetic field is also capable of generating an electric field, with which an electromagnetic wave will have been generated. [8]

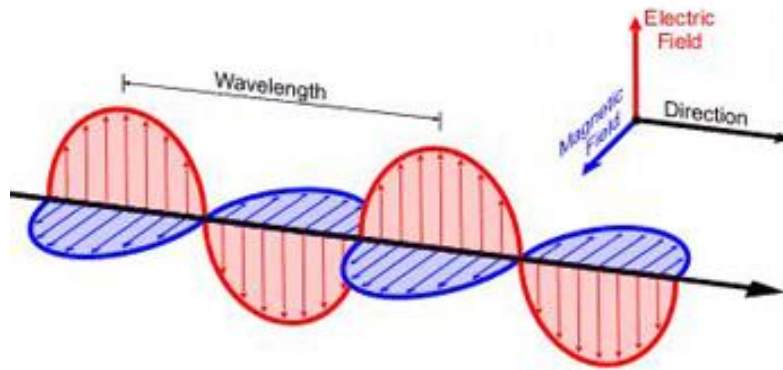


Figure 3.2. Electromagnetic Wave propagation

3.2.3 Fundamentals of Electromagnetism

The Maxwell equations describe mathematically the physics of the electromagnetic fields, which are commanded by: The electromagnetic induction law of Faraday (Equation 3.4), the Ampere-Maxwell equation (3.5), and the Gauss law for closed surfaces (3.2,3.3). These 2 last equations show that the two fields are linked. Maxwell describe the propagation of electromagnetic waves with the following equations:

$$\text{Div}\vec{D} = q \quad \text{Equation 3.2}$$

$$\text{div}\vec{B} = 0 \quad \text{Equation 3.3}$$

$$\text{Rot}\vec{E} = -\frac{\partial\vec{B}}{\partial t} \quad \text{Equation 3.4}$$

$$\text{rot}\vec{H} = \vec{J} + \frac{\partial\vec{D}}{\partial t} \quad \text{Equation 3.5}$$

Where the parameters are:

\vec{D} Electric displacement [C/m²]

q Electric charge [C/m³]

\vec{E}	Electric field intensity [V/m]
\vec{j}	Electric current density [A/m ²]
\vec{H}	Magnetic field intensity [A/m]
\vec{B}	Magnetic field flux [T or Wb/m ²]

3.2.4 Constitutive equations

Constitutive relationships are the approach to describe a material's response to EM fields. For GPR, the electrical and magnetic properties are important. Constitutive equations (Equation 3.6, 3.9, 3.10) provide a macroscopic (or average behavior) description of how electrons, atoms, and molecules respond to the application of an EM field. [5]

$$\vec{j} = \sigma \vec{E} \quad \text{Equation 3.6}$$

$$\vec{D} = \epsilon \vec{E} \quad \text{Equation 3.7}$$

$$\vec{B} = \mu \vec{H} \quad \text{Equation 3.8}$$

σ, ϵ and μ are the electric conductivity, electric permittivity and magnetic permeability, already described in section 3.1 .

Maxwell also consider some electromagnetic parameters:

$$\epsilon = \epsilon_r \epsilon_0 \quad \text{Equation 3.9}$$

$$\mu = \mu_r \mu_0 \quad \text{Equation 3.10}$$

$$\epsilon_0 = 8.85 \times 10^{-12} \quad \text{Equation 3.11}$$

$$\mu_0 = 4\pi \times 10^{-7} \quad \text{Equation 3.12}$$

In which the subscript r stays for relative and 0 for vacuum. Combining the constitutive equations in conjunction with the set of equations described in section 3.2.4 and with the electromagnetic parameters above, Maxwell obtained 2 partial differential equations for the electric and magnetic fields (\vec{E} and \vec{H})

$$\Delta^2 \vec{H} = \mu \sigma \frac{\partial \vec{H}}{\partial t} + \mu \epsilon \frac{\partial^2 \vec{H}}{\partial t^2} \quad \text{Equation 3.13}$$

$$\Delta^2 \vec{E} = \mu\sigma \frac{\partial \vec{E}}{\partial t} + \mu\epsilon \frac{\partial^2 \vec{E}}{\partial t^2} \quad \text{Equation 3.14}$$

The solution for both equations Equation 3.13 and 3.16 has the following form:

$$V(z) = V_0 e^{-\alpha z} e^{i(\omega t - \beta z)} \quad \text{Equation 3.15}$$

This similarity of equations and solutions of the electric and magnetic fields allows to analyze only E and the analysis will work for H too. In GPR we analyze an E field oscillating along the x direction, and propagating along the z direction, so the solution can be described as the solution of a dissipative wave by the following:

$$E(z, \omega, t) = E_x(0, \omega, 0) e^{-\alpha z} e^{i(\omega t - \beta z)} \quad \text{Equation 3.16}$$

Where the parameters are:

- α Attenuation factor [1/m]
- β Propagation factor [rad/m]
- ω Angular frequency ($\omega = 2\pi f$) [rad/s]
- f Frequency [1/s]
- v Propagation velocity ($v = \frac{\omega}{\beta}$) [m/s]
- λ Wavelength ($\lambda = \frac{2\pi}{\beta} = \frac{v}{f}$) [m]

From the first exponential function it can be seen that at a distance $z=1/\alpha$, the attenuation is $1/e$. This distance is known as the skin depth, d , and provides an indication of the penetration depth of surface-penetrating radar system.

Finally, the parameters α and β known, can be related to σ and $j\omega\epsilon$ as shown below [9]

$$\alpha = \beta \sqrt{\left[\frac{\mu\epsilon'}{2} \sqrt{1 + \left(\frac{\epsilon''}{\epsilon'}\right)^2} - 1 \right]} \quad \text{Equation 3.17}$$

$$\beta = \omega \sqrt{\left[\frac{\mu \varepsilon'}{2} \sqrt{1 + \left(\frac{\varepsilon''}{\varepsilon'} \right)^2} + 1 \right]} \quad \text{Equation 3.18}$$

Knowing these two parameters we can calculate the loss tangent and the wave number in function of α and β

$$tg(\theta) = \frac{\sigma}{\omega \varepsilon} \quad \text{Equation 3.19}$$

$$\gamma = \alpha + j\beta \quad \text{Equation 3.20}$$

3.2.5 Propagation Velocity

The propagation velocity of an electromagnetic wave is defined by:

$$V = \lambda f = \frac{\omega}{\beta} [ms^{-1}] \quad \text{Equation 3.21}$$

Where λ is the wave length of the signal, ω is the angular velocity and β is the propagation factor, which is the inverse of the wavelength. For a dielectric medium, where there is no conduction of electric current, the wave velocity is independent from the frequency, for low-dissipative, homogeneous and isotropic materials, the relative propagation velocity can be calculated from: [10]

$$v_r = \frac{c_0}{\sqrt{\varepsilon_r}} [ms^{-1}] \quad \text{Equation 3.22}$$

Where ε_r is the relative permittivity and $c_0=2.998 \times 10^8$ [m/s].

In most practical trial situations, the relative permittivity will be unknown. The velocity of propagation must be measured in situ, estimated by means of direct measurement of the depth to a physical interface or target (i.e. by borehole), or by calculation by means of multiple measurements. [9]

3.2.6 Energy losses: absorption, dispersion and spherical divergence.

Ground Penetrating Radar (GPR) uses a pulse with duration around nanoseconds and frequency in the range 50 MHz–2 GHz. As the pulse propagates in the geologic medium, it suffers attenuation as the result of absorption, dispersion and spherical divergence.

The real 3-D GPR pulse can be simulated as a sum of monochromatic waves of form as in the Equation 3.23, with corrections due to spherical divergence. This latter is a frequency independent effect, if the Earth's subsurface can be modeled as a perfect dielectric (constant v , $\alpha = 0$), the received propagated pulse has the same shape of the starting pulse. [11] However, real geologic media usually present pronounced attenuation effects.

$$E(z, \omega, t) = E_x(0, \omega, 0)e^{-\alpha z} e^{i(\omega t - \beta z)} \quad \text{Equation 3.23}$$

Where $E(x, t)$ is the value of the electric field in the position x and time t , $E_0 = E(0,0)$, $i = \sqrt{-1}$, α is the attenuation coefficient, v is the phase velocity, and $\omega = 2\pi f$, with f being the frequency. In general, α and v are frequency dependent.

Absorption is associated to amplitude decay due to the energy loss related to heat conversion, dispersion refers to the pulse deformation related to the frequency dependence of the wave parameters, the pulse detects magnetic and electric heterogeneities, the small heterogeneities generates a weaker and undetectable response (scattering), but whose presence has impact in the signal. Those heterogeneities extract energy once the wave passes and is dispersed in all directions, like in the Figure 3.3.

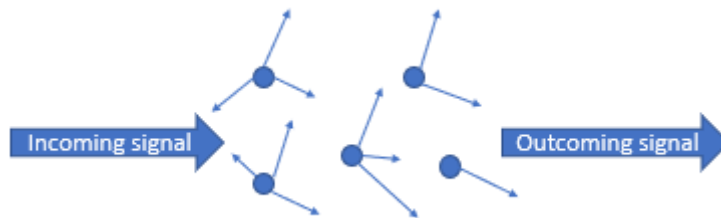


Figure 3.3. Dispersive attenuation (for scattering) [11]

The resulting signal will have an energy that has been decreased in function of the distance r and proportionally to an attenuation for dispersion coefficient (α_s) as the following equation shows

$$E = E_0 e^{-\alpha_s r} \quad \text{Equation 3.24}$$

$$\alpha_s = \frac{NA}{2} \quad \text{Equation 3.25}$$

Where A is the transversal section of the particles and N the number of particles per unit of volume. [5].

Finally, spherical divergence or geometrical spreading refers to the energy spreading in the wave front, which is a pure geometrical factor, generally the energy decays approximately with a ratio of $1/r^2$, where r is the distance source-object [12].

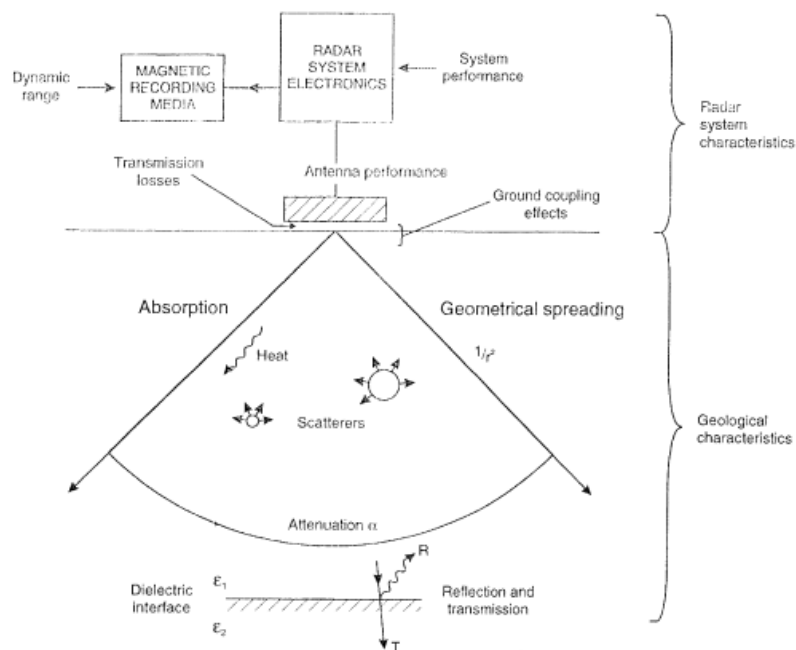


Figure 3.4. Energy losses scheme

3.2.7 Reflection, refraction and transmission in the interfaces.

The GPR pulse, travels in media as any other wave phenomena, when the EM wave finds a discontinuity in the electromagnetic properties (ϵ, σ, μ) is reflected, refracted and transmitted through the following media (Figure 3.5). In the case of the GPR, the refraction phenomena is not considered, because the usual survey are mainly based on reflection and diffraction. The Snell law, establishes that the reflected angle is the same than the incident angle, as shown in Equation 3.26 [7]

$$\sin \theta_i = \sin \theta_r \quad \text{Equation 3.26}$$

In the case of the refraction, using the Snell law and the relationship between the velocity and the electric permittivity [13] the equation becomes:

$$\varepsilon_1 \sin^2 \theta_i = \varepsilon_2 \sin^2 \theta_t \quad \text{Equation 3.27}$$

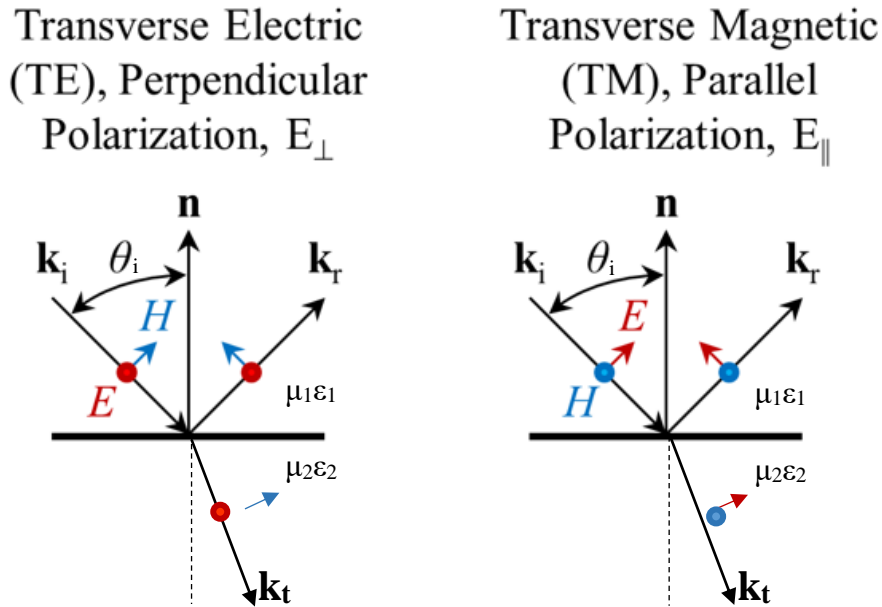


Figure 3.5. Reflection of electromagnetic waves [14]

As in the figure, the polarization can be transversal or parallel, it depends on the preferential direction of the object with respect to the direction of incidence of the electromagnetic pulses. The polarization of a wave is described by the locus of the tip of the E vector as time progress when the locus is a straight line, the wave is said to be linearly polarized. If the locus is a circle then the wave is said to be circularly polarized. In the case of GPR waves they can only be linearly polarized, the only thing that changes is the direction of that polarization with respect to the studied object.

3.2.8 Electromagnetic impedance

The electromagnetic impedance of an electromagnetic wave is the relation between the transversal components of the electric and magnetic fields

$$Z = \frac{E}{H} = \sqrt{\frac{j\omega\mu}{\sigma + j\omega\varepsilon}} \quad [\Omega] \quad \text{Equation 3.28}$$

Where μ is the magnetic permeability, ε is the electric permittivity and σ is the electric conductivity of the material in which the wave is traveling. In the equation, j is the imaginary unit and ω is the angular frequency.

The quantity of energy that is reflected and transmitted by the wave can be defined by the transmission and reflection coefficients [14]

$$R = \frac{Z_2 - Z_1}{Z_2 + Z_1} \quad \text{Equation 3.29}$$

$$T = -\frac{2Z_2}{Z_2 + Z_1} \quad \text{Equation 3.30}$$

Where R and T indicate the reflected and transmitted wave (Figure 3.5) while the subscripts 1 and 2 are for first and second medium that the wave cross [15]. These equations work for $\theta < 20^\circ$ and medium 2 thickness much greater than the wavelength in the medium.

The other possibility in the wave propagation is the diffraction, generally due to a point-like object, in this case, it can be seen in the radargram the diffracted pulses arranged on a hyperbola which can be seen at times:

$$twt = \frac{2\sqrt{(x - x_0)^2 + h^2}}{v_1} \quad \text{Equation 3.31}$$

It can easily be recognized that if the propagation velocity can be measured, as shown in section 3.2.5, an absolute measurement of depth or thickness can be made:

$$d = v_R \frac{twt}{2} [m] \quad \text{Equation 3.32}$$

Where twt is the two-way travel time to and from the target.

In particular, the reflection of the signal depends on the distance between the antenna and the detected discontinuity, which is calculated as a function of the delay between the emitted pulse and the reflected impulse which returns to the surface. For this reason, the geophysical analyzes take into account the Two-Way Travel time (twt). [16]

3.2.9 Vertical and horizontal resolution

As the transmitting antenna emits large part of EM energy in a “cone of radiation” the resolution of a ground penetrating radar can be defined as the capacity to distinguish between two nearby reflectors or small objects, it depends on the wavelength and it can be divided in vertical and horizontal resolution.

Vertical resolution: It is defined that an object or reflector with a thickness less than $\lambda/4$ will not be able to reflect the energy towards the receiving antenna, therefore it cannot be detected. [17] From this it can be concluded that the smallest reflector that can be detected with a certain wavelength $\lambda = \frac{c}{\sqrt{\epsilon_r}f}$ is one of dimensions equal to that expressed in Equation 3.33. The vertical Spatial Resolution Δz is usually not supposed to vary with depth [14].

$$\Delta z = \frac{\lambda}{4} [m] \quad \text{Equation 3.33}$$

Horizontal resolution: In this case, it cannot be expected the distinction of two objects that are located horizontally closer than Δx . The horizontal Spatial Resolution Δx varies with depth mainly in function of the EM characteristic of the soil and of the frequency.

$$\Delta x = \sqrt{\frac{\lambda D}{2}} [m] \quad \text{Equation 3.34}$$

Where D is the depth and λ is the wavelength.

Chapter 4 Data acquisition

The GPR data acquisition was carried out in the entering part of the Candoglia quarry, the 13th and 26th of July of 2018. A total of 157 profiles were measured, distributed in five study zones, in the Figure 4.5 is shown the disposition and relative location of the acquired profiles. In the first day, the acquisition was made with the 200MHz antenna only, while in the second day, the 200MHz was used for the measurements on the ground and the 900MHz, for the walls, the detail of each acquisition is listed below.

4.1 Equipment and tools

For the acquisition of the profiles a pulsed-radar IDS K2 GPR with a TR200 IDS and a GSSI 900 MHz antennas, was used. The equipment was then composed of:

- IDS K2 GPR Central Unit
- 200-MHz and 900MHz central-frequency bistatic antenna.
- Wheel odometer
- Transporting base
- Computer
- Batteries and cables

In this case, a GPS wasn't used due to the closed space in which the profiles were made, it would not have been an exact measure, instead, the starting and ending point of each area were marked with red spray for a topographical survey, after supplied to us by Studio Bertinotti.



Figure 4.1. Equipment: at the left, the 900MHz antenna with the wheel odometer, in the center the computer, in the right the GPR Unit and the 200MHz antenna



Figure 4.2. Survey in the points 19-20-21-22 with the 200MHz antenna

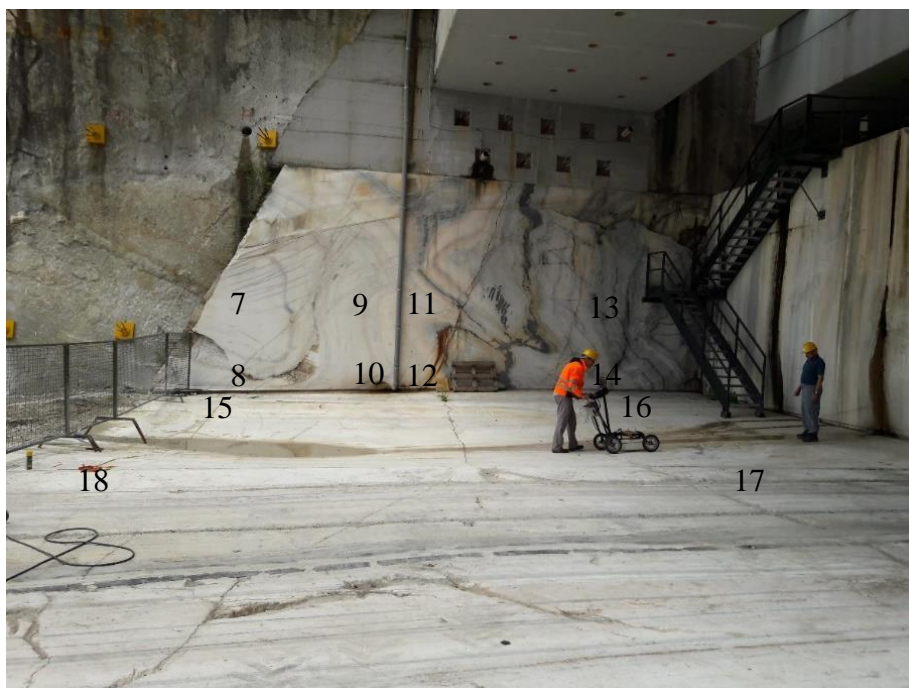


Figure 4.3. Survey in the points 15-16-17-18 with the 200MHz antenna



Figure 4.4. Survey in the points 1-2-3-4 with the 200MHz antenna

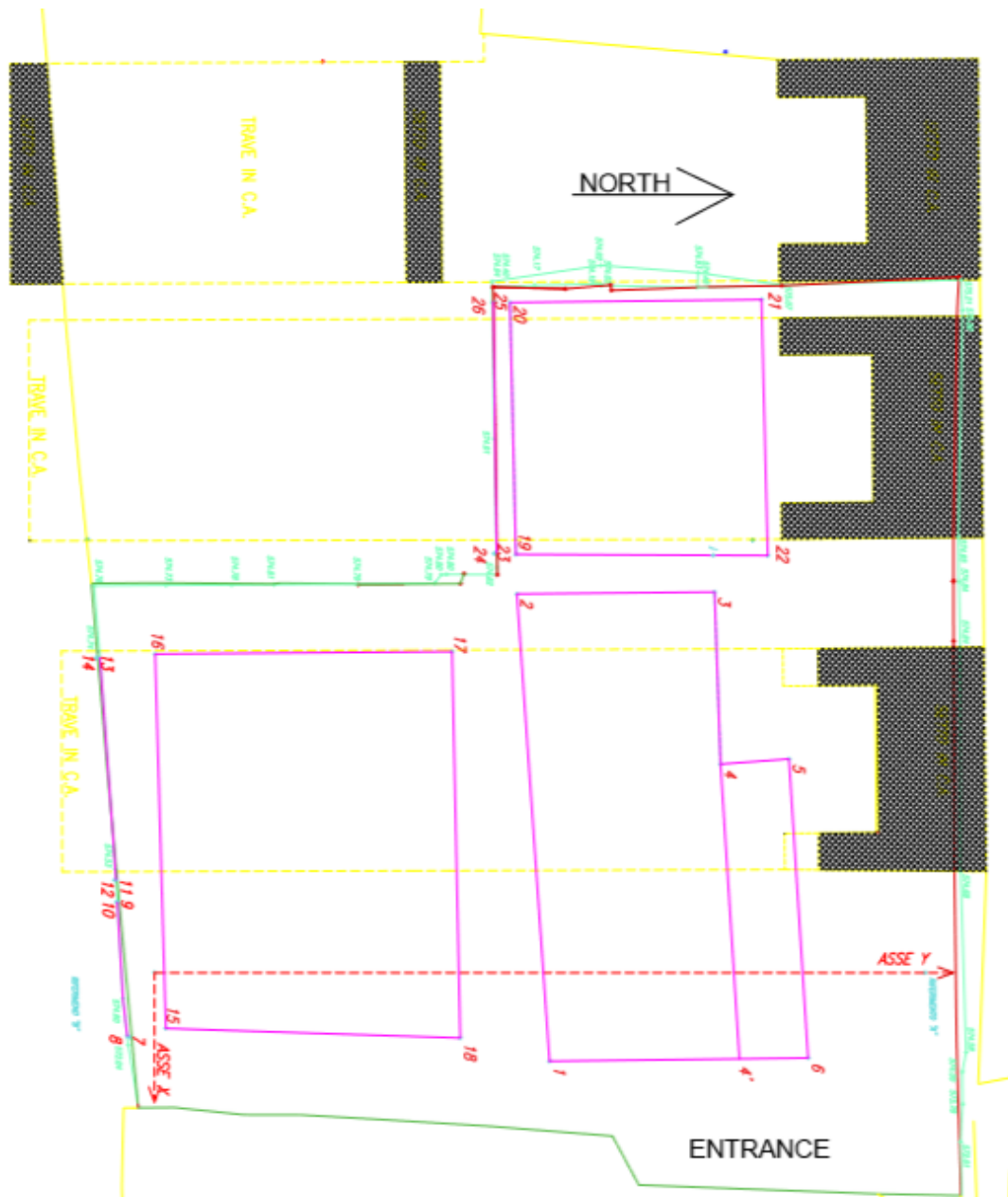


Figure 4.5 Modification from the image provided by studio bertinotti

4.2 Acquisition parameters for each survey

In the 13th July 2018, the first acquisition was carried out on the floor, at the north part of the entrance (Figure 4.5) along the Y orientation in the reference system given by Studio Bertinotti, each profile spaced 0.3m without meandering, and with the acquisition parameters shown in Table 4.1.

Table 4.1. Acquisition parameter- 200 MHz

Trace duration [ns]	Samples per trace [-]	Sampling interval [ns]	Sampling frequency [GHz]	Trace interval (y) [m]	Profile length [m]	Number of profiles [-]	Profile interval (x) [m]
500	1024	0.488	2	0.024	6.7 (4.9)	42	0.3

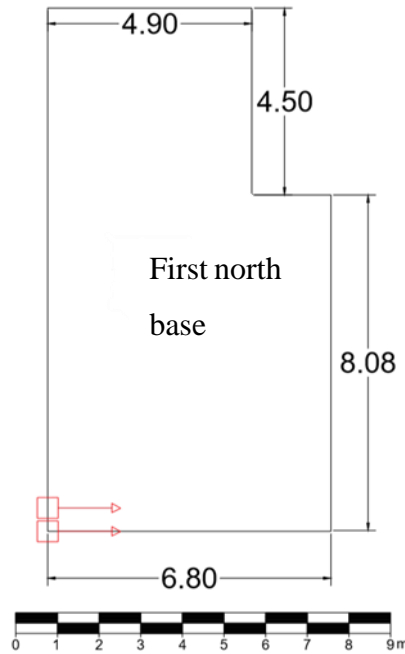


Figure 4.6. Points 1-2-3-4-5-6 from the image provided by studio Bertinottii

While the south wall, was acquired in two parts: the inner and the outer part of the wall, because in the middle there was a pipe of approximately 10cm of diameter, which did not allow the passage of the radar. 18 profiles were made, 9 in the inner wall, and 9 in the outer wall, both along the x orientation in the reference system, and 0.2m spacing in the z direction without meandering. (Table 4.2 and 4.3)

Table 4.2. South outer wall acquisition parameters- 200 MHz

Trace duration [ns]	Samples per trace [-]	Sampling interval [ns]	Sampling frequency [GHz]	Trace interval (x) [m]	Profile length [m]	Number of profiles [-]	Profile interval (z) [m]
300	1024	0.293	3.4	0.024	5.9	9	0.2

Table 4.3. South inner wall Acquisition parameter- 200 MHz

Trace duration [ns]	Samples per trace [-]	Sampling interval [ns]	Sampling frequency [GHz]	Trace interval (x) [m]	Profile length [m]	Number of profiles [-]	Profile interval (z) [m]
300	1024	0.293	3.4	0.024	3.3	9	0.2

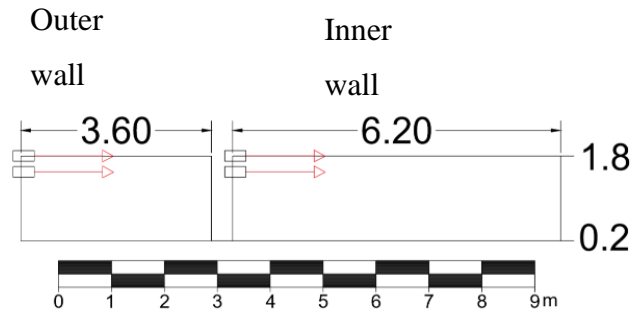


Figure 4.7. South wall: points 7-8-9-10 from the image provided by studio bertinotti

In the survey carried out on 26th July 2018, secondary acquisitions in the floor (named north, south and west base) with the 200MHz antenna and in the walls with the 900MHz antenna were made. In particular, the first floor acquisition was repeated in a perpendicular direction, due to interpretation difficulties in the radargram response. The first 3 acquisitions were made along the Y direction in the reference system given by Studio Bertinotti, with a profile interval of 0.3m with meandering, technical details in the Table 4.4, 4.5 and 4.6.

Table 4.4. North base acquisition parameters 200MHz

Trace duration [ns]	Samples per trace [-]	Sampling interval [ns]	Sampling frequency [GHz]	Trace interval (y) [m]	Profile length [m]	Number of profiles [-]	Profile interval (x) [m]
500	1024	0.488	2	0.062	12.2	19	0.3

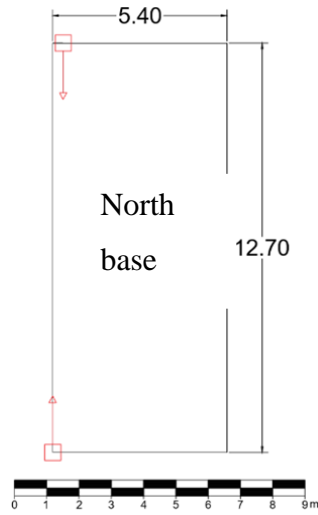


Figure 4.8. Points 1-2-3-4' from the image provided by studio bertinotti

Table 4.5. South base acquisition parameters 200MHz

Trace duration [ns]	Samples per trace [-]	Sampling interval [ns]	Sampling frequency [GHz]	Trace interval (y) [m]	Profile length [m]	Number of profiles [-]	Profile interval (x) [m]
500	1024	0.488	2	0.062	9.8	28	0.3

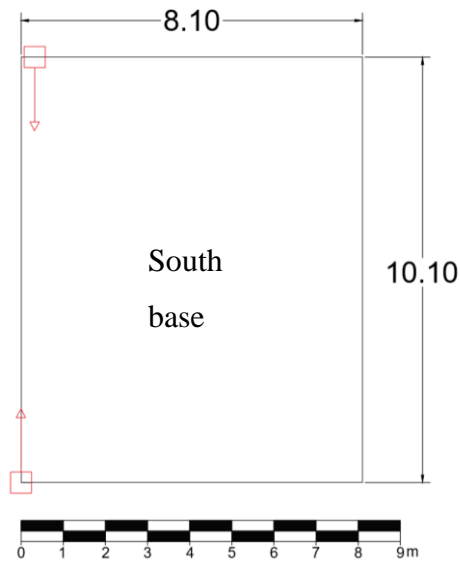


Figure 4.9. Points 15-16-17-18 from the image provided by studio bertinotti

Table 4.6 West base acquisition parameters 200MHz

Trace duration [ns]	Samples per trace [-]	Sampling interval [ns]	Sampling frequency [GHz]	Trace interval (y) [m]	Profile length [m]	Number of profiles [-]	Profile interval (x) [m]
500	1024	0.488	2	0.062	9.8	28	0.3

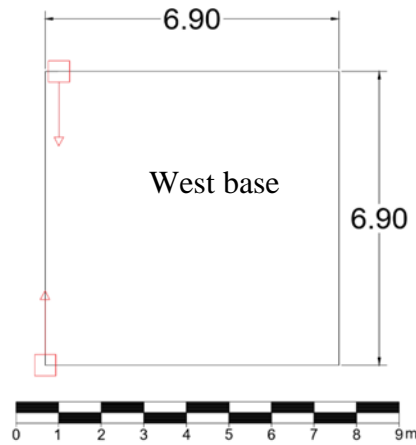


Figure 4.10. Points 19-20-21-22 from the image provided by studio bertinotti

The last 3 surfaces (Table 4.7, 4.8 and 4.9) were performed in the North wall, and a repetition on the south wall, with the GSSI 900 MHz antenna, all with an interval of 0.2m and an X orientation in the reference system given by Studio Bertinotti.

Table 4.7 North wall acquisition parameters 900MHz

Trace duration [ns]	Samples per trace [-]	Sampling interval [ns]	Sampling frequency [GHz]	Trace interval (x) [m]	Profile length [m]	Number of profiles [-]	Profile interval (z) [m]
200	2048	0.09766	10	0.024	6.3	8	0.2

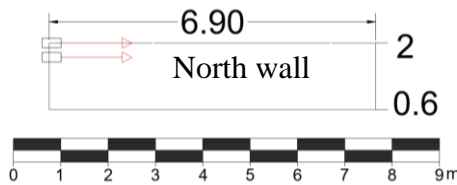


Figure 4.11. North wall, points 23-24-25-26 from the image provided by studio bertinotti

Table 4.8. South outer wall acquisition parameters 900MHz

Trace duration [ns]	Samples per trace [-]	Sampling interval [ns]	Sampling frequency [GHz]	Trace interval (x) [m]	Profile length [m]	Number of profiles [-]	Profile interval (z) [m]
200	2048	0.09766	10	0.024	3.3	9	0.2

Table 4.9. South inner wall acquisition parameters 900MHz

Trace duration [ns]	Samples per trace [-]	Sampling interval [ns]	Sampling frequency [GHz]	Trace interval (x) [m]	Profile length [m]	Number of profiles [-]	Profile interval (z) [m]
200	2048	0.09766	10	0.024	5.9	9	0.2

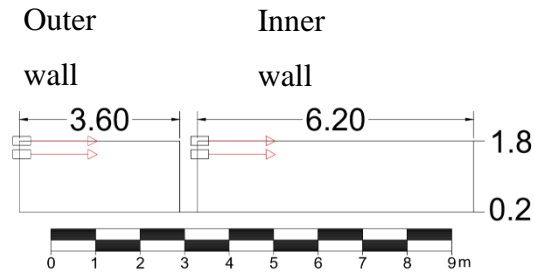


Figure 4.12. South wall: points 7-8-9-10 from the image provided by studio bertinotti

Chapter 5 Processing

This chapter will present the procedures used to enhance the quality of the raw data collected in the field. The aim of the processing of the radargrams is to highlight and identify the information contained in the signals. The unprocessed signal of a GPR usually presents reverberations, background noise, attenuation of the energy with depth, signal interference, etc. that can mask the data of interest. [18]

The processing software used to improve the raw data was Reflex-Win software for the majority of radargrams, and Matlab 2015b for a special processing in the south wall, where we had data areas along the same profiles, acquired with two different frequencies. The processing sequence basically consist in the application of different types of filters and graphical procedures, each one described in the following sections.

5.1 Data import

The first step to follow to visualize the data acquired in the survey is to perform the correct import to the Reflex platform, according to the parameters chosen during the acquisition. In the following image it is shown, the data import table for the acquisition in the area delimited by the points 15-16-17-18 (Figure 4.9, Table 4.5)

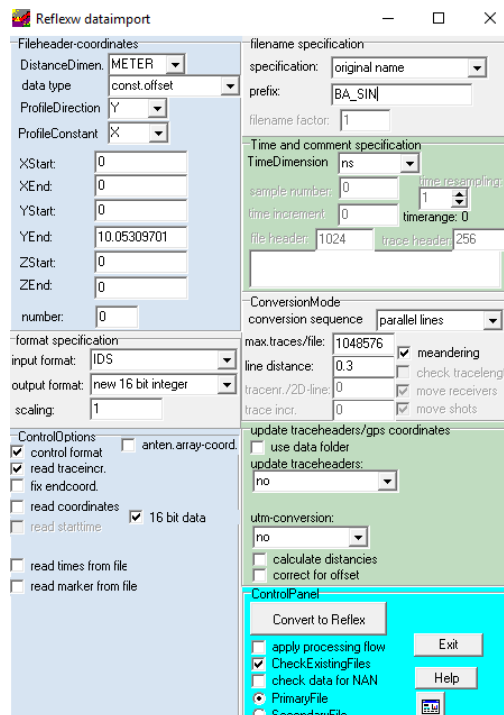


Figure 5.1. Data import table

After that, certain modifications are needed, for example, for the profiles acquired in the walls, the acquisition was made from the high to the low part, so the values by default of the radar starts at zero in the higher height that in this case was 1.80m. Also, for each profile the initial trace starts not in the edge of the profile but in correspondence to the position of the center of the antenna. Since all the acquisitions were made with the antenna bottom aligned with the edge of the area, the equivalent to half antenna of the initial and final position should be added. For this reason, a modification is made in the file header table that contains the spatial data (x and y position) and the trace increment data. In the image, an example of the table before and after the height modification.

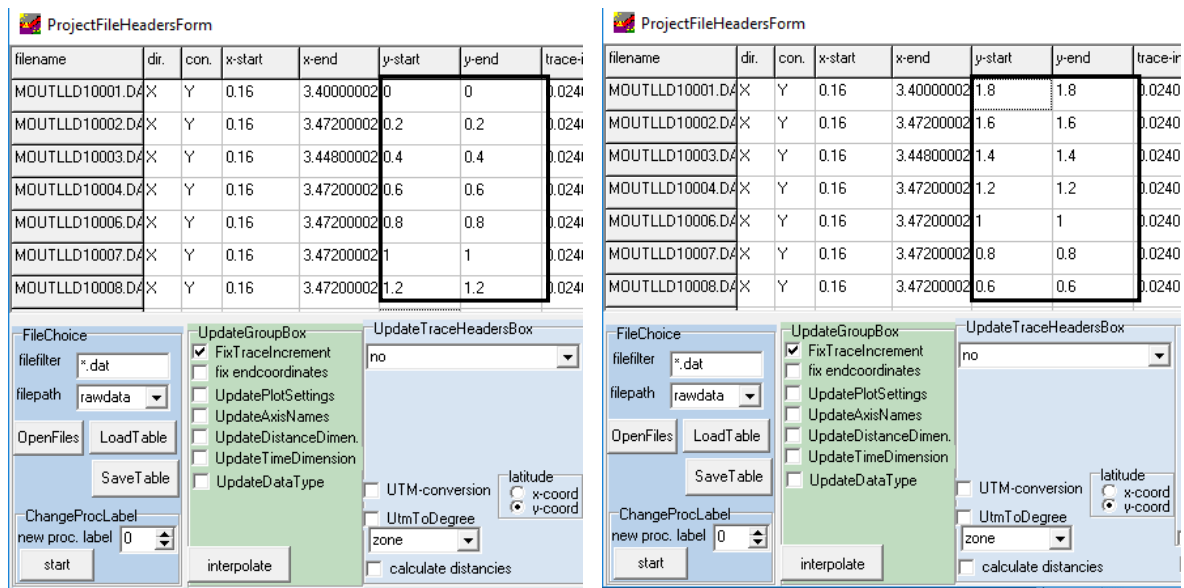


Figure 5.2. X Y coordinates data table

5.2 Graphical modifications

Due to the fact that the studied areas were very close to each other, the union of the profiles of certain areas was carried out to make a global interpretation of the studied area. For this it is necessary to modify again the coordinate table illustrated in Figure 5.2, placing as starting point the first profile of the first area and as last point the last profile of the second area, then, having both surveys in the same file, is necessary to perform a processing procedure called “insert profile”, which consist in the combination of two files with different ending and starting coordinates and basically attaches a selected profile to the current one, obviously this procedure needs to be done independently for each profile of the survey.

5.2.1 South inner and outer wall

The first profiles attached were the ones in the south wall, in the Figure 5.3. South inner and outer wall 900MHz the first profile of the 900MHz survey is shown, the same procedure was carried out for all the other profiles until completing the area, and also for the 200MHz survey.

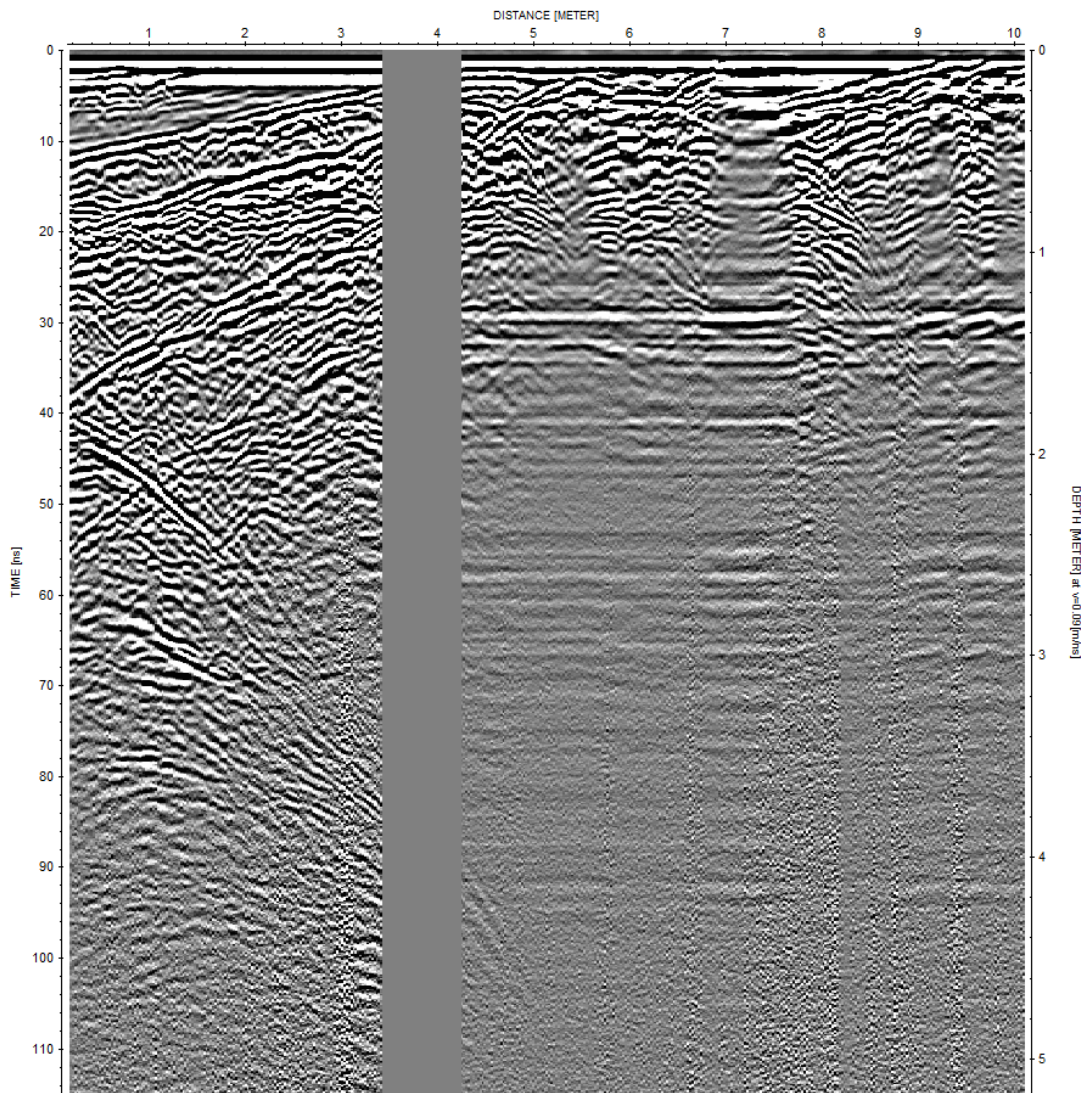


Figure 5.3. South inner and outer wall 900MHz

As it can be seen in the Figure 5.4 the coordinate table was modified, the black box data corresponds to the outer wall in which the length the profiles goes from 0.16m to 3.4m, then there is certain distance due to a plastic tube placed in the middle of the two surveys, after that we have the red box data, which begins at 4.23m and ends at about 10m.

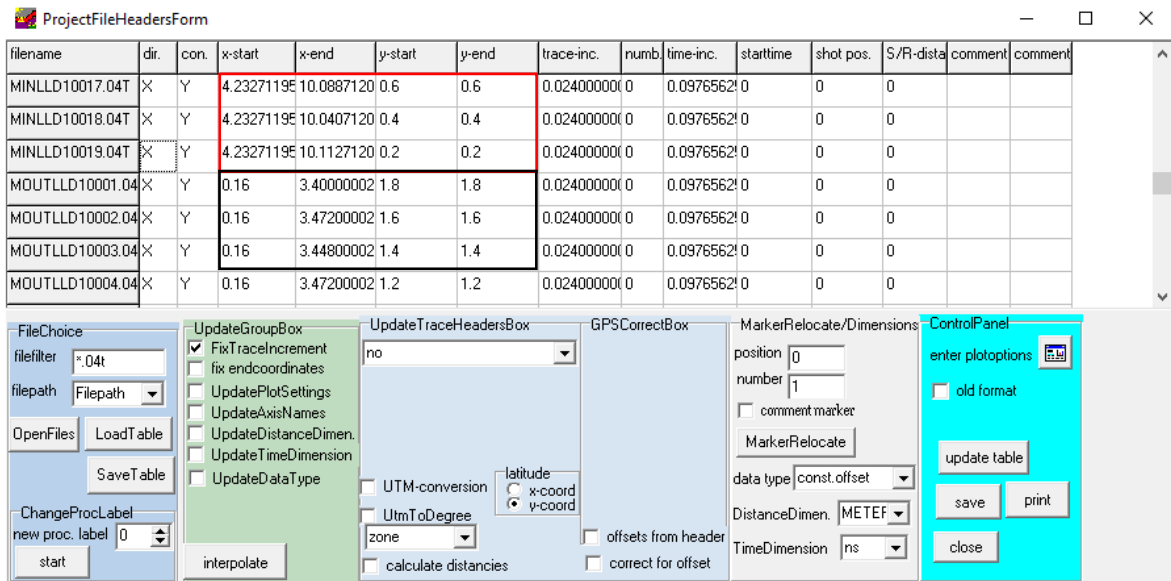


Figure 5.4. South inner and outer wall 900 MHz coordinate table

5.2.2 South base and north base

Both south and north bases were carried out with X direction, so an interesting procedure was to unite those two areas to have a wider study area. The starting point of the north base survey was not aligned with the first point of the last profile of the south base, this means that the starting value of the Y coordinate for both of them were different, for that reason in the Figure 5.5 the “y-start” column starts at zero when corresponding to the south base profiles, and at -0.55m for the north base survey, decreasing profile by profile.

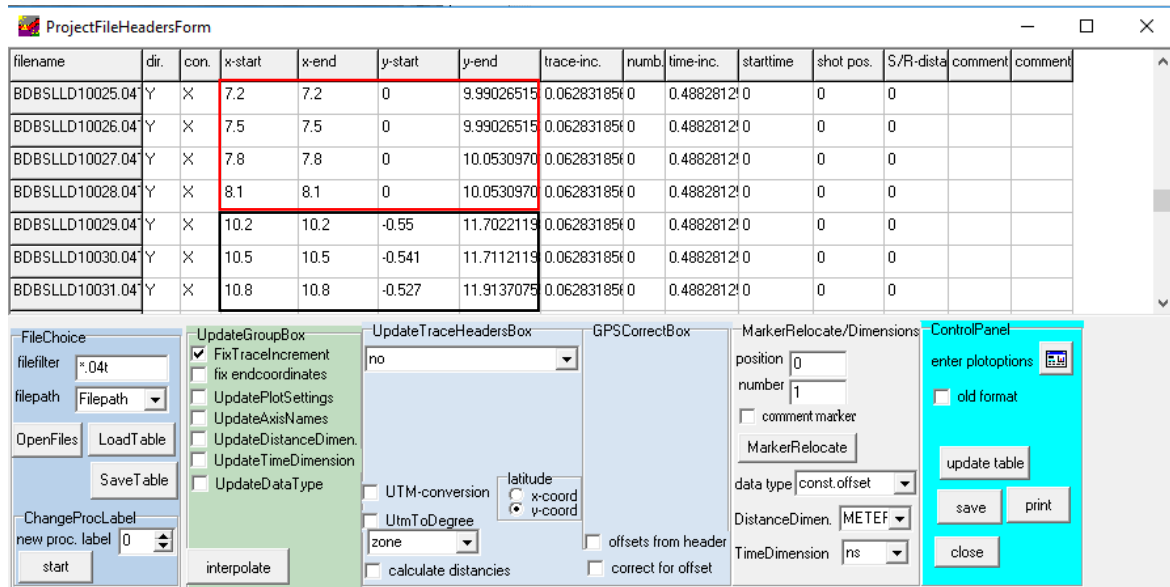


Figure 5.5. South and north base 200 MHz coordinate table

Also, in the X direction, (Figure 5.5) due to the short distance variation between both surveys, a mean value was chosen for separating the last south base profile from the first north base profile, therefore, the profiles in the red box had distance increment of 0.3m, while between the red box and the black box the increment is 1.1m, corresponding to the mean value chosen.

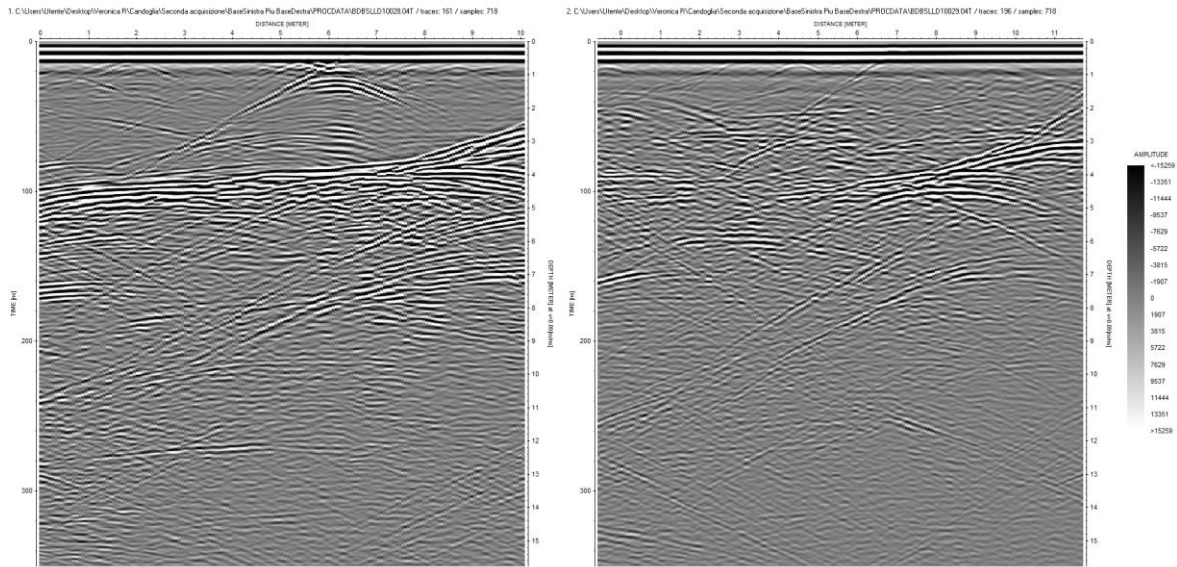


Figure 5.6. South base (on the left side) and north base (on the right side)

On the left side of the Figure 5.6 is shown the last profile of the south base (length about 10m), on the right side the first profile of the north base (length around 12m), both acquisitions are in the same file, each located correctly in the space allows realizing a future 3D interpretation in where both areas are included.



Figure 5.7. South and north base profiles

5.2.3 North base and west base

In this case, because the profiles were quite aligned, (see Figure 5.9) the union of the north base and the west base was carried out profile by profile, as a result, each profile is longer, corresponding to 12.70m of the north base plus 6.90 of the bottom base and some distance that was approximately 0.8m between the areas, for a total of around 20.5m (Figure 5.8). It also can be seen in the Figure 5.10 that the west base starts at a minor time than the north base, this is because between both there is a height difference of approximately 40cm, therefore there must be a difference in the initial time between them.

filename	dir.	con.	x-start	x-end	y-start	y-end	trace-inc.	numb.	time-inc.	starttime	shot pos.	S/R-dista	comment	comment
BA_DESLLD10001	Y	X	0	0	0.215	20.4468577	0.062831856	0	0.4882812	0	0	0		
BA_DESLLD10002	Y	X	0.3	0.3	0.215	20.5096895	0.062831856	0	0.4882812	0	0	0		
BA_DESLLD10003	Y	X	0.6	0.6	0.215	20.5096895	0.062831856	0	0.4882812	0	0	0		
BA_DESLLD10004	Y	X	0.9	0.9	0.215	20.5096895	0.062831856	0	0.4882812	0	0	0		
BA_DESLLD10005	Y	X	1.2	1.2	0.215	20.5096895	0.062831856	0	0.4882812	0	0	0		
BA_DESLLD10006	Y	X	1.5	1.5	0.215	20.5096895	0.062831856	0	0.4882812	0	0	0		
BA_DESLLD10007	Y	X	1.8	1.8	0.215	20.5096895	0.062831856	0	0.4882812	0	0	0		

Figure 5.8. North base and west base 200 MHz coordinate table

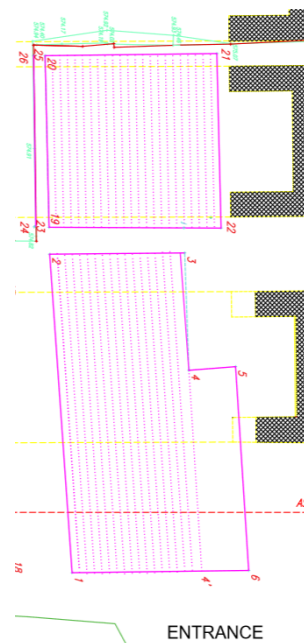


Figure 5.9. North base and west base profiles

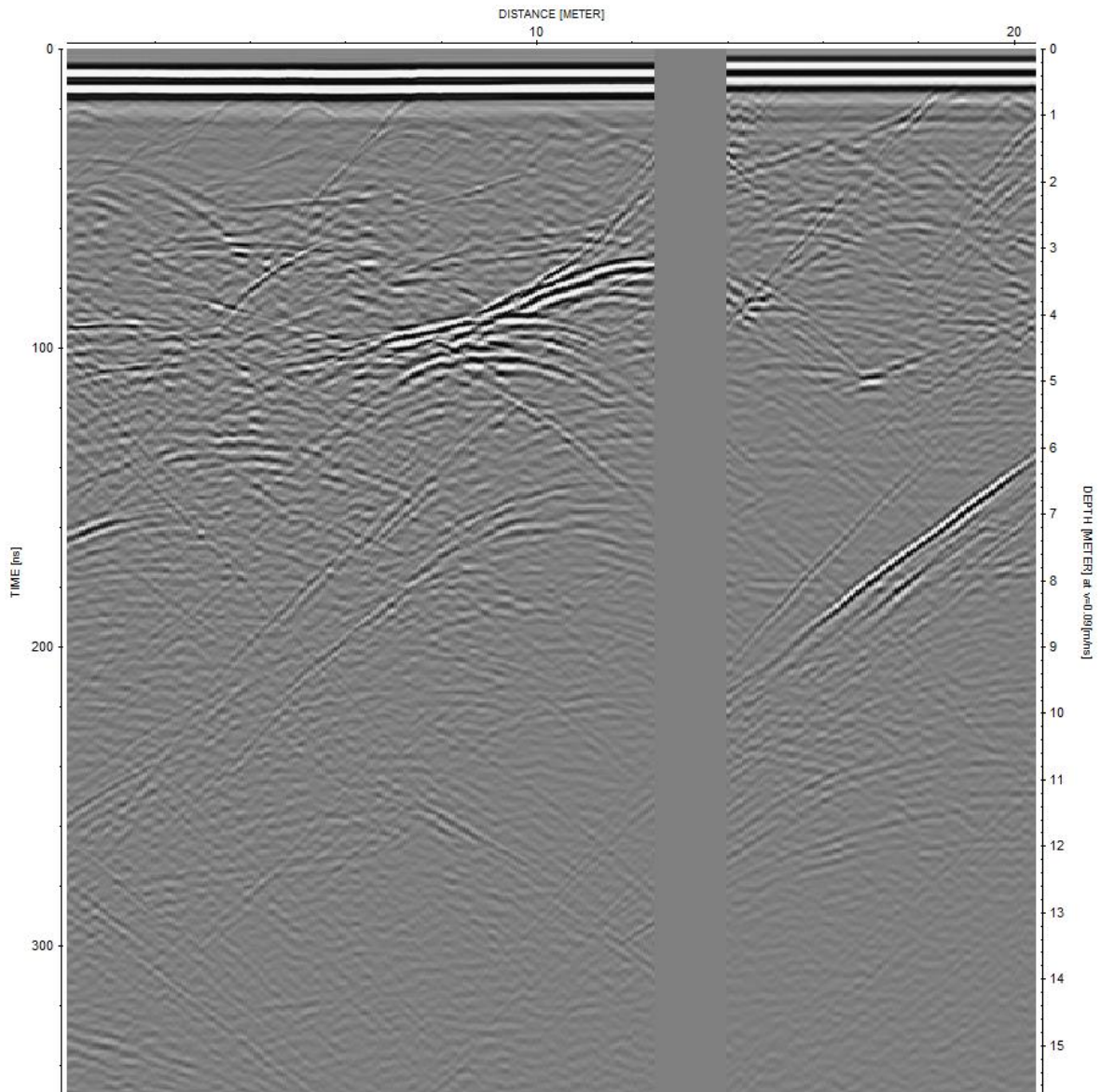


Figure 5.10. North base and west base radargram

To carry out a 3D representation later, the union of the north base, the south base and the west base were carried out in a single file, in this case, the profiles are seen equal to those reported in the Figure 5.6 and Figure 5.10, as well as the tables. Another file was also made, including the first acquisition made in the north base, for a total of 4 joined areas. In this case a last modification was made in the table corresponding to this first acquisition, to position the points appropriately Figure 5.11 and 5.12.

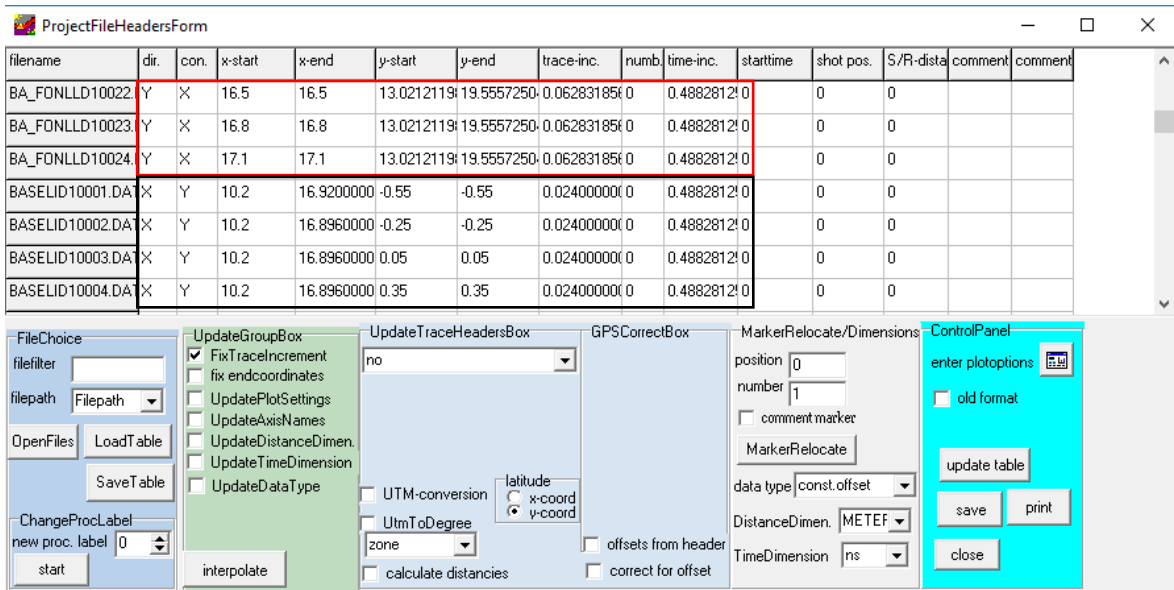


Figure 5.11. 4 bases merging coordinate table, part one (west base+ first north base)

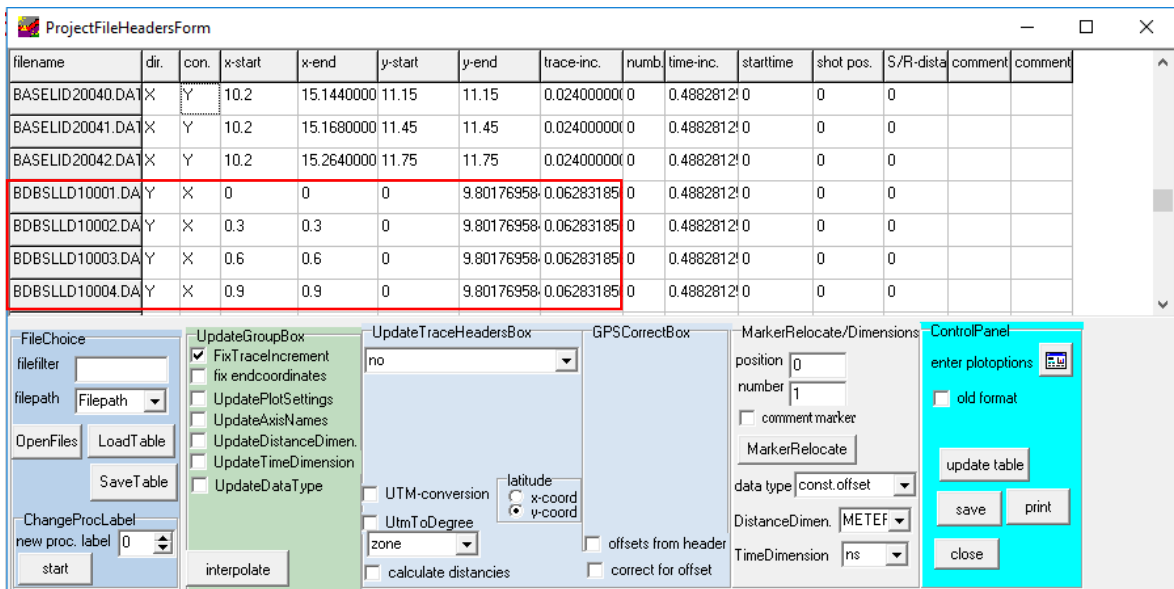


Figure 5.12. Four bases merging coordinate table, part two (north base+ south base)

In the following image (Figure 5.13) the succession of profiles that make up the 4 acquisitions are shown; the first acquisition is distinguished since it is the only one that has direction of the profiles towards the Y axis from the studio bertinotti reference system.



Figure 5.13. The 4 acquisitions made on the floor.

5.3 Processing on the signal using Reflex-Win

The processing implemented was quite similar in the various areas, in this section a profile of the south base is shown from the start to the final result. The processing begins with the raw radargram acquired in the field (Figure 5.14), which does not have any modification in the signal, and continues the following processing flow extracted from Reflexw:

```
Subtract mean(dewow) / 5 / 0 / 0 / 0 // 1 / 0 / 1 / 157  
move starttime / -20 / 0 / 0 / 0 // 1 / 0 / 1 / 157  
time cut / 350 / 0 / 0 / 0 // 1 / 0 / 1 / 157  
div. compensation / 1 / 0 / 0 / 0 // 0 / 0 / 1 / 104  
spectral whitening / 50 / 450 / 1 / 0 // 0 / 0 / 1 / 103  
bandpassbutterworth / 50 / 450 / 0 / 0 // 0 / 0 / 1 / 103
```

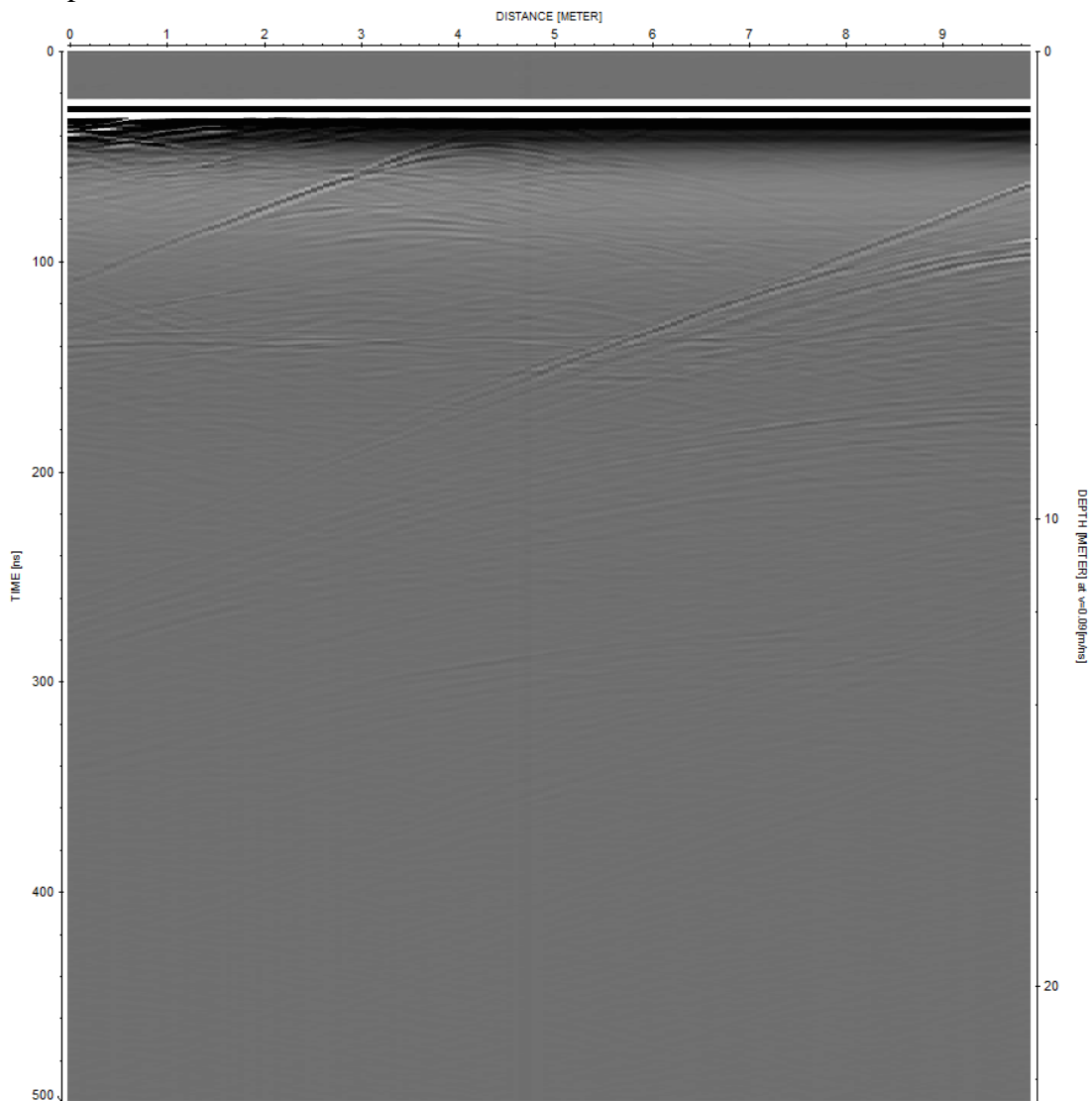


Figure 5.14. Raw radargram

5.3.1 Subtract mean Dewow

The GPS data is acquired with small distance between receiver and transmitter. The fields near the transmitter contain low-frequency energy associated with electrostatic and inductive fields, which decay rapidly with distance. This low-frequency energy often yields a slowly time-varying component to the measured field data. This energy causes the base level of the received signal to bow up or down. This effect is known as “wow” in the GPR lexicon. The “wow” signal can be eliminated applying a high-pass temporal filter, and this process is known as “Dewow” [5]. In the following figure, the original radargram (Figure 5.15) after the dewow procedure.

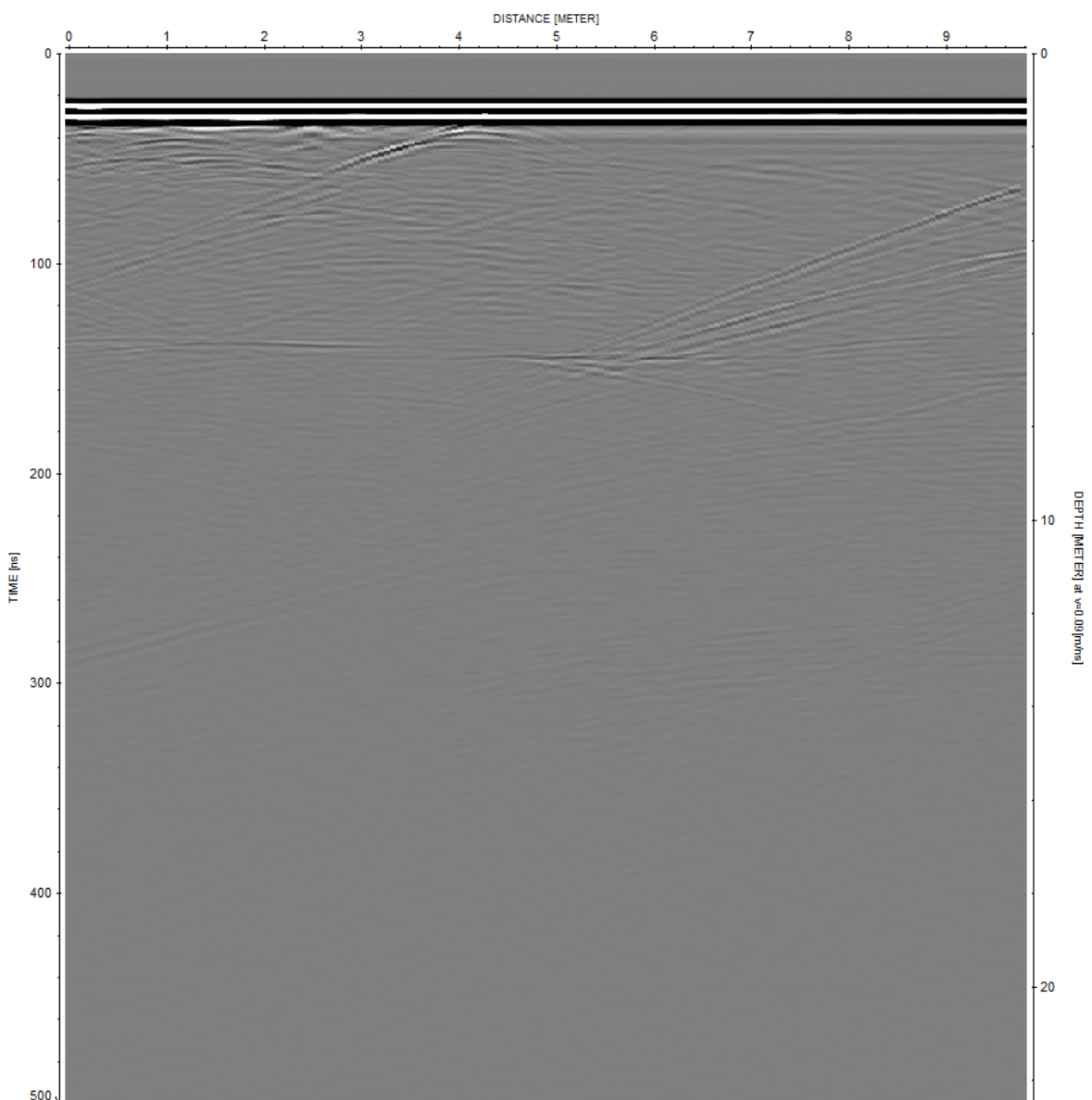


Figure 5.15. Radargram after dewow

5.3.2 Move start time

The move start time is a type of processing usually always used, it needs to be done before any interpretation because leads to errors in the estimation of depths. It consists of correcting the starting position of the time axis (the $t=0$). Radars use as time origin the first significative reflection that arrives to the receiver antenna, that correspond to the interface air-soil, so there is a first part of the radargram that actually is above the soil. After determining the zero-time, that is generally located before the beginning of the main bang, that represents those strong reflections air-ground, the traces are translated to the settled new origin time, in which the big amplitudes of the main bang begin at $t=0$ [19]. It can be seen in the Figure 5.16 the radargram after the procedure.

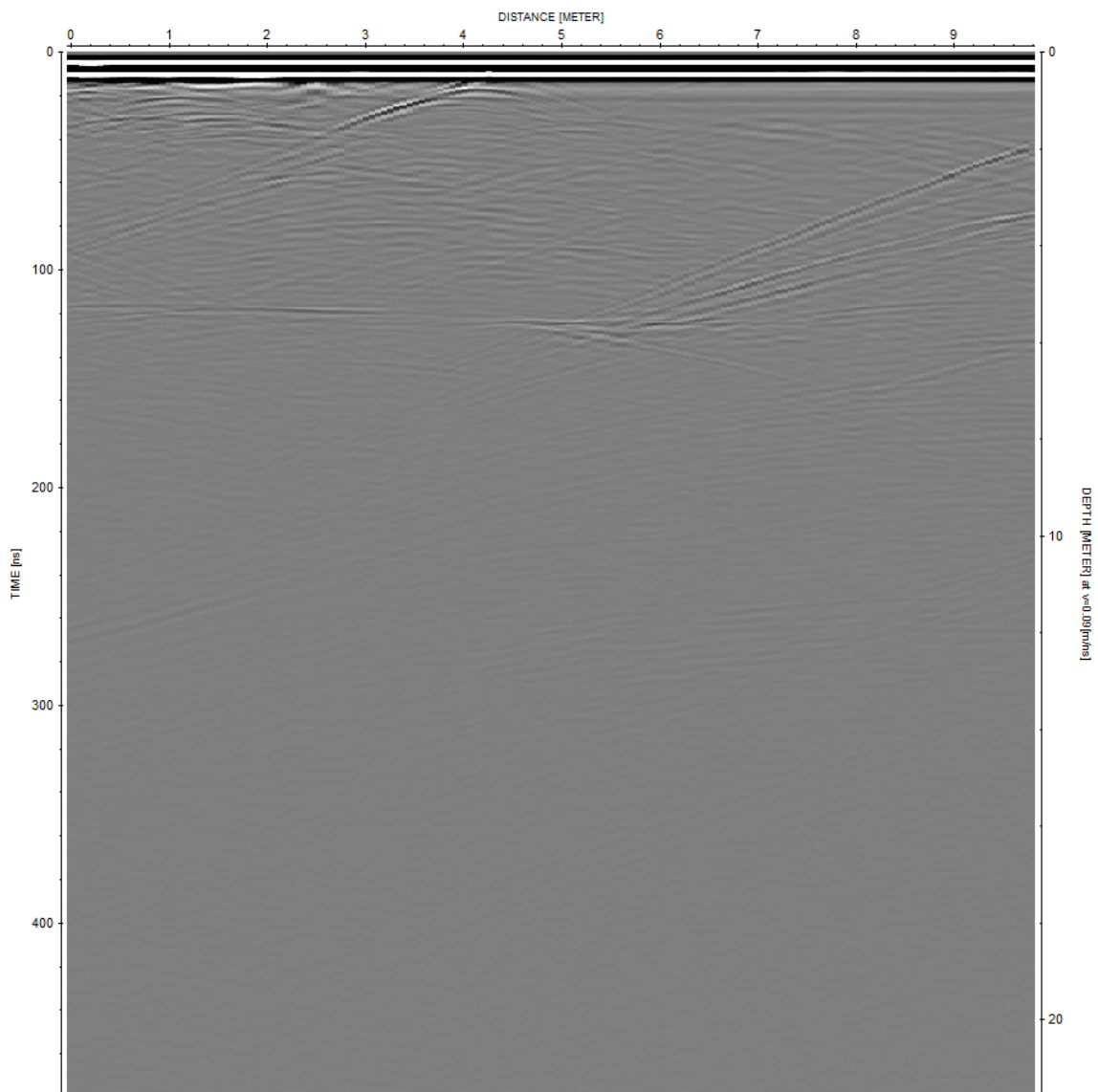


Figure 5.16. Radargram after moving start time

5.3.3 Time cutting

In this case, time cutting is a procedure that is not always necessary, but useful if we need to focus on certain depth, or if the radargram after certain time has no more useful information in it. It consists in physically cut the radargram, setting the maximum time wanted to be seen, and discarding all the information after that, as shown in Figure 5.17 [19].

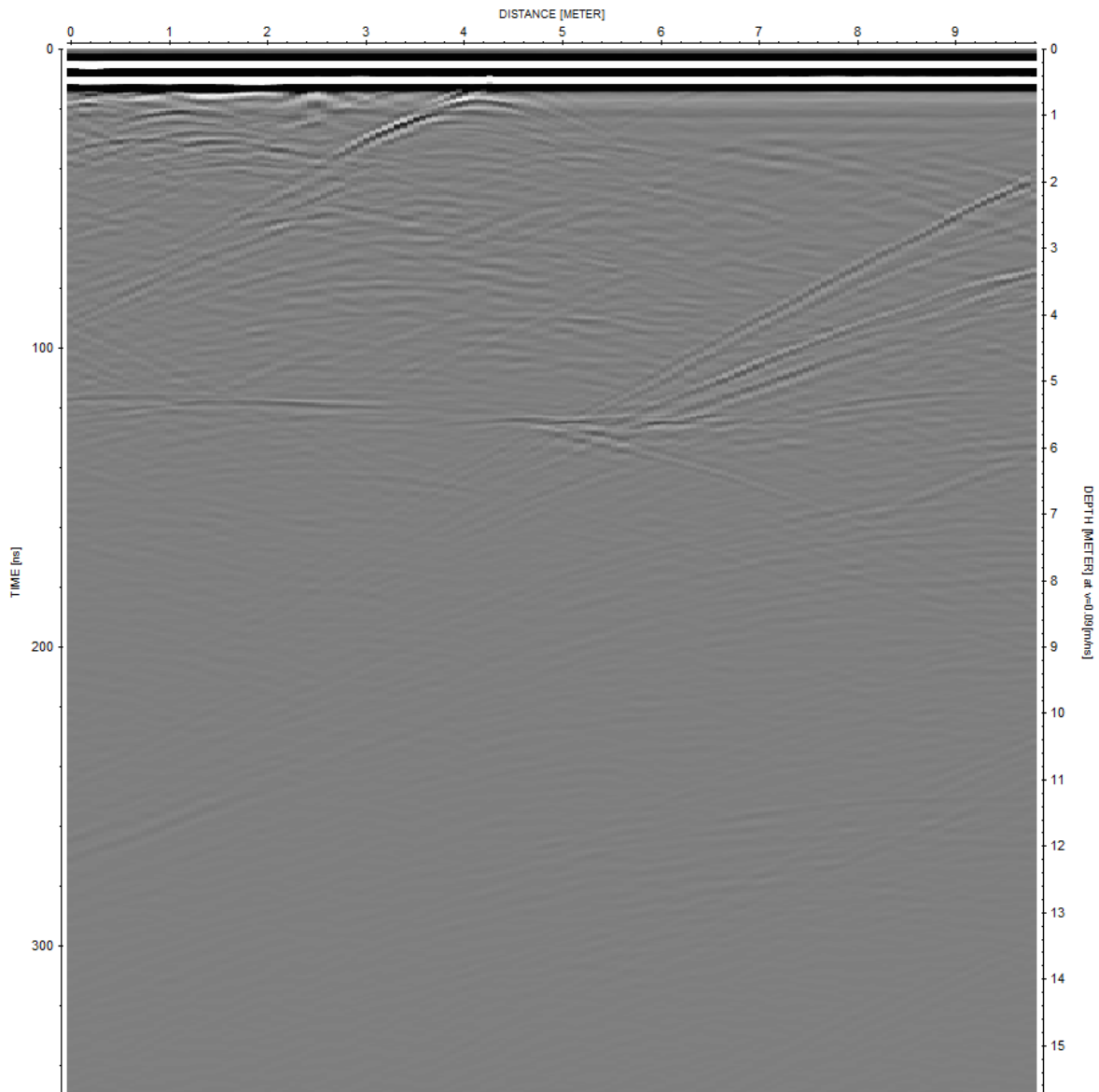


Figure 5.17. Radargram after time cutting

5.3.4 Divergence compensation

As it has already been explained in previous chapters, electromagnetic waves lose energy as they propagate through the medium, one of the causes of energy loss is geometrical spreading and depends only on geometric factors. This filter allows to compensate the energy lost by this phenomenon, acting on each trace independently. [19]

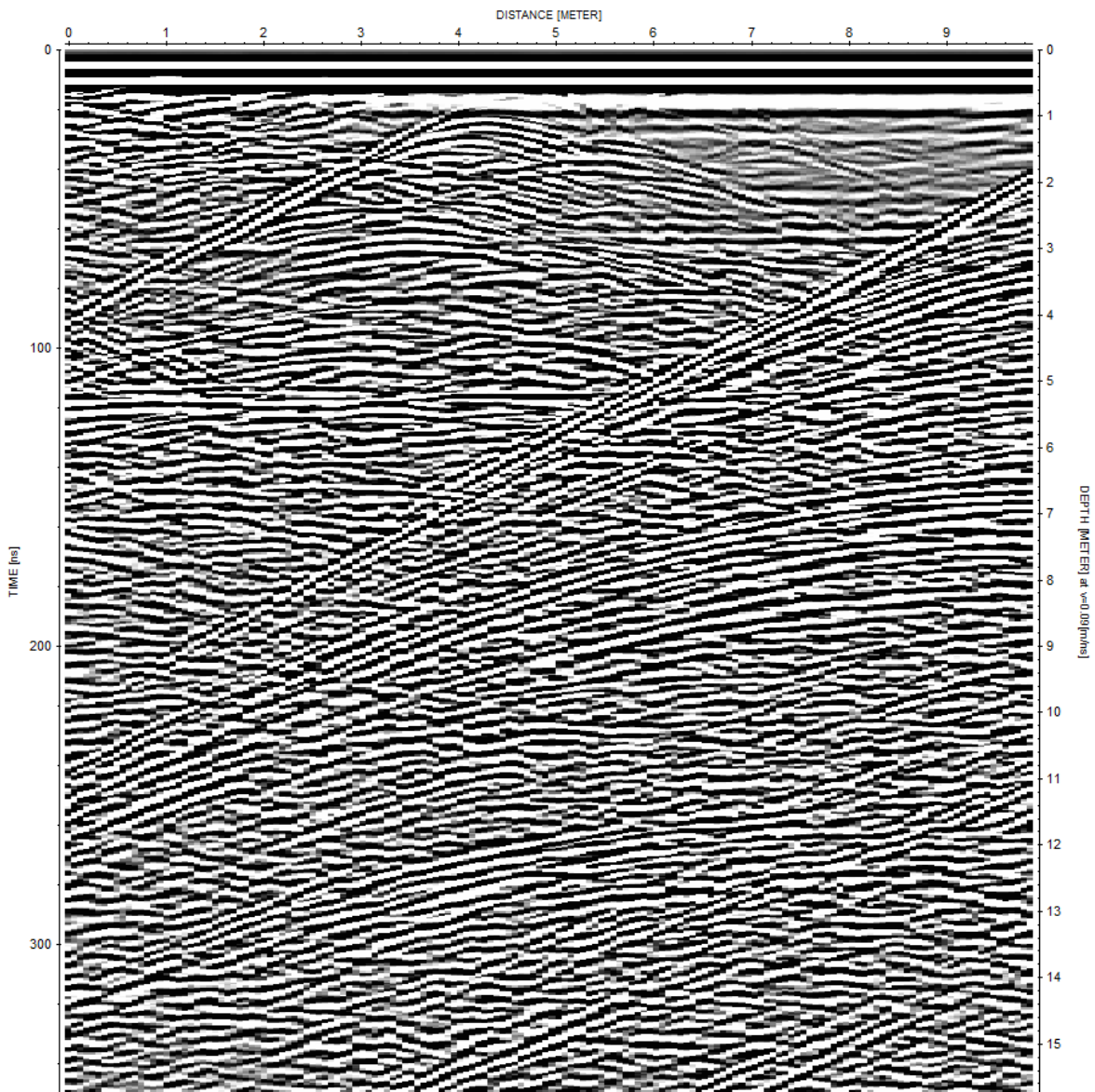


Figure 5.18. Radargram with divergence recovery

Clearly, in the image on the right the energy recovery makes the identification of the relevant information a bit more difficult, so within the visualization mode, Reflex W has two options to adapt the visualization: the `tracenormalize` option (Figure 5.19), in where the data is plotted with amplitude normalized for each trace, the maximum amplitude of

each visible trace is normalized to 1. And the second is manually adjust the plotscale, which changes proportionally the amplitudes of each trace (Figure 5.20). Both options plotoptions are only a graphical and does not affect the filtering/stacking process

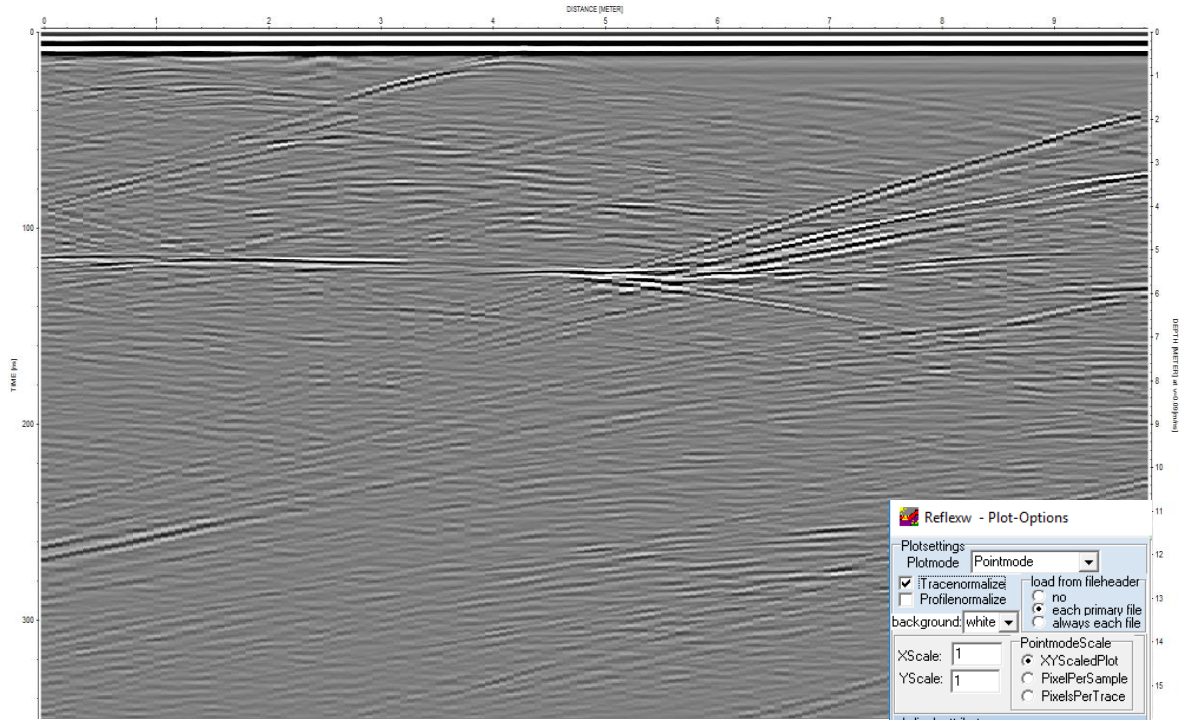


Figure 5.19. Radargram with divergence recovery and trace normalization

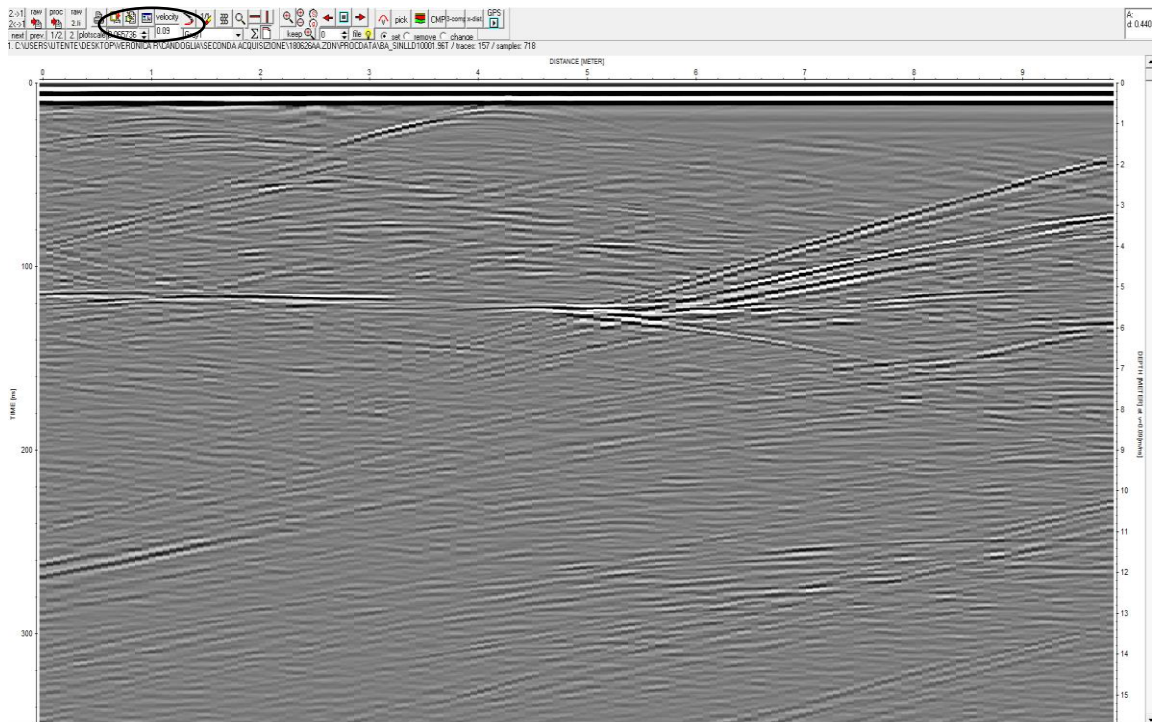


Figure 5.20. Radargram with divergence recovery and plotscale modification

5.3.5 Gain function

A second alternative to recover energy in depth is through a procedure called Manual Gain (y). The filter acts on each trace independently and facilitates the possibility of multiplying the data points by a given function $g(y)$ or $g(t)$ respectively [19]. The user constructs its own function allowing to specify the parts in which more or less energy will be recovered. In general, the function must have a logical sense, starting from low values close to the surface, gradually increasing and then decreasing again, because high depth information is not very reliable, and will probably add rumor to the signal.

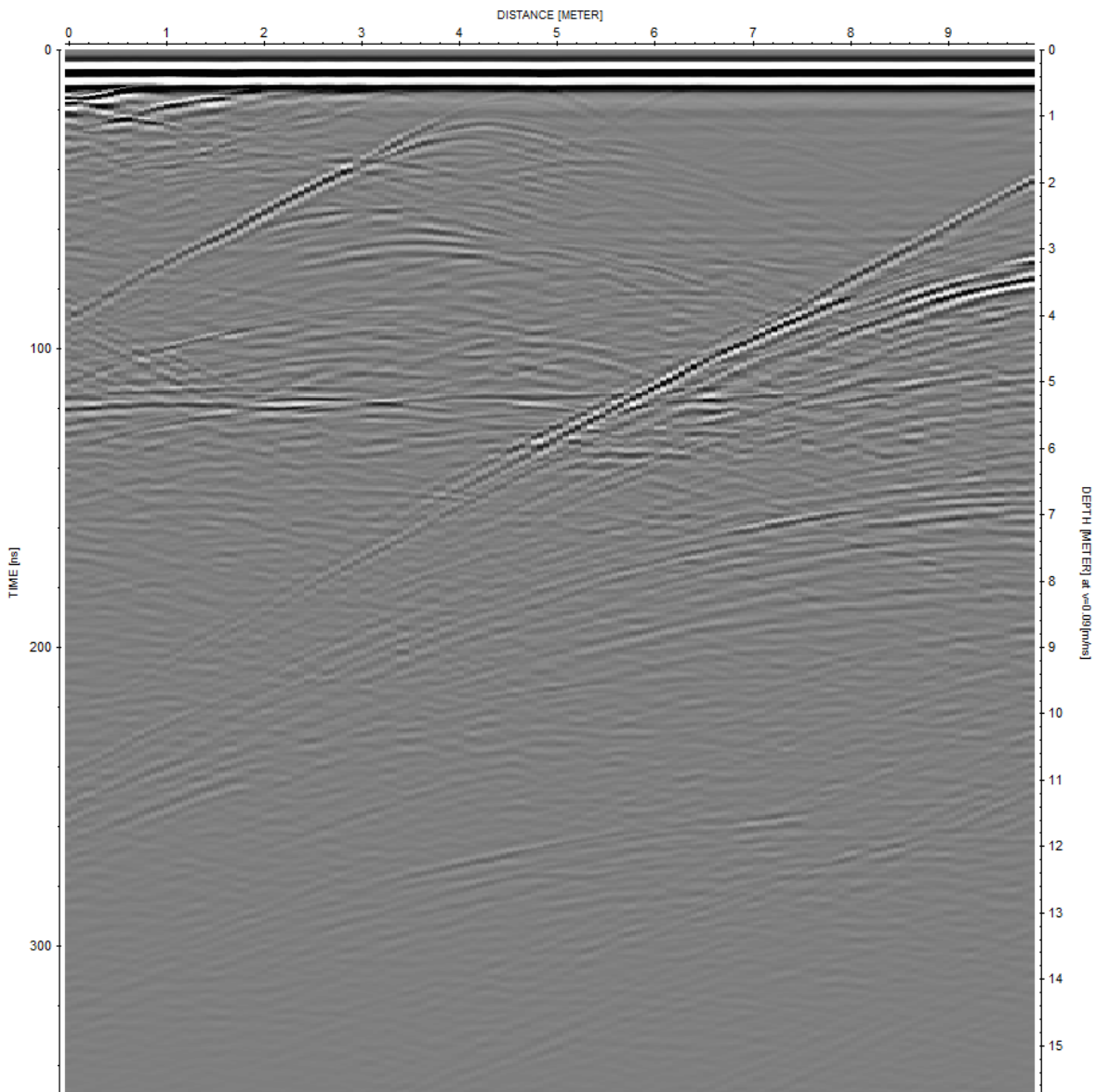


Figure 5.21. Radargram with Manual Gain (y)

5.3.6 Spectral Whitening

The objective of this filter is to flatten the spectrum within a certain frequency band, as input parameters select the input frequency and the output frequency. The filter works by applying a series of narrow overlapping band-pass filters on each trace. The same series of amplitude decay curves is then computed to describe the decay rates for each frequency band. The inverses of these decay curves are applied to each bandpass filtered trace and the results are summed. In order to preserve the amplitude characteristics of the original trace the summed trace is then multiplied with the amplitude decay curve of the original trace. The filter changes the overall amplitudes. The spectral whitening allows to compensate for frequency attenuation with time. [19]

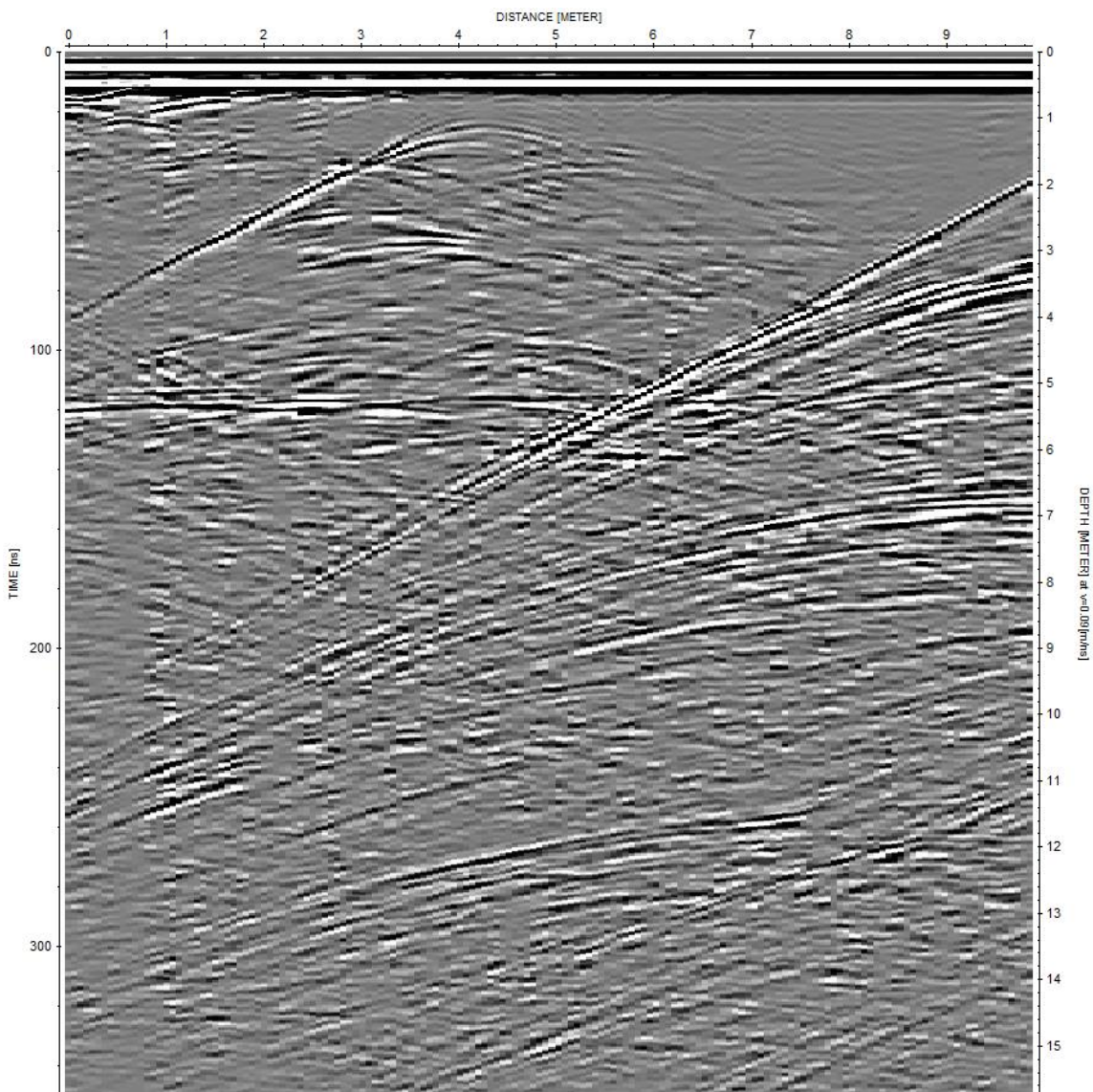


Figure 5.22. Radargram with spectral whitening

5.3.7 Band-Pass Butterworth

The filter band is specified by setting two frequency values. The first point determines the low-cut frequency, the second one the high cut frequency. The frequency spectrum below the low cut and above the high cut frequency is attenuated. By the corresponding choice of the points of the bandpass either a low-pass or a high-pass can be approximately realized. Noise can be suppressed with the bandpass filter when it differs from the signal in its frequency content. [19]

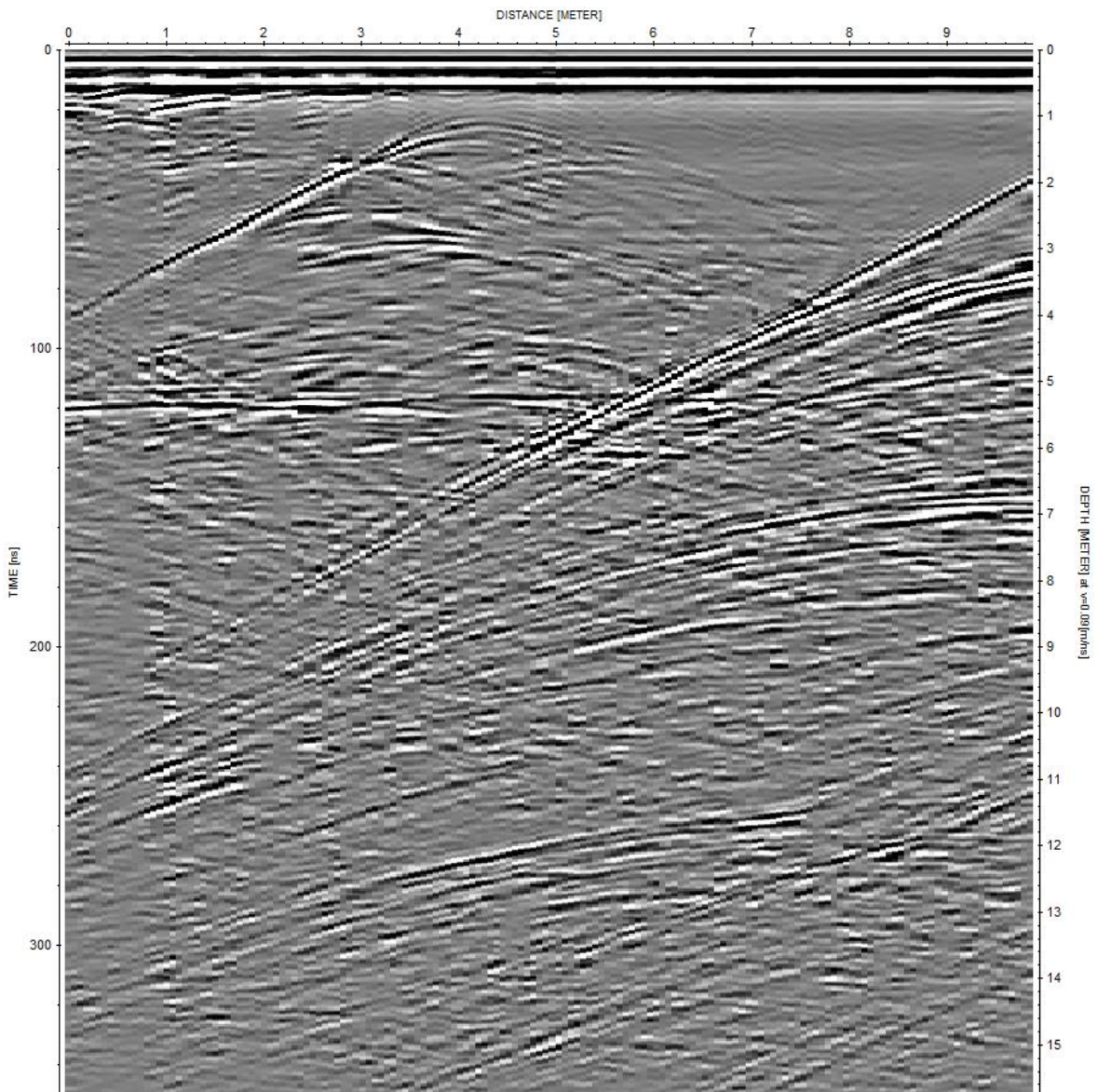


Figure 5.23. Radargram with bandpass butterworth

5.4 3D Assembling

To finalize the processing, a 3D assembly was made to have a better visualization of the acquired data. The module 3D data-interpretation of Reflex allows the interpretation of 3-dimensional data by displaying x-, y- or z-slices or the full 3D-data volume.

Having all the processed files, the procedure to import the data consist in specifying certain parameters and choose the already well-located surveys, (Figure 5.24) [19].

The screenshot shows the 'Generate 3D-file from 2D-lines' dialog box. The '3D filename' is '3D model'. The 'type of interpolation' is 'use interpolation scheme for freely distributed 2D-lines'. The 'add x-y-scans by choosing the max. abs. value' checkbox is unchecked. The 'apply mean filter in time direction' checkbox is checked, with a value of 1. The '3D coordinates' section includes: XStart: 0, XEnd: 17.1, YStart: -0.55, YEnd: 19.61855689, XRasterincrement: 0.1, YRasterincrement: 0.1, XInterpolation: 0.7, YInterpolation: 0.7, interpol.weight: linear weight, and data scaling: 1. The 'timerange/sorting' section includes: time end: 350, timeincrement scale: 1, and sorting: fileheader coordinates. The '2D-files choice' section includes: filepath: procdata, filefilter: *.07t, a 'load 2D-files' button, a list of files (BA_FONLLD10001, BA_FONLLD10002, BA_FONLLD10003), and min/max.xy coord. (BA_FONLLD10003). The 'update traceheader coordinates' checkbox is checked. 'Start' and 'Cancel' buttons are at the bottom.

Figure 5.24. 3D data import table

Within the import parameters, the X and Y start and end coordinates are updated automatically when the 2D files are selected, the “time end” must be the same for all the files, otherwise some of them will be cutted. Finally, the X-Y Rasterincrement and X-Y interpolation parameters, need to be selected depending on the parameters of the survey.

XRasterincrement and YRasterincrement specify the grid interval of the two coordinate axes spanning the plane in the given distance dimension. A useful value for both is the traceincrement used for the individual 2D-profiles. [19]

XInterpolation and YInterpolation: define the interpolation area (a rectangle) in the given distance dimension. To guarantee a complete filling of the 3D-data cube the interpolation range in x- and y-direction has to comply with the greatest occurring distance between two data points in the corresponding direction whereby a too large range leads to an averaging. [19]

Subsequently, visualization mode can be chosen between absolute values, envelope, envelope timeslices only or none of the above. As a result, a 3D interpolated cube (Figure 5.25) is generated.

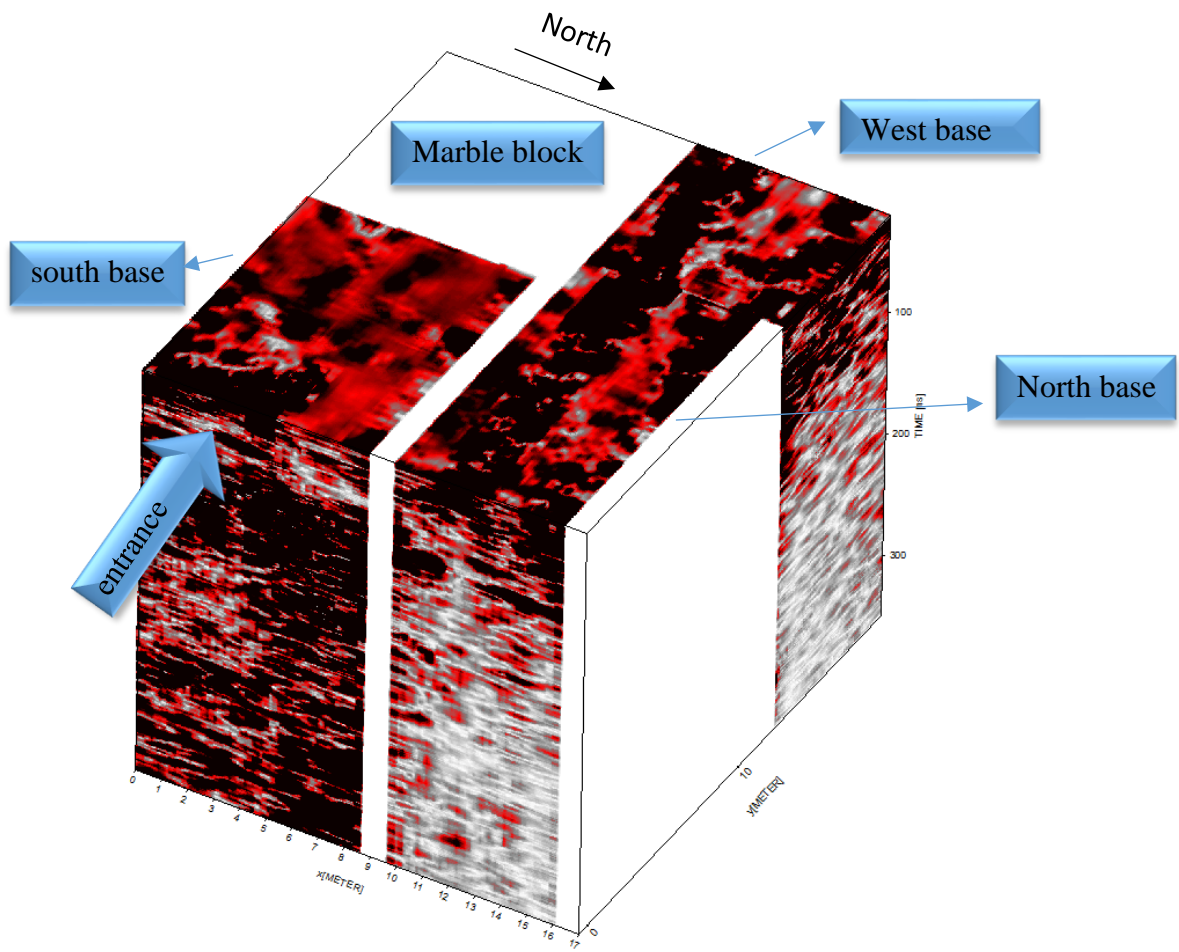


Figure 5.25. 3D Cube result

In white, the areas on which no profiles are present, due to the small space between the north base and the west base, the program makes an interpolation, for this reason it looks like the two areas are continuous.

Chapter 6 Test on Matlab: Mixing of GPR data acquired with different frequencies

MATLAB is a mathematical software that offers an integrated development environment with its own programming language (M language). In engineering area and many others, it represents a very useful tool for data analysis. In the case of geophysics, Matlab is known because it allows to develop custom data processing.

The objective of this chapter is to describe the procedure followed by a code programmed in Matlab, carried out in order to achieve a complementation between the information given by two signals, specifically, the data of two acquisitions where we had data areas along the same profiles, acquired with two different frequencies. The processing flow of the code, which will be later described one by one, is summarized in the Figure 6.1. The entire code is available in annexes.

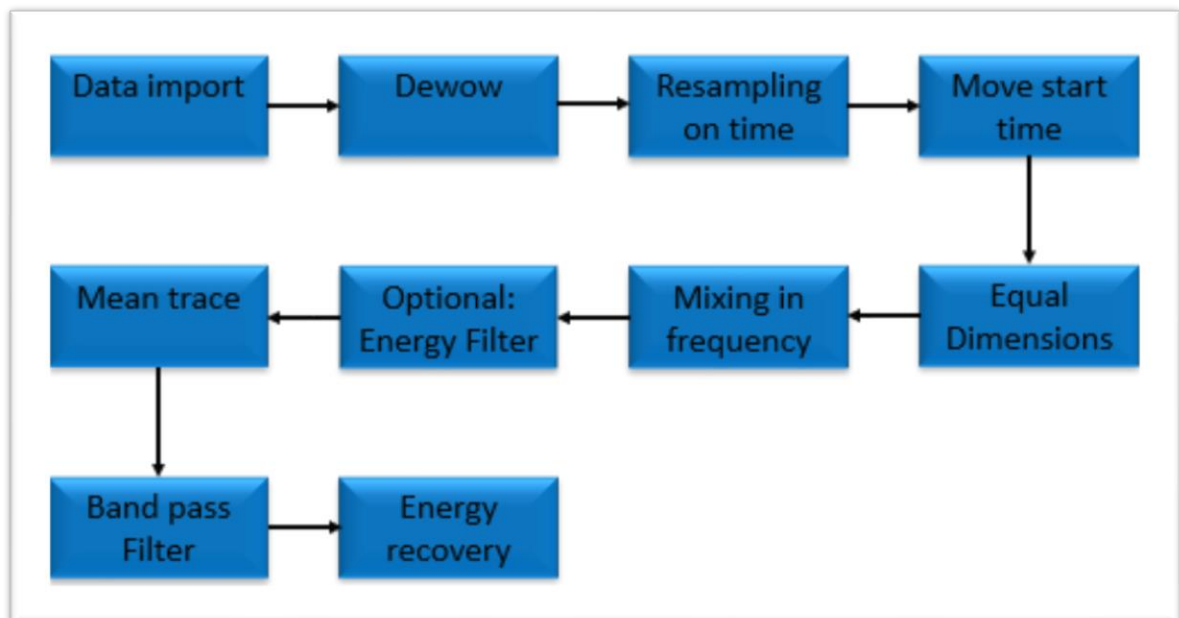


Figure 6.1. Processing flow of the matlab program

6.1 Data import

The radar data is imported into the program in the form of a matrix, where each column represents a trace, and each row represents the value of the amplitude at a certain time.

The program initially requests the input of two radargrams, one of high frequency and one of low frequency, which must belong spatially to the same line. In the following figures the radargrams imported and the parameters for each one

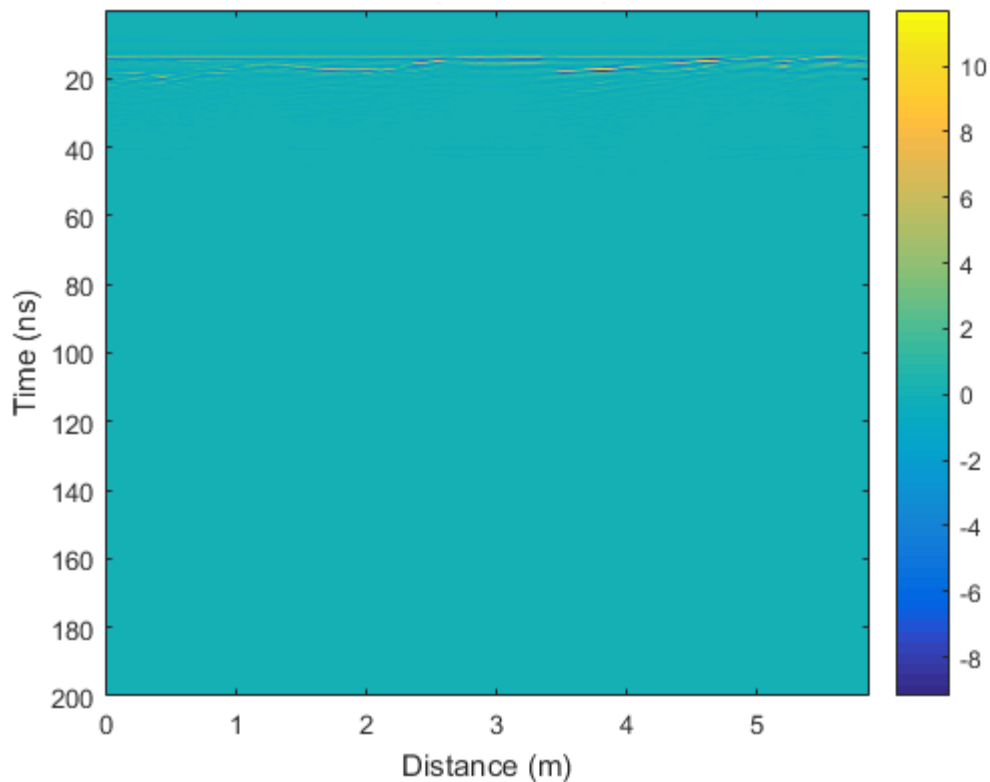


Figure 6.2. High frequency radargram

Name ▲	Value
HAntF	900000000
HAtov	3.0518e-04
Hdt	9.7656e-11
Hdx	0.0240
HNosa	2048
HNotr	245
Hraw	2048x245 double
HStruvar	1x1 struct
Ht	1x2048 double
Hx	1x245 double

Figure 6.3. Parameters imported for the High frequency antenna

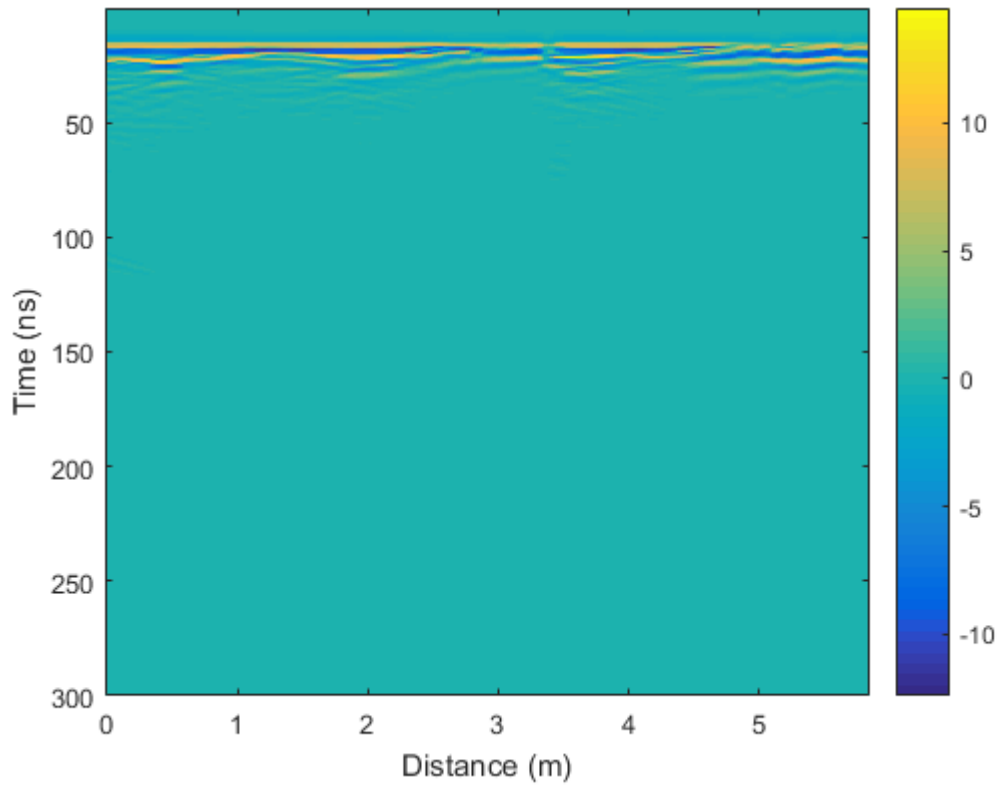


Figure 6.4. Low frequency radargram

Name ▲	Value
LAntF	200000000
LAtov	3.0518e-04
Ldt	2.9297e-10
Ldx	0.0240
LNosa	1024
LNotr	244
Lraw	1024x244 double
Lstruvar	1x1 struct
Lt	1x1024 double
Lx	1x244 double

Figure 6.5. Parameters imported for the low frequency antenna

6.2 Dewow

This filter may be used for eliminating a possible low frequency part, as explained in section 5.3.1 for this, the program applies a high pass filter that is given by the complement of a low pass filter.

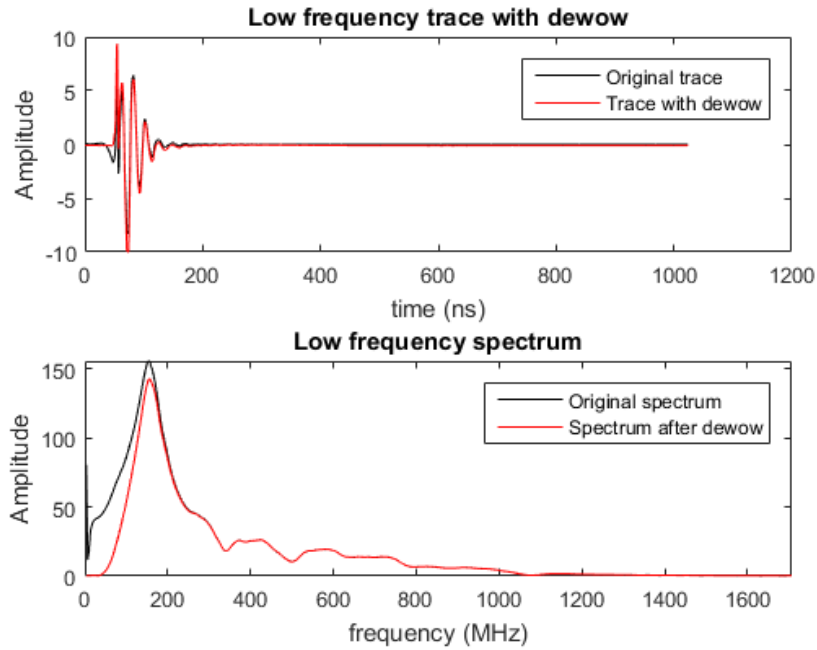


Figure 6.6. Dewow effect in one trace of the low frequency radargram

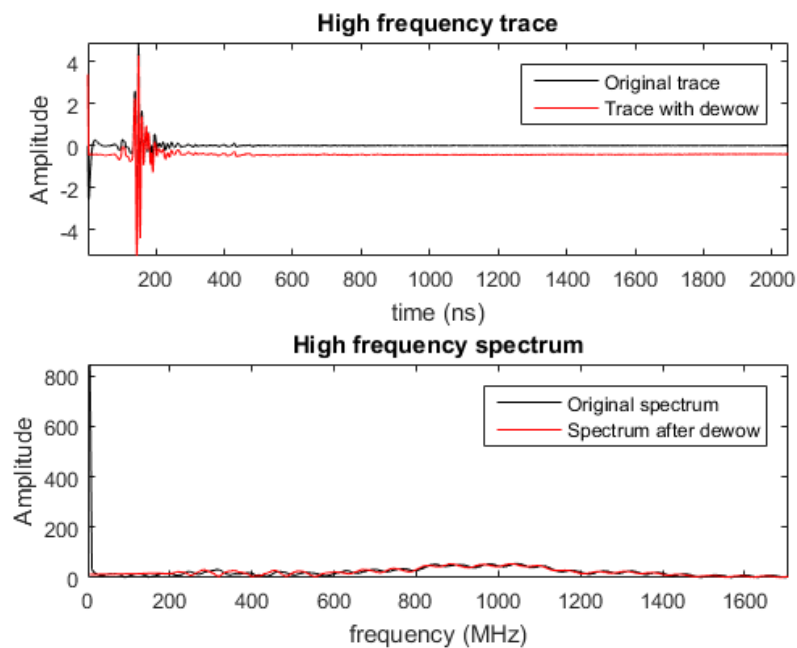


Figure 6.7. Dewow effect in one trace of the high frequency radargram

6.3 Resampling on time

Generally, GPR data acquired with high frequency antennas have a higher sampling frequency than lower frequency ones, this is due to the fact that with high frequency antennas more detailed information can be obtained, but at a lower depth, since the wavelength is minor. Therefore, the two matrices imported into Matlab have different sampling interval.

The resampling consists on increasing the sampling frequency of one of the two radargram matrices, with the aim of obtaining the same delta t in both. The procedure used is to identify the data matrix that was acquired with the largest delta t, as well as the relationship between the smallest and largest deltas, then the “resample” command allows increasing the number of samples in each trace, increasing the number of sampling points on the signal, in a fairly precise way. The Figure 6.8 shows the original trace in contrast to the resampled one. It can be seen that the black x’s fit well the original signal.

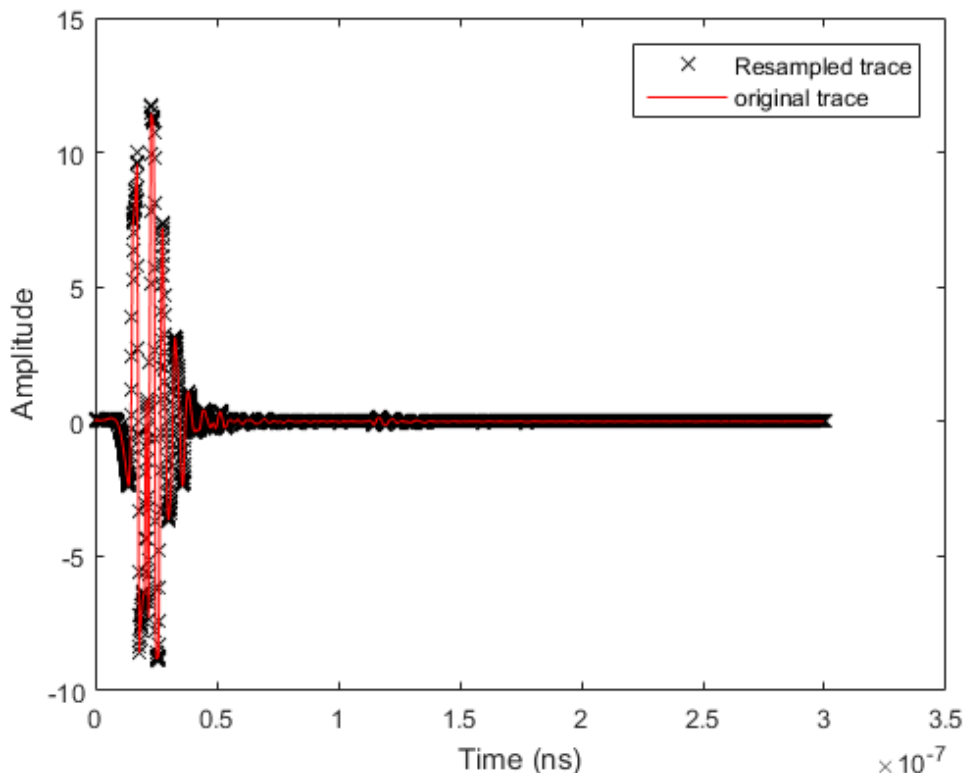


Figure 6.8. Adjustment of the resampled trace

6.4 Remove initial delay

This procedure is equivalent to the one mentioned in section 5.3.2 For a better identification of the arrival time of the first wave corresponding to the previously described "main bang", the average trace was calculated, through the application of a mean in horizontal direction. Next, the "ginput" command allows the user to select the desired point in the image. In the Figure 6.9 and 6.10 can be appreciated the radargram before and after the removing of the initial delay.

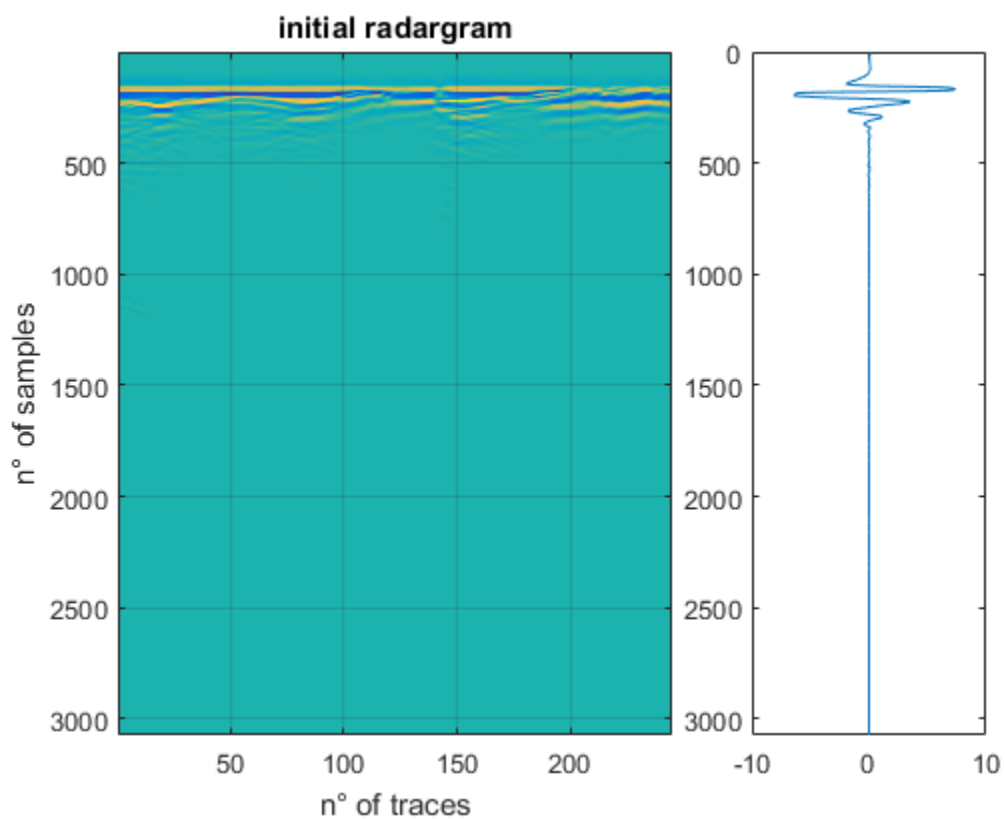


Figure 6.9. Tool for the selection of the time for the removing of the initial delay

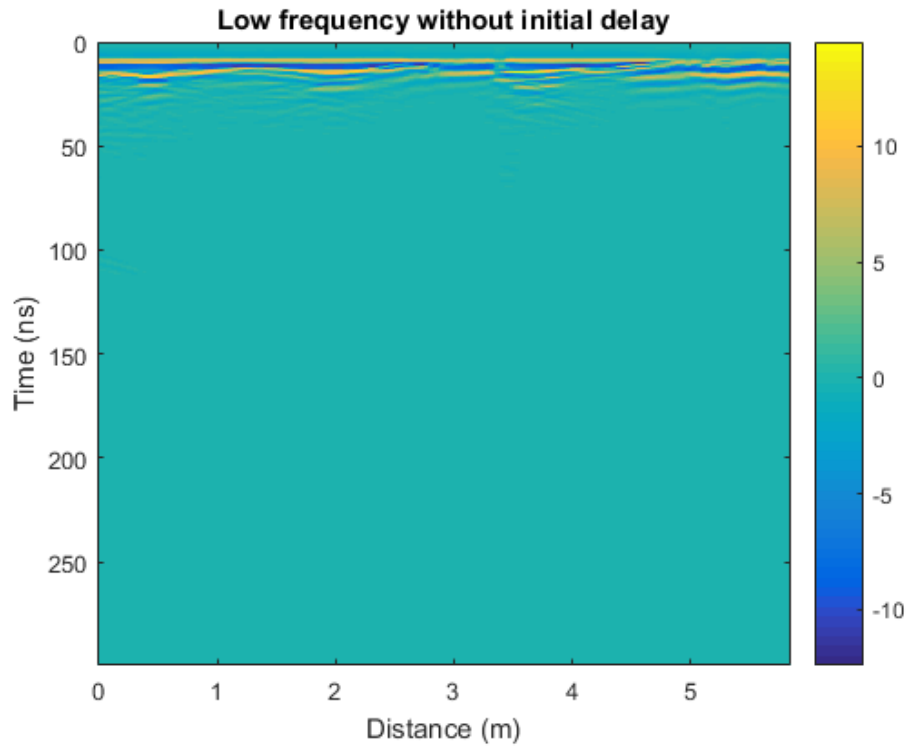


Figure 6.10. Result after removing of the initial delay

6.5 Equal dimensions

Having both radargrams the same Δt , the equal dimension process consists basically in cutting the larger one to make it of the same size of the smallest one- This procedure is necessary to later perform the mixing of the signals, the code makes a verification on the vertical axis (time), comparing both sizes, and eliminating the time difference between one and the other. On the horizontal axis (traces) compare the amount of traces between them and eliminate the excess. In the following images (Figure 6.11 and 6.12) can be seen that both frequency radargrams have the same end time and the same distance in the X direction

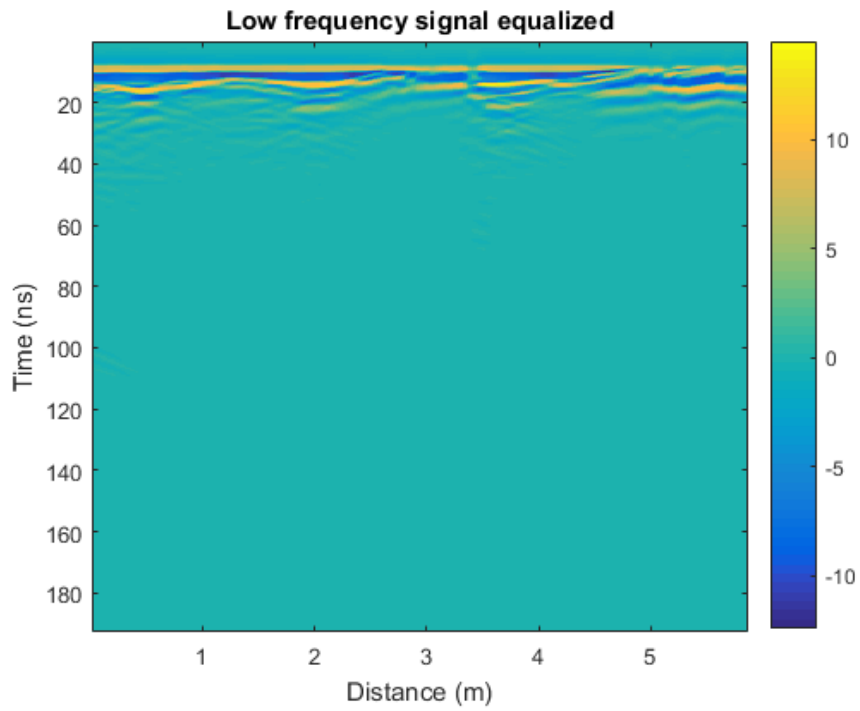


Figure 6.11. Low frequency signal with equal dimensions

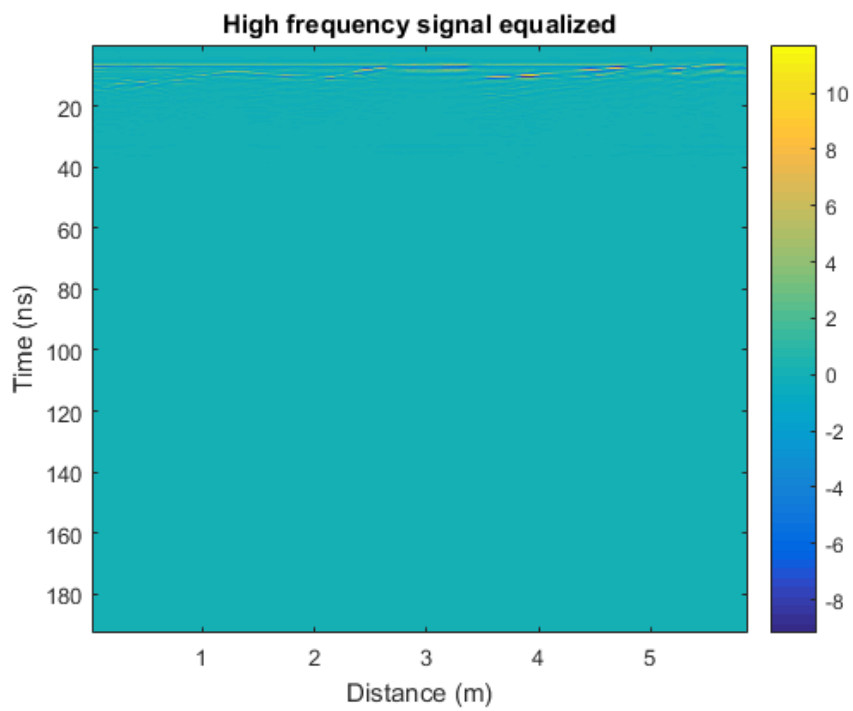


Figure 6.12. High frequency signal with equal dimensions

6.6 Mixing in frequency

The procedure of mixing in frequency, consists of applying the Fourier transform to each signal, to later perform the sum in frequency domain. The Figure 6.13 contains already the information of both antennas, some different details can be seen in contrast to the 200MHz original radargram.

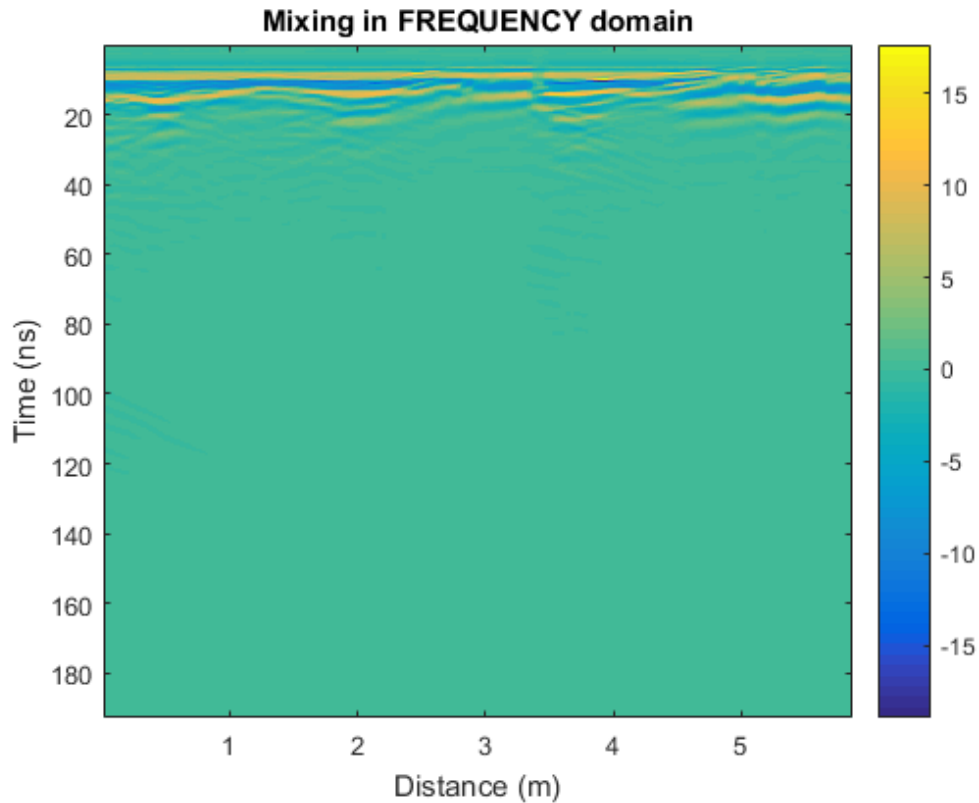


Figure 6.13. Mixed in frequency radargram

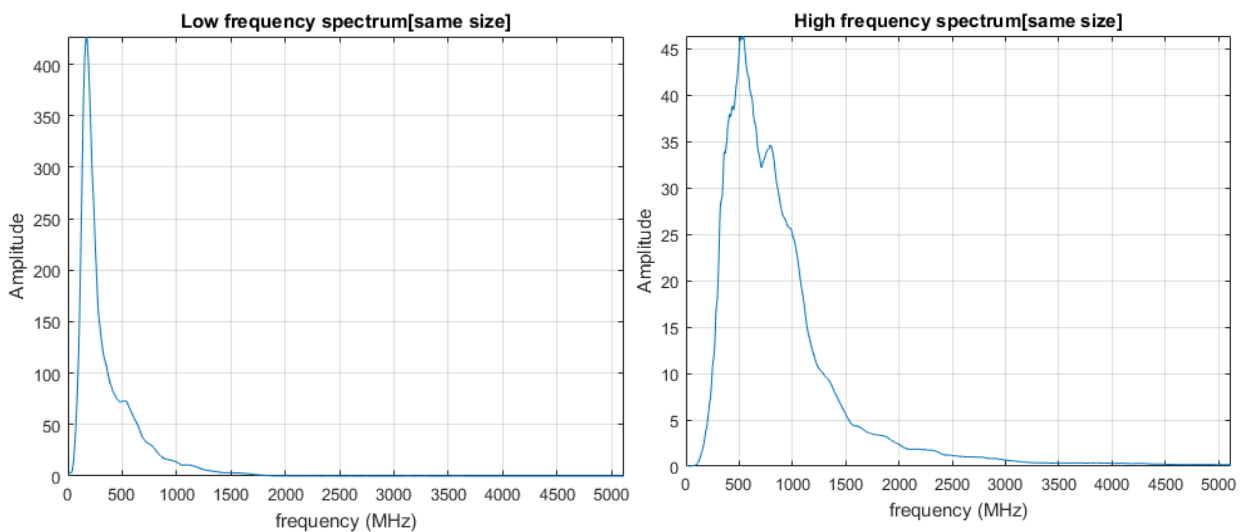


Figure 6.14. At the left, the low frequency amplitude spectrum, at the right, the high frequency amplitude spectrum

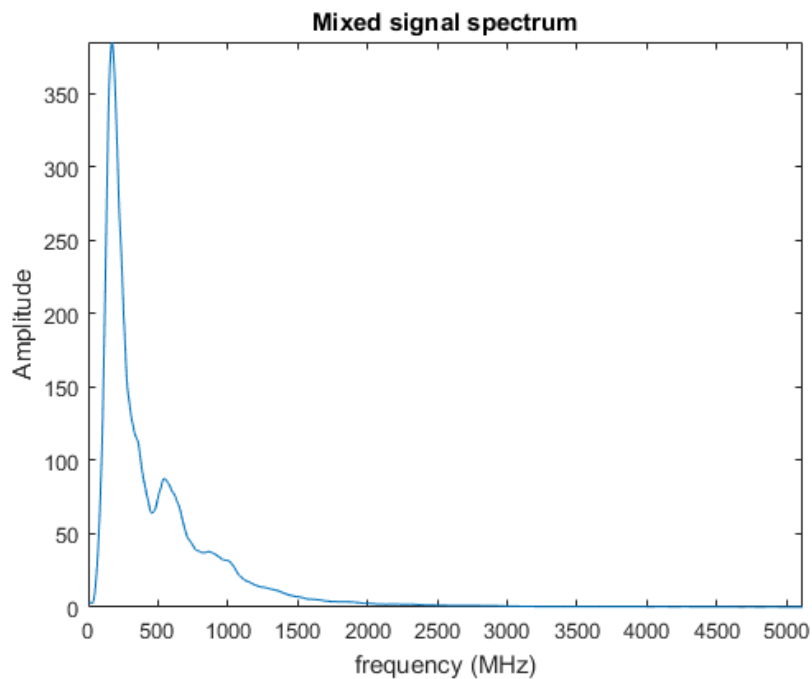


Figure 6.15. Amplitude spectrum of the mixed signal

6.7 Energy filter

The energy filter is applied in the spectrum of amplitudes; the greater the amplitude, the more energy the signal contains. The code calculates the spectrum of amplitudes of the signal already mixed and then is represented in a histogram (Figure 6.17), by applying zoom, the cutting of low or high energy can be made, the program search in the matrix the values that are lower than the low cut or higher than the high cut and eliminates them. The result is represented as a 2D spectrum. in Figure 6.18, it can be appreciated the difference between the initial spectrum which contains all the data and the filtered spectrum, from which part of the low energy (in blu, in the corners) and some of the high energy (in yellow, in the center) has been filtered.

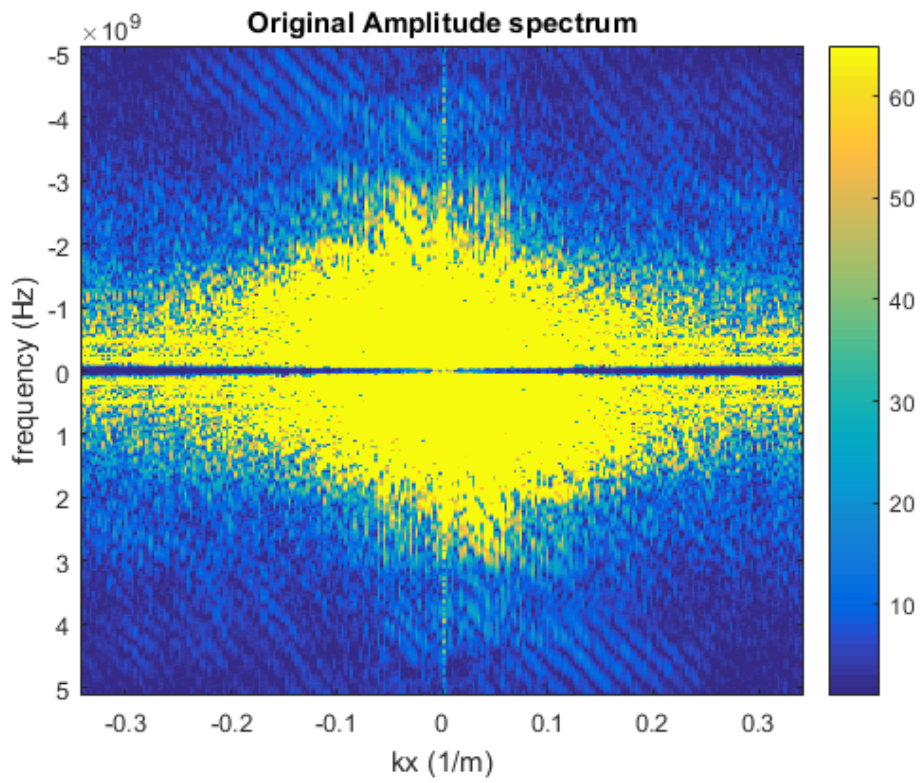


Figure 6.16. 2D Amplitude spectrum before filter

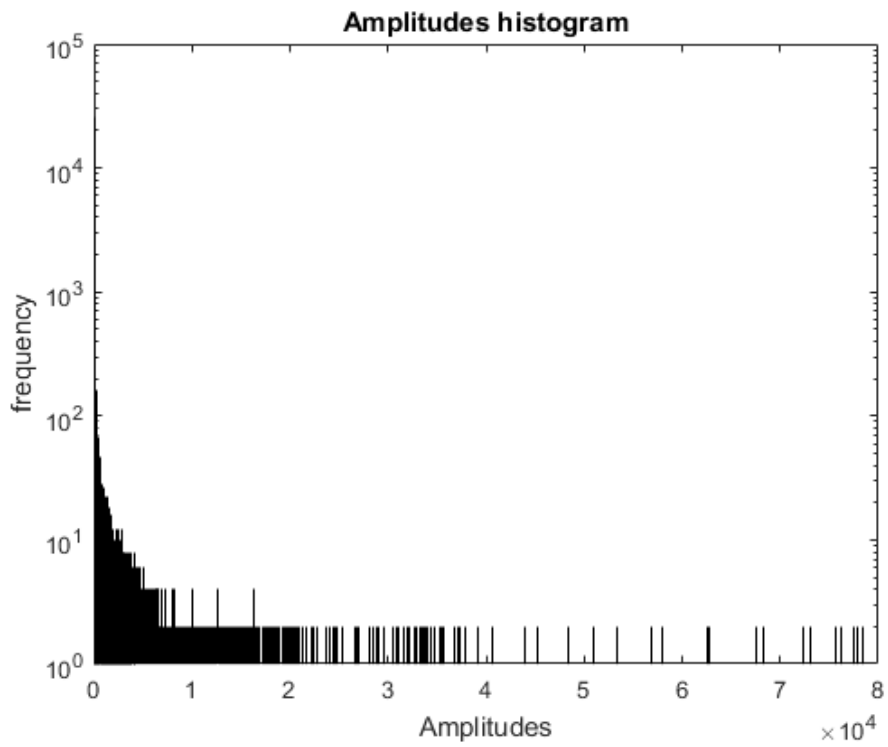


Figure 6.17. Amplitude histogram

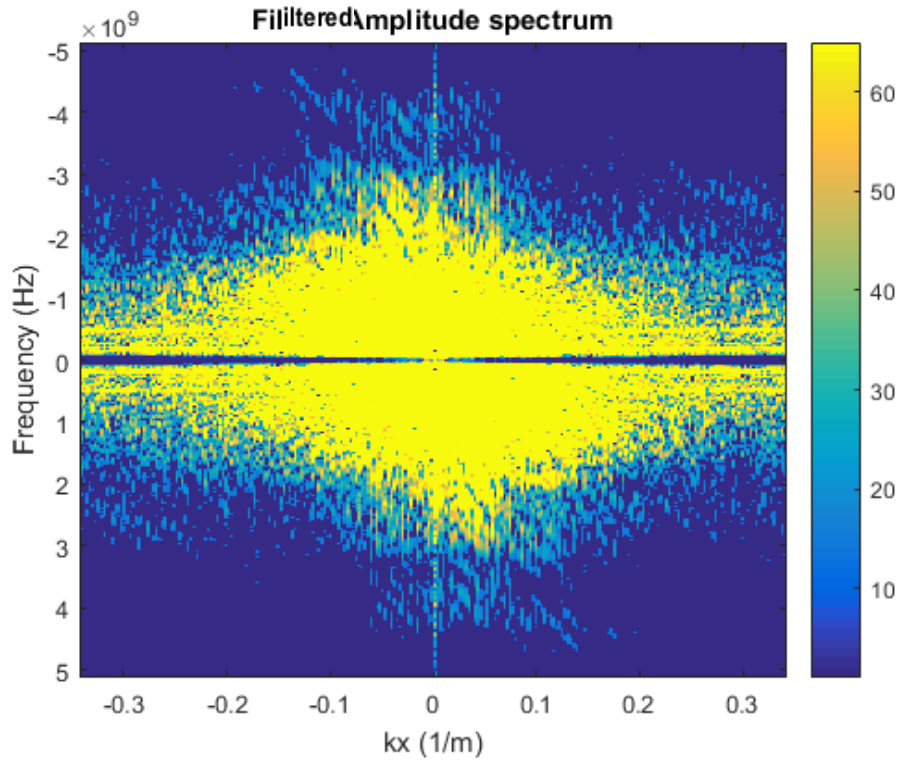


Figure 6.18. 2D amplitude spectrum after the filter

6.8 Mean trace

This simple procedure consists of calculating the mean trace of a radargram matrix, through the function “repmat” the program constructs a matrix with the same quantity of traces than the entrant radargram, and then subtract the mean matrix to the original. In the Figure 6.19 the trace before and after this step.

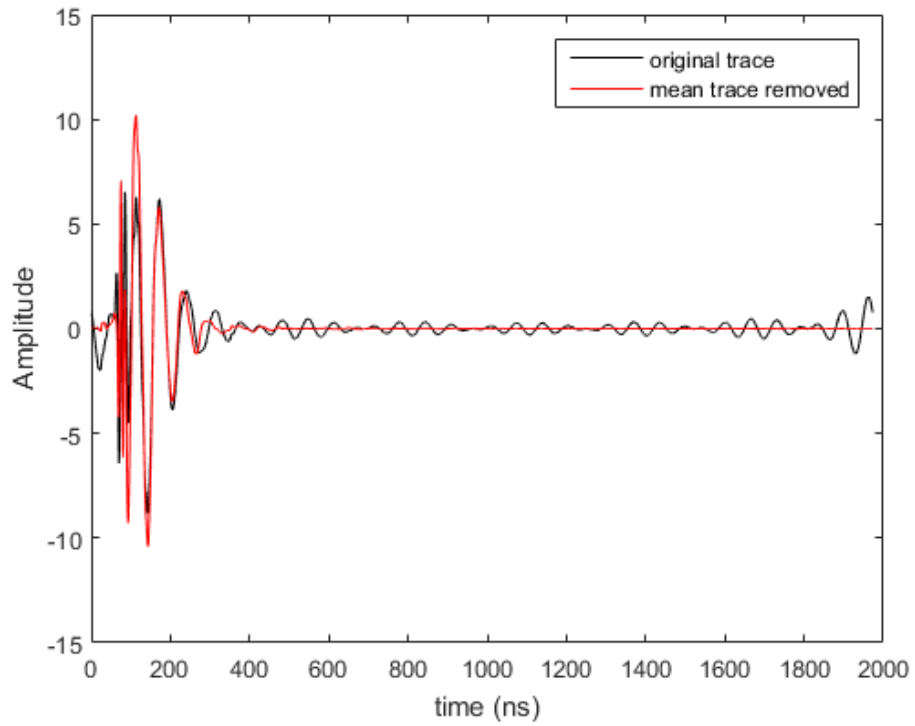


Figure 6.19. Trace with mean removed

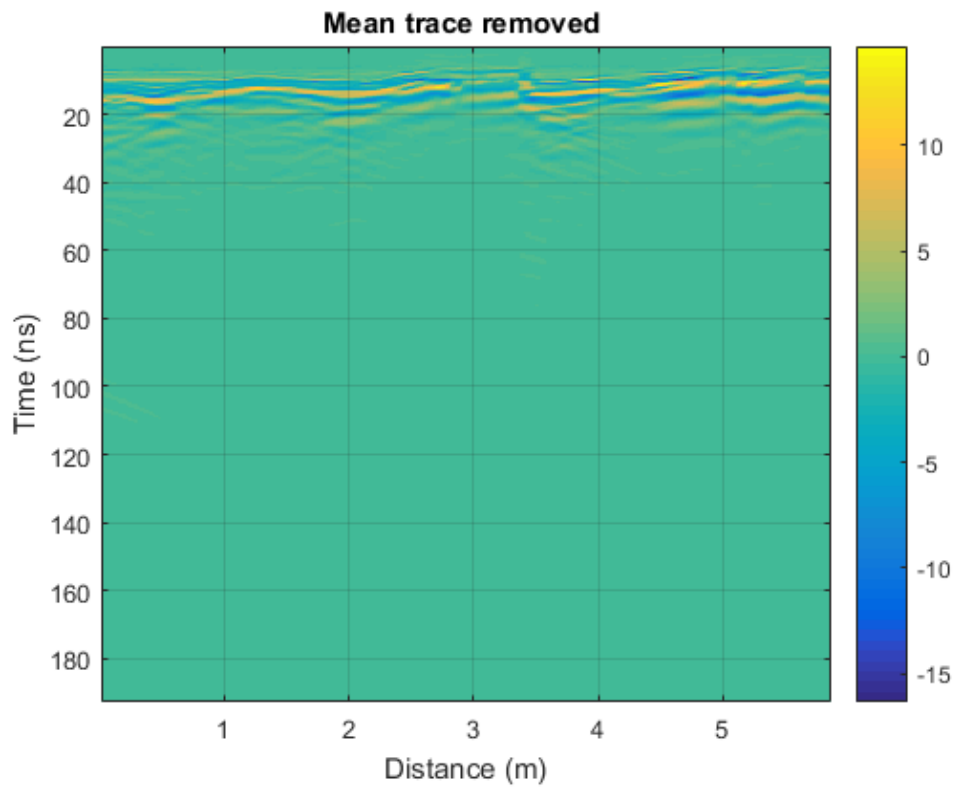


Figure 6.20. Radargram with mean trace removed

6.9 Band pass filter

The band pass filter is used to attenuate certain frequencies that are above and below the selected frequency band, in this case there are 2 filter options, one where the band is fixed at 1.5 times the maximum frequency between the two antennas, and another where the cutoff frequencies are given by the maximum values of the amplitude matrix, a cutoff frequency before and after this value is automatically selected by the program. The program also gives the frequency spectrum shown in figure 6.18, on which it can be seen the low influence of the 900Mhz antenna (values close to 1).

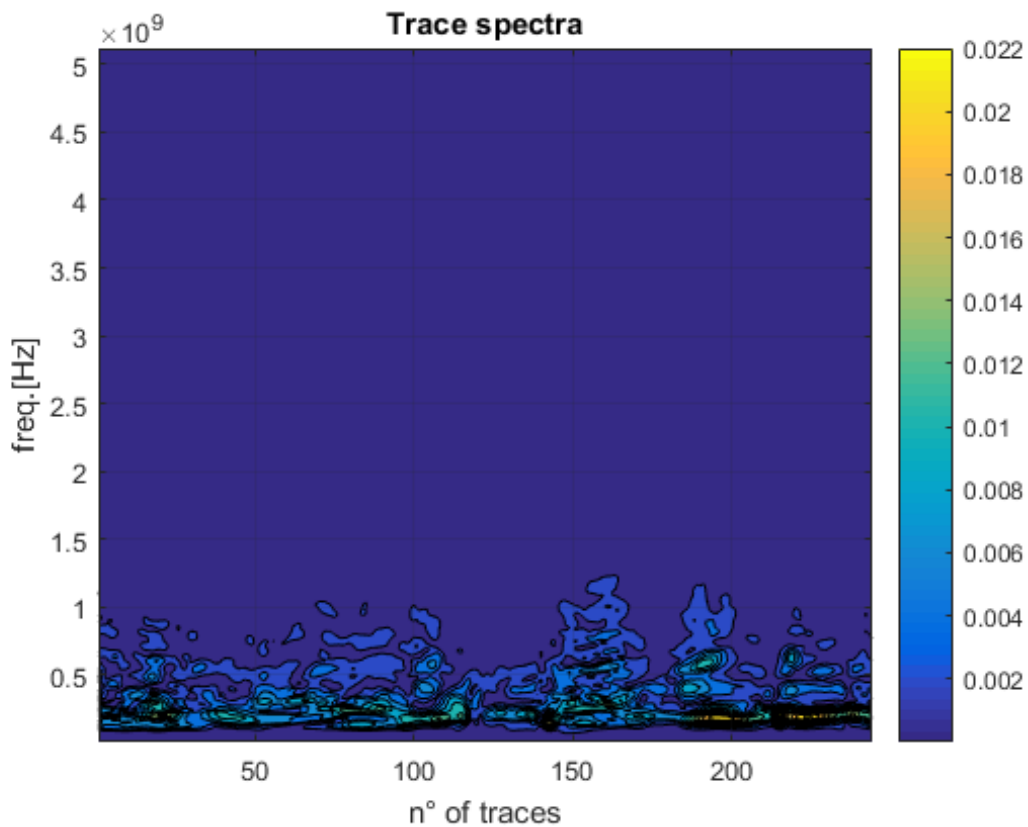


Figure 6.21. Trace amplitude spectra

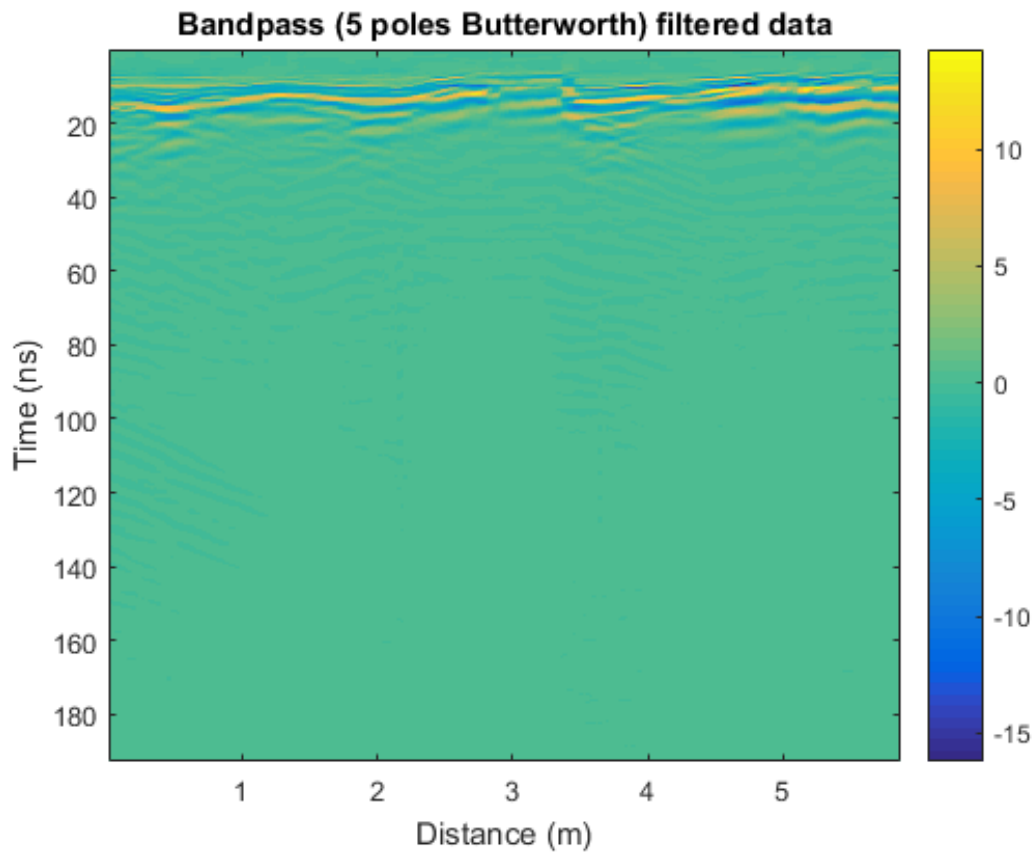


Figure 6.22. Bandpass filter fixed at 1.5 high frequency antenna

6.10 Energy recovery

With the aim of recover some information in depth, an energy recover procedure is necessary, the procedure aims to recover energy that has been loss for the distance between the source and the target. In this case, the program ask for a velocity, which should be the estimated velocity of the material, then ask for the point from where the recovery will be done (in time), with these two parameters calculates a distance, that will be elevated to an exponential value, chosen by the user between square root (0.5), linear (1), quadratic (2) and cubic (3). Depending on the exponent the amplitudes will increase more or less. As a result, can be appreciated in the Figure 6.23 that the information between 100 and 120ns was not present in the previous radargrams.

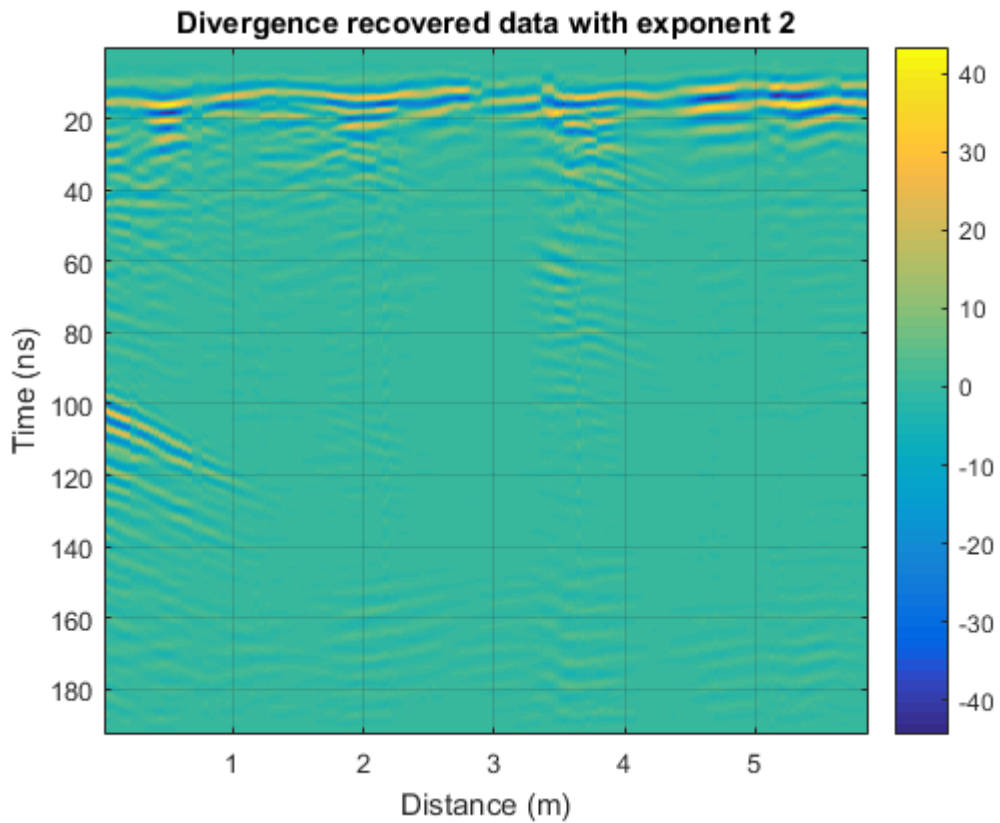


Figure 6.23. Radargram with Divergence recovery

This chapter has represented a very important part of this thesis work, but, after analyzing in a very detailed way the radargrams on each individual step, testing different filter combinations, among others. The conclusion was not satisfactory, because the frequency bands of each antenna are (obviously) dislodged, and no procedure was found that would allow them to be coupled, therefore, the information that results from the mixing is not totally true, given that the position of the events it is a bit different for the 900Mhz antenna (whose response has shorter wavelengths) than for the 200Mhz, where the wavelength is longer, as well as the frequency band.

Chapter 7 Results and interpretation

Mainly, the results of this thesis work are summarized in 3D cubes generated from the radargrams already processed, where several structures of great importance for the fulfillment of the stated objective are observed; Next, the cubes with the most relevant cuts are shown, as well as the explanation of each one.

The figures from 7.1 to 7.6 correspond to the cube constructed using the acquisitions made in the floor, in the 3 areas identified above, using different cuts to understand the continuity of the main anomalies observed.

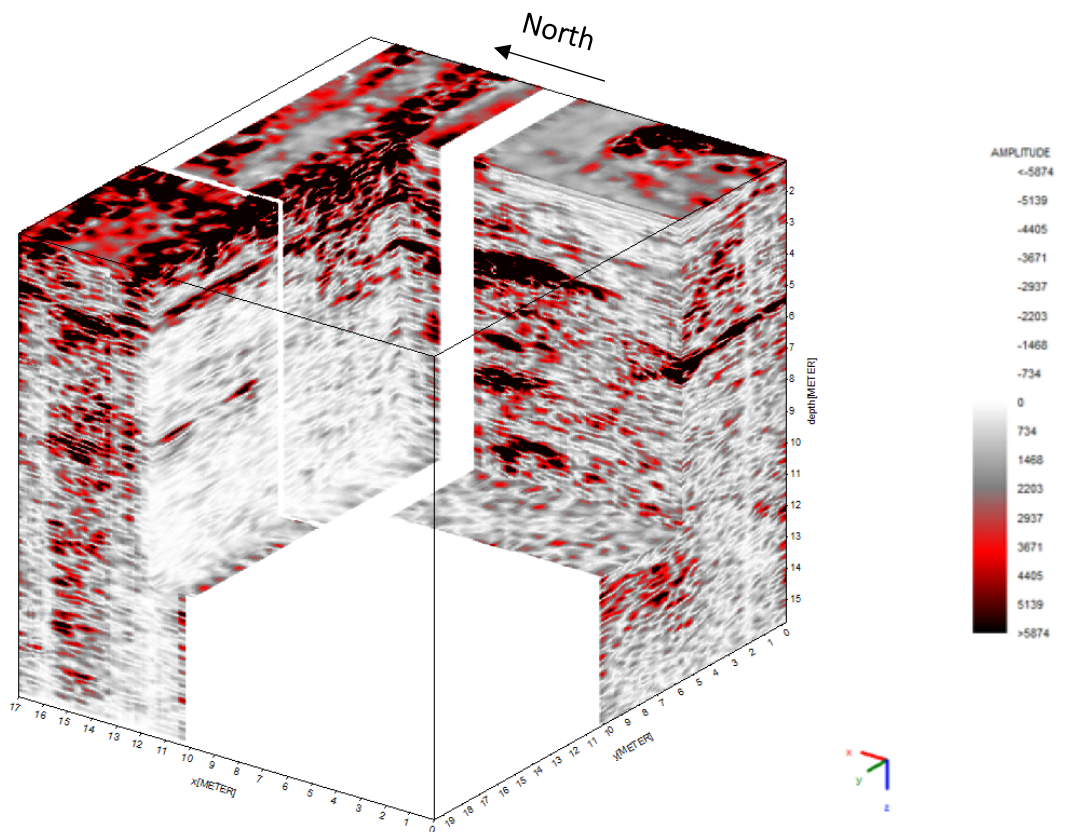


Figure 7.1. 3D cube containing the acquisitions made in the floor, with a X,Y,Z cut showing the main fractures found.
Radar acquisition plane: y

In the image 7.1 we see the cube that has been cut starting from the corner where no acquisition was made, because there is an intact marble block, in this it can be seen that there is a possible plane of fracture or contact, which has a dip-slope direction, this would make sense because according to the geology explained above in section 2.4, the area should have this type of fracture.

For a better visualization the interpretation of the Figure 7.1, the Figure 7.2 is presented, where those first planes described above can be easily observed, delimited with yellow lines.

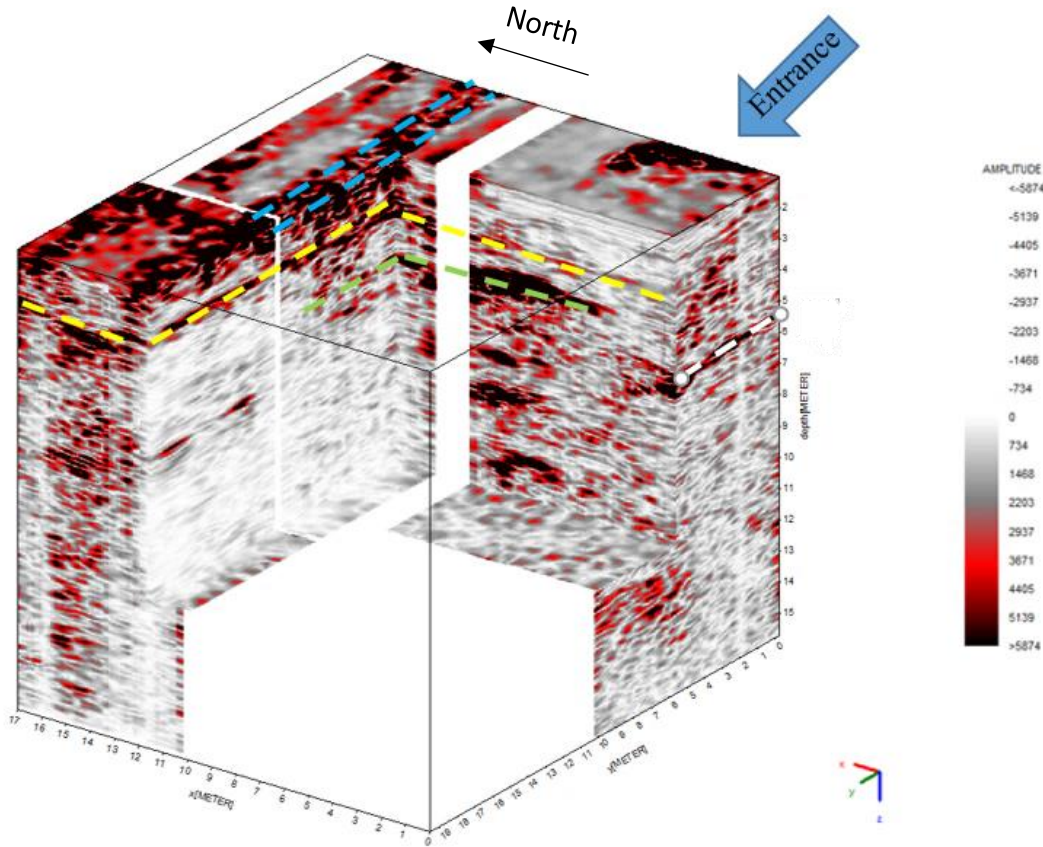


Figure 7.2. Interpretation of the figure 7.1 showing the main fracture plains found. Radar acquisition plane: y

The estimated depth of this shallow foreground is approximately 2.5m in its most superficial part (on the opposite side of the entrance) to about 3.5m near the entrance of the quarry, considering a wave speed for the marble of 0.09. m/ns.

In this first cube it can also be seen high amplitudes aligned on the surface corresponding to the north base, which correspond exactly to an amphibolite vein found in that area, which can be seen in the Chapter 4, Figure 4.4, which is parallel to a vein of black marble. In the interpreted figure this detail is demarcated by the lines in light blue.

Lastly, the areas delimited in green and white, could correspond to subsequent fractures, at approximate depths of 4.5m and 5.5m, however, these cannot be recognized perfectly in this first cube.

Figure 7.3 corresponds to a lateral cut made to check if it was possible to observe some continuity in the fracture delimited in green (the second in depth), finding that, at a quite similar depth of approximately 4.5m in its deepest part, it is found a surface, also dip-slope direction. The surface cannot be seen in the space between the two veins (amphibolite and black marble) by an attenuation effect on se signal caused for these materials, which can be seen in the area framed in a yellow circle.

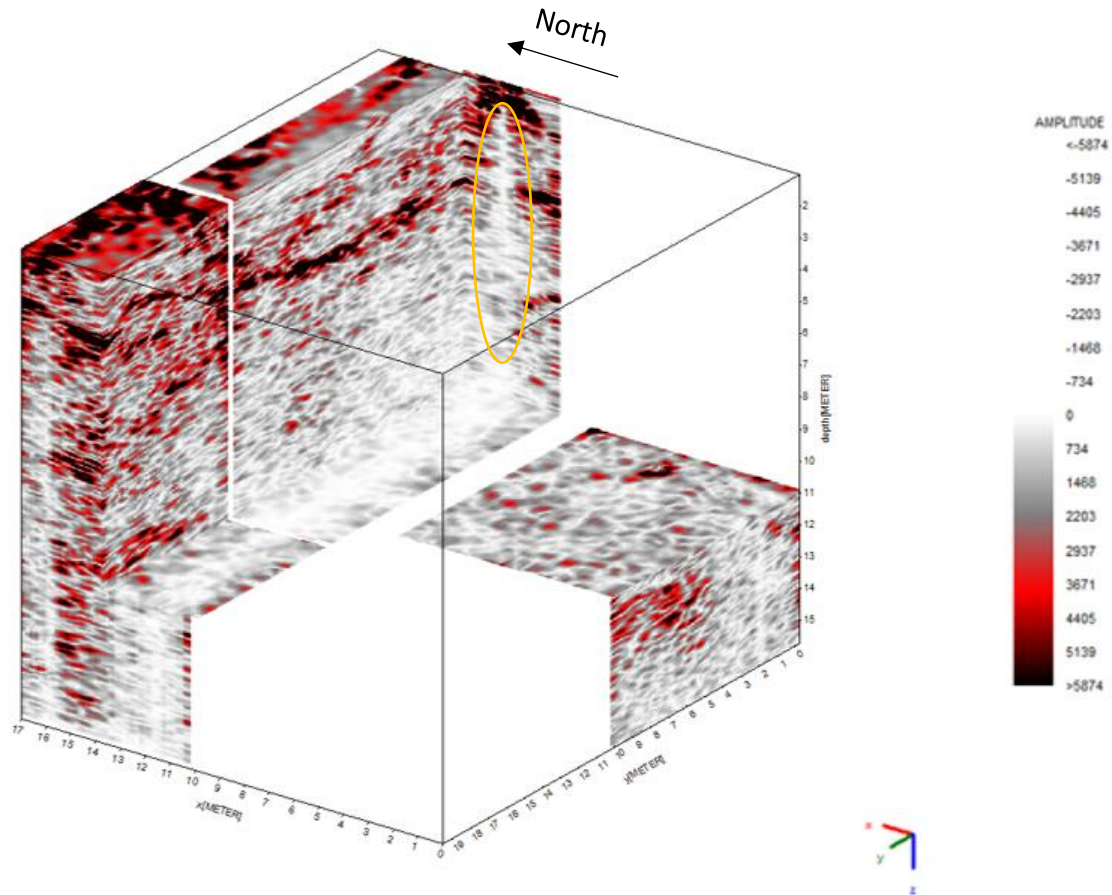


Figure 7.3. Lateral cut positioned north the amphibolite vein, showing the attenuation effect of this material, and the continuity of the fracture plain. Radar acquisition plane: y

In the Figure 7.4 we can see a cut made through the same value of Y used in the cut 1 (Figure 7.1), it is found that the plane found in the figure 7.3 seems connected to the same surface previously identified in green, thus verifying that it has continuity and it likely corresponds to a second plane of fracture.

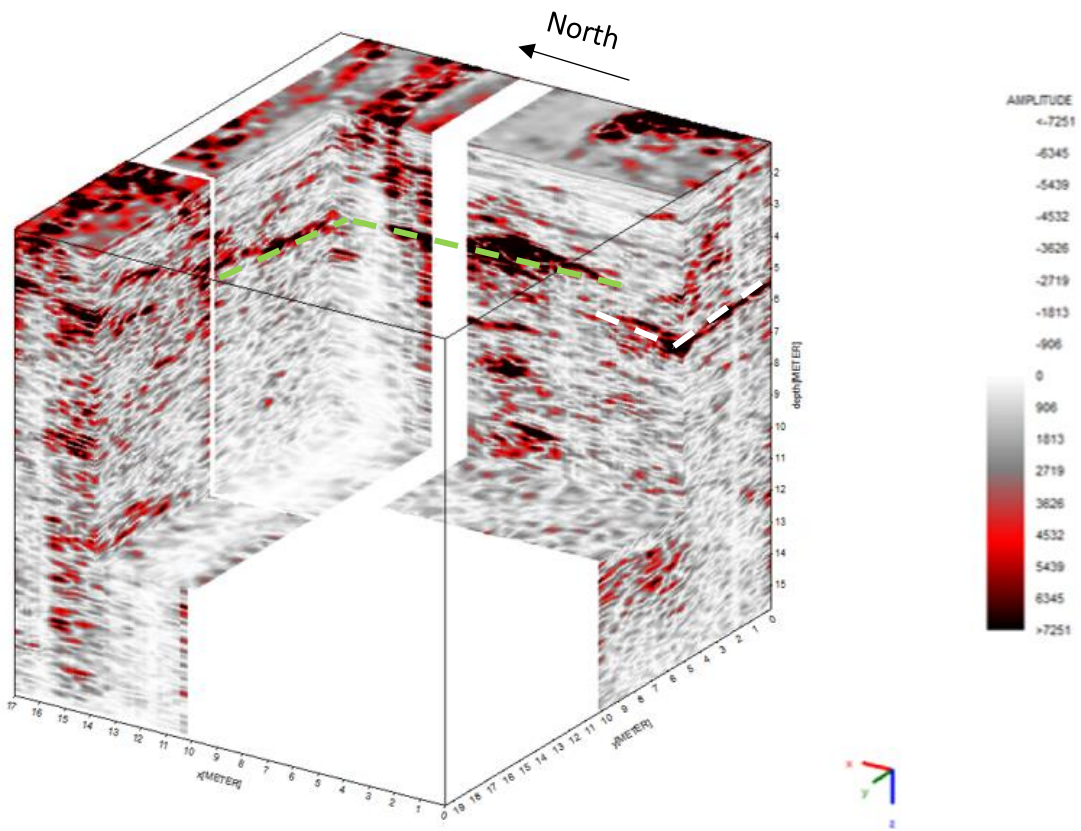


Figure 7.4. View of the continuity of the fracture identified earlier with a green plane, radar acquisition plane: y

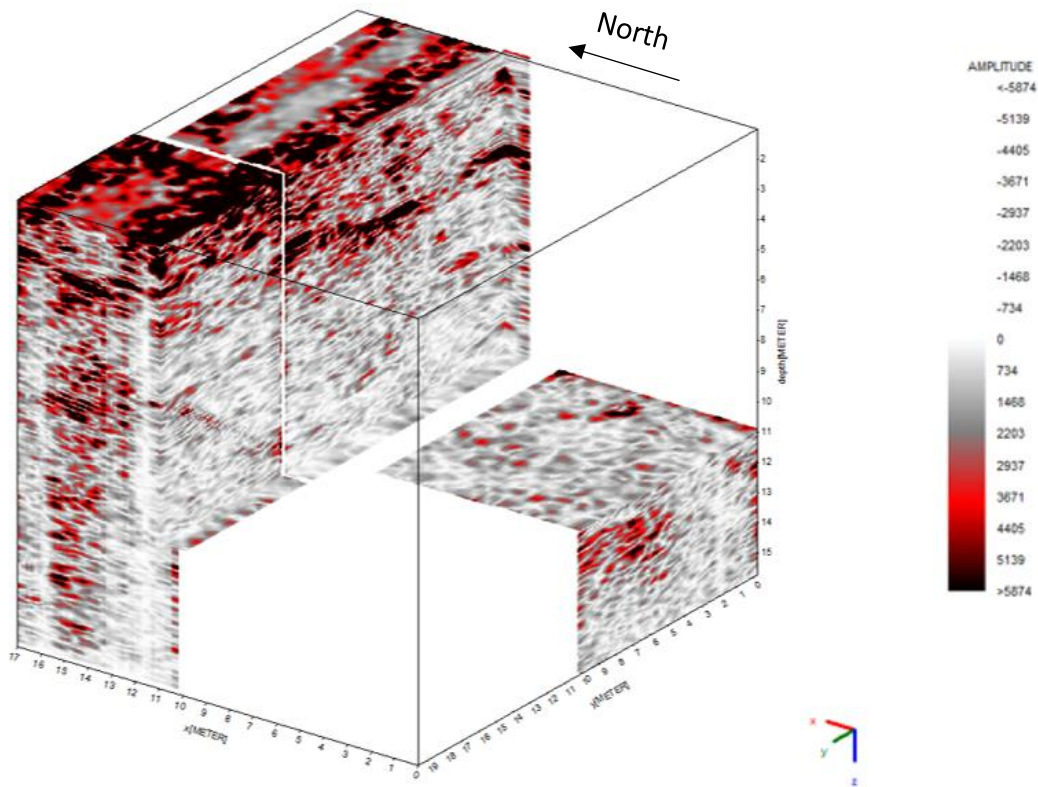


Figure 7.5. Lateral cut positioned south the amphibolite vein, radar acquisition plane: y

Finalizing this section of the interpretation, figure 7.5 shows a final cut, made before the amphibolite and black marble vein, to verify the extension of this plane, resulting that the presence of the same is still observed, so it can be said that it has a horizontal extension of approximately 15m of the total 17m that conform the 3 bases acquisition, an inclination towards the entrance of the mine, and a depth that varies between 3m and 4.5m.

The last possible fracture initially identified by white lines, is small, is located at a slightly higher depth, and it is not connected to the green one.

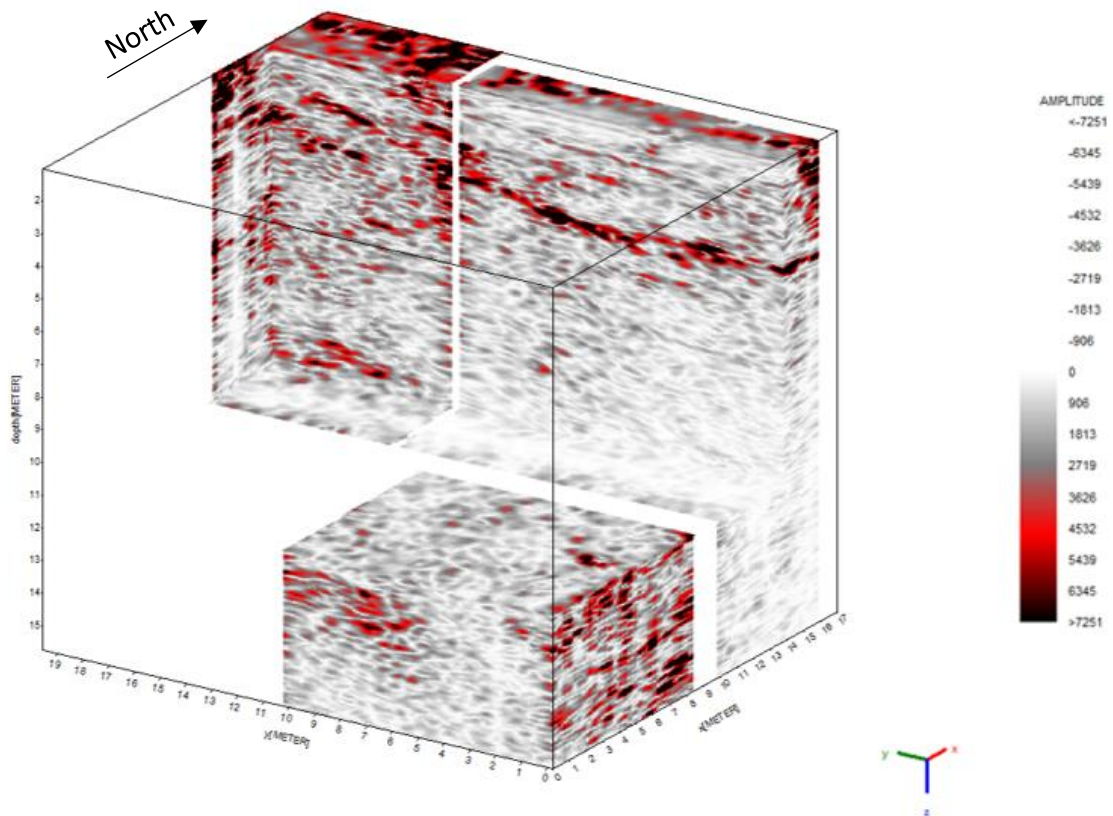


Figure 7.6. Visualization of the main fracture found, radar acquisition plane: y

This last view (figure 7.6) was made to have a complete and well-directed visualization of the main fracture found.

The following figures (7.7 and 7.8) correspond to the north wall acquisition (points 23,24,25,26 of the figure 4.2). In the 7.7 figure three planes can be identified, one at approximately 1m, then there is another which is more prominent and defined at 4m and a last one at 5.5m.

In this particular case, as the survey was made in a wall that was part of a cube of marble which had a lateral free-to-see wall (figure 4.3), the more prominent plane was associated with a part of the wall from which water was coming out constantly.

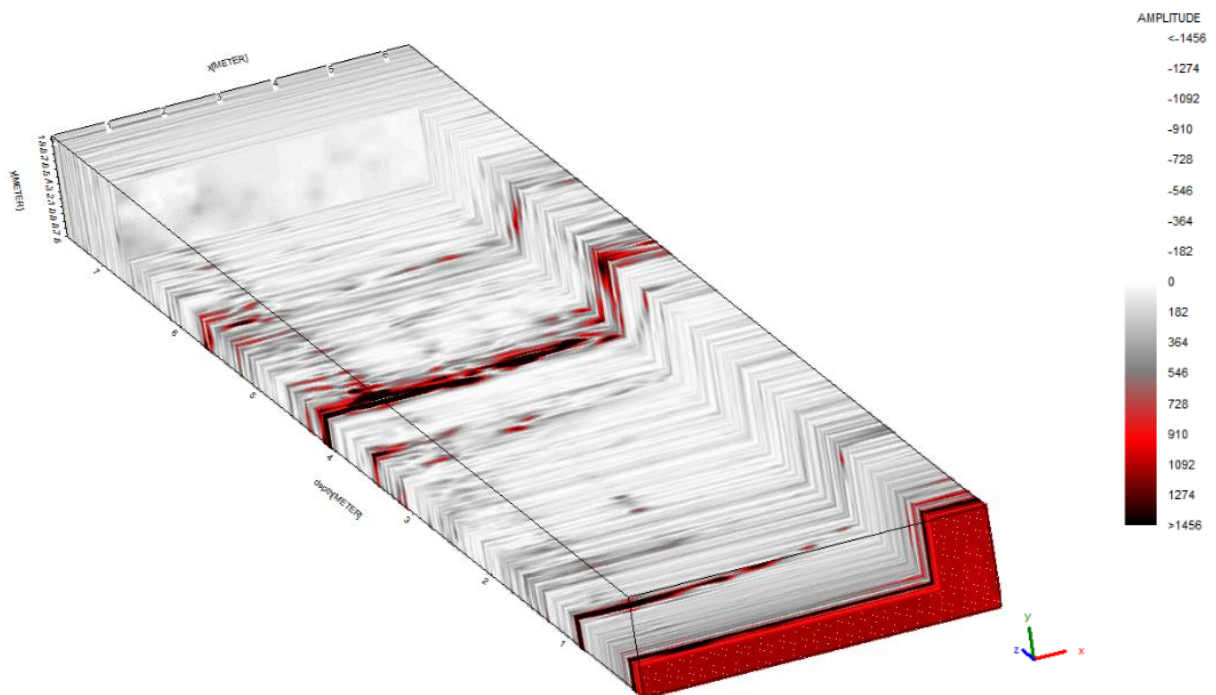


Figure 7.7. North wall, scale enhancing the visibility of the bigger fracture at 4,2m, radar acquisition plane: x

The other two planes can be associated with fractures, but in this case is not that relevant because this block of marble is the last one of the current stage, and is practically isolated, so those fractures will not compromise the stability of the quarry.

For a final view, trying to fit a good color scale that highlights the deepest fracture, the figure 7.8 is presented, on which the contrast of colors improves the visualization of all 3 fractures.

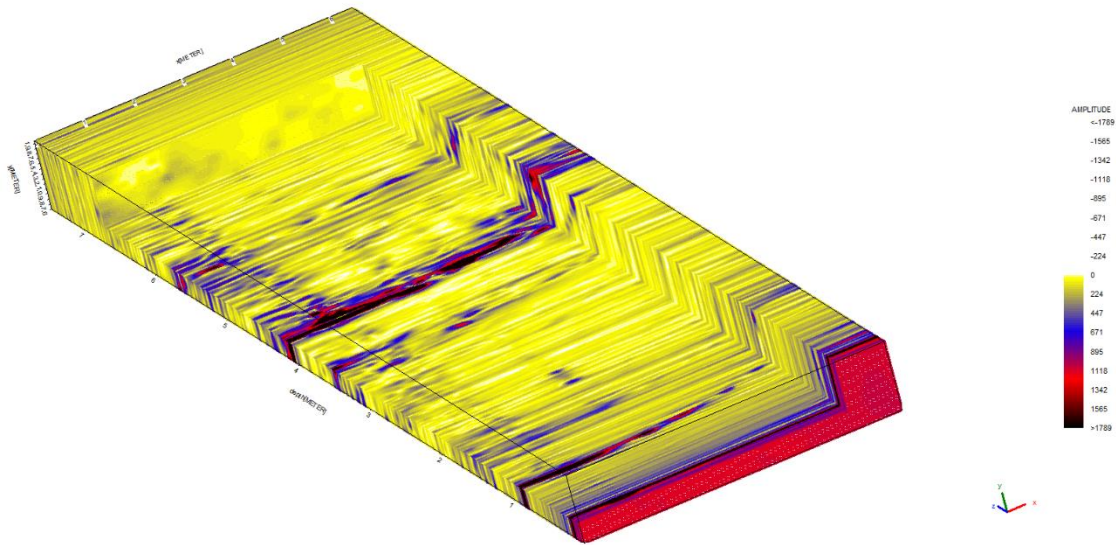


Figure 7.8. North wall, scale trying to improve the visualization of the deeper fracture, radar acquisition plane: x

It can be noticed that the cube of the south inner and outer wall is not shown in the results, the reason for this is that for that section, we couldn't obtain relevant information, in addition to finding very large hyperbolas that suggested some type of error, however one of the profiles acquired with the 200Mhz antenna is shown below, followed by the same profile acquired with the 900 antenna, where it can be observed that there is apparently some contact or fracture on the left side.

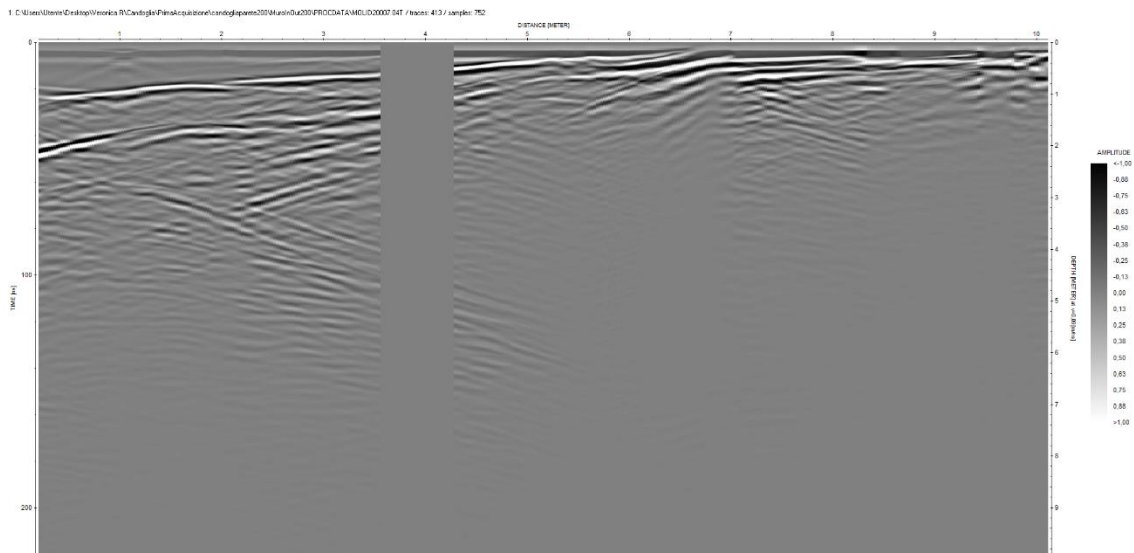


Figure 7.9. Profile 07 of the inner and outer wall acquisition with the 200Mhz antenna

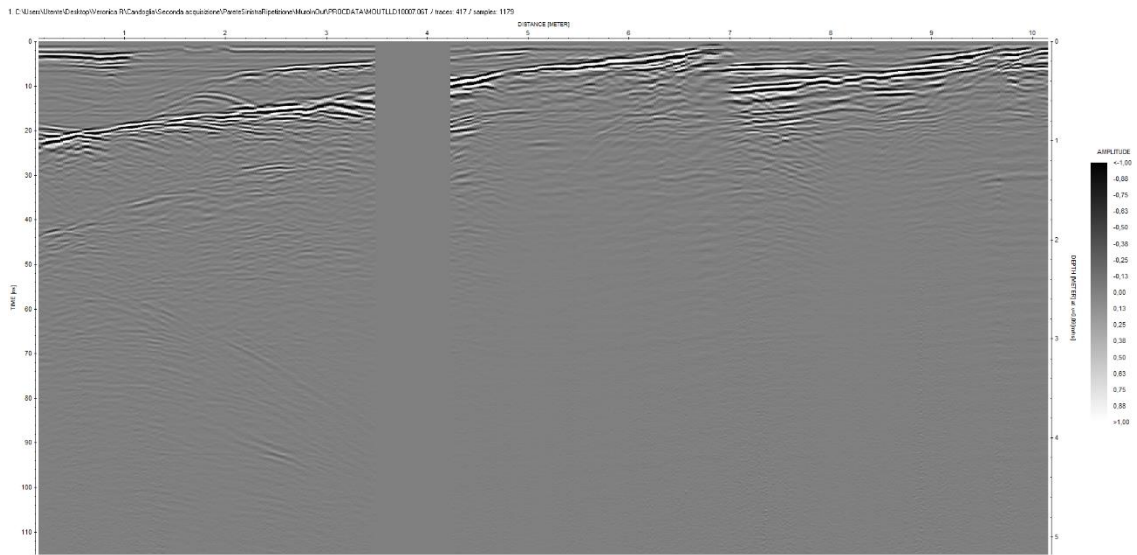


Figure 7.10. Profile 07 of the inner and outer wall acquisition with the 900 MHz antenna

According to the geology and the excavation methodology, at least 5m of marble should have been left in that wall (for stability reasons a certain marble thickness was left between the excavation and the contact with the adjacent rock), being this a shallow surface (2 meters maximum) could be attributed to a small fracture, or to the contact between two marbles with different mineralogical properties. In any case, the shallow information is not very useful, and after the processing, the information in depth is not relevant, in fact, is almost null.

Still, it is important to emphasize the good quality of the data, this can be seen by the persistence fractures observed in the union of the profiles, remembering that the internal and external wall were acquired separately and joined profile by profile used the software ReflexW, the united profiles show a precise continuity of the fractures that starts more superficially in the internal wall and deepens in the external wall.

Chapter 8 Conclusions and future works

8.1 Conclusions

Considering that geophysical methods are indirect methods based on theoretical physical principles, the conclusions presented below may not be entirely true. Generally, the geophysical acquisition campaigns are carried out using at least two different methods to have a contrast and comparison of results, generating more reliable and accurate information, however, in this case the only applied method was the ground penetrating radar.

According to the information presented above, it can be said that, mainly, there are at least two almost parallel fractures, which are disposed with dip-slope direction, these fractures are of relevance for future excavations, which would probably be carried out in the middle of 2025. It is probable that the section that contains this fracture represents an unusable part of the marble for the reconstruction of the Cathedral of Milan, because useful blocks must be intact. However, from another point of view, more detailed studies should be carried out to verify if these fractures could affect or not the stability of the mine.

On the other hand, the presence of some dark materials such as amphibolite, and black marble, generate an attenuation of the energy and a distortion of the resulting radargram, in fact, in multiple occasions the information in depth in the parts corresponding with those materials was almost completely lost, an example of this is the south wall, where in the inner part a big part of this material was found and no useful information was generated. The lack of information in depth in this area can also be related to the presence of wet soil particles inside the fracture, according to some investigations [20], this condition will show a great delimitation of the fracture because of the high reflectivity of the water, but an attenuation of information in depth, which could be the reason of the lack of information in this case.

Finally, Ground Penetrating Radar is a wide used method that in general gives very good results, from shallow details to deep evidence, in fact, the information obtained in the floor acquisitions was important and relevant for the future of the cave, still, more information is necessary, for this particular case, using just GPR is not adequate.

8.2 Future works

As a result of the aforementioned, it is considered of great importance to carry out a second acquisition campaign, on which other geophysical methods such as seismic are included and thus obtain a comparison of results.

On the other hand, given that on the south wall the radar response is not effective, it would be useful to make a small perforation, to check the depth of the marble at that point, and to identify with closeness the contact between the marble and the adjacent rocks, which is important to the stability of the quarry.

Finally, it is important to make an integration between the results obtained in this thesis work, and numerical analysis of stability, to check the stability of the mine in the future in order to preserve the safety of the workers.

Appreciations

To my parents, Martha & Alfredo, and my brothers Natalia & Gerardo, for always giving me support, love and encouragement to follow my dreams and achieve my goals even in the distance,

To Vicente Manuel, for being my rock and unconditional source of love, energy, joy and laughter,

Last but not least, to my tutor, Luigi Sambuelli, for giving me the opportunity of continuing to discover the beauty of geophysics, and for teaching me something new each day,

Thank you.

Chapter 9 Bibliography

- [1] C. Oggeri, P. Oreste, D. Peila, P. S, E. Corbetta e B. Morlin, «UNA GRANDE CAVERNA PER L'ESTRAZIONE DI PIETRA ORNAMENTALE: IL CASO DELLA CAVA MADRE DEL DUOMO DI MILANO A CANDOGIA (VCO),» in *GEAM*, Torino, 2006.
- [2] S. Pelizza, O. P, D. Peila e C. Oggeri, «Stability Analysis of a Large Cavern in Italy for Quarrying Exploitation of a Pink Marble,» *Pergamon*, vol. 15, n. 4, pp. 421-435, 2001.
- [3] H. Keppler e J. Smyth, «Geological Excursion Field Guide,» ETH, Verbania-Pallanza, 2003.
- [4] N. Adrian, «Ground-penetrating radar and its use in sedimentology: principles, problems and progress,» *Earth Science Reviews*, vol. 66, n. 3-4, pp. 261-330, 2004.
- [5] H. M. Jol, *Ground Penetrating Radar: Theory and Applications*, Amsterdam: Elsevier B.V., 2009.
- [6] E. Parkhomenko, *Electrical Properties of Rocks*, New York: Plenum Press, 1967.
- [7] W. Lowrie, *Fundamentals of Geophysics*, Cambridge University Press, 2007.
- [8] R. WANGSNESS, «Campos Electromagneticos,» *Editorial Limusa S.A*, pp. 459-519, 2001.
- [9] D. J. Daniels, *Ground Penetrating Radar*, 2nd edition, London, United Kingdom: The Institution of Electrical Engineers, 2004.
- [10] A. Von Hippel, *Dielectrics and waves 1st Edition*, Cambridge, United States: MIT Press, 1954.
- [11] A. Annan, «Transmission dispersion and GPR,» *JEEG*, pp. 125-136, 1996.

- [12] P. X. Neto e W. E. de Medeiros, «A practical approach to correct attenuation effects in GPR data,» *Journal of Applied Geophysics*, vol. 59, pp. 140-151, 2005.
- [13] F. Ulriksen e C. Peter, *Application of Impulse Radar to Civil Engineering*, Doctoral Thesis, Geophysical Survey Systems, Inc., 1982.
- [14] L. Sambuelli, *Basic GPR*, Torino: Politecnico di torino (DIATI), 2016.
- [15] V. Jimenez, *Caracterizacion arqueologica en el parque san felipe usando el metodo de georadar*, Caracas: Tesis. Universidad Simon Bolivar, 2016.
- [16] W.-c. Wang, *Electromagnetic wave theory*, Washington, 2007.
- [17] M. De la vega e N. Bonomo, *Metodo de Georadar*, Caracas, 2007.
- [18] Lopez, *Aplicacion el radar de penetracion en tierra (georadar) a la aplicacion no destructiva de yacimientos arqueologicos*, Thesis of the university of Grenade, 2008.
- [19] K. Sandmeier, *REFLEXW Version 8.5 user's guide*, Germany, 2017.
- [20] L. Sambuelli e C. CALZONI, «Estimation of thin fracture aperture in a marble block by GPR sounding,» *Bollettino di Geofisica Teorica ed Applicata*, vol. 51, n. 2-3, pp. 239-252, 2010.

Appendix 1. Main code for the mixing of two frequency signals

```
%import raw data from IDS files
%
%needs: Idsris_read_2
%
%OUTPUT
% Struvar                All: header and data
% Number of traces       Notr
% Number of sample/trace Nosa
% Sampling interval      dt
% Sampling time vector   t
% Trace interval         dx
% Trace positions vector x
% Antenna frequency      AntF
% Conversion constant ampl/Volts AtoV
% Radargram              raw
%
clc
close all
clear all

display ('*****SELECT LOW FREQUENCY FILE*****')

LStruvar=Idsris_read_2;
LNotr=LStruvar.n_acq_sweep; ORI_LNotr=LNotr;%[-]
LNosa=LStruvar.n_acq_sample; ORI_LNosa=LNosa;%[-]
Ldt=2*LStruvar.y_cell;    ORI_Ldt=Ldt;%[s]
Lt=2*LStruvar.Y;         ORI_Lt=Lt;%[s]vector
Ldx=LStruvar.x_cell;     ORI_Ldx=Ldx;%[m]
Lx=LStruvar.X;          ORI_Lx=Lx;%[m]vector
LAntF=LStruvar.radar_freq; %[MHz]
LAtov=LStruvar.conv_int_volts;%[V]
Lraw=LStruvar.MAPPA;    ORI_Lraw=Lraw;%[-]matrix
%
%                               figure(10)
%image(x,t*10^9,raw);
%xlabel('Distance [m]');
%ylabel('twt [ns]');

display ('*****SELECT HIGH FREQUENCY FILE*****')
HStruvar=Idsris_read_2;
HNotr=HStruvar.n_acq_sweep; ORI_HNotr=HNotr;%[-]
HNosa=HStruvar.n_acq_sample; ORI_HNosa=HNosa;%[-]
Hdt=2*HStruvar.y_cell;    ORI_Hdt=Hdt;%[s]
Ht=2*HStruvar.Y;         ORI_Ht=Ht;%[s]vector
Hdx=HStruvar.x_cell;     ORI_Hdx=Hdx;%[m]
```

```

Hx=HStruvar.X;          ORI_Hx=Hx; %[m]vector
HAntF=HStruvar.radar_freq;  %[MHz]
HAtoV=HStruvar.conv_int_volts; %[V]
Hraw=HStruvar.MAPPA;    ORI_Lraw=Lraw; %[-]matrix

```

```

%% %%%%%%%%%%% DEWOW %%%%%%%%%%%

```

```

%%% Low frequency signal

```

```

dwL=dewowFX(Lraw, 8, 2, 0.05);

```

```

j=(1:(LNosa));
tl=j*Ldt*10^6;
fl=(j/max(tl));

```

```

figure(100)

```

```

subplot (2,1,1)
plot(dwL(:,200),'k');
hold on
plot(Lraw(:,200),'r');
title('Low frequency trace with dewow')
legend ('Original trace','Trace with dewow')
xlabel('time (ns)')
ylabel('Amplitude')

```

```

LAspori2=abs(fft(Lraw(:,200)));
LAsporif2=abs(fft(dwL(:,200)));

```

```

subplot (2,1,2)
plot(fl,LAspori2,'k',fl,LAsporif2,'r');
axis ([0 fl(LNosa/2) 0 inf]);
title('Low frequency spectrum')
legend ('Original spectrum','Spectrum after dewow')
xlabel('frequency (MHz)')
ylabel('Amplitude')

```

```

%%% High frequency signal

```

```

dwH=dewowFX(Hraw, 8, 2, 0.05);

```

```

j=(1:HNosa);
th=j*Hdt*10^6;
fh=(j/max(th));

```

```

figure (120)

```

```

subplot (2,1,1)
plot(dwH(:,200),'k');
hold on
plot(Hraw(:,200),'r');
axis ([-inf inf -inf inf]);
title('High frequency trace')

```

```

legend ('Original trace','Trace with dewow')
xlabel('time (ns)')
ylabel('Amplitude')

```

```

HAspori2=abs(fft(Hraw(:,200)));
HAsporif2=abs(fft(dwH(:,200)));

```

```

subplot (2,1,2)
ph=plot(fh,HAspori2,'k',fh,HAsporif2,'r');
axis ([0 fl(LNosa/2) 0 inf]);
title('High frequency spectrum')
legend ('Original spectrum','Spectrum after dewow')
xlabel('frequency (MHz)')
ylabel('Amplitude')

```

```

display ('dewow done')

```

```

%%%%%%%%%% RESAMPLING %%%%%%%%%%%
%**dopo il resampling il delta t per tutte e due è pari al minimo

```

```

[NLt, NHt, dwrL, dwrH]=resamp2FX(dwL,dwH,Ldt,Hdt);

```

```

figure (132)
imagesc(Lx',NLt*10^9,dwrL)
xlabel('Distance (m)')
ylabel('Time (ns)')
title ('Resampled low frequency antenna')
colorbar

```

```

figure (134)
imagesc (Hx',NHt*10^9,dwrH)
xlabel('Distance (m)')
ylabel('Time (ns)')
title ('Resampled high frequency antenna')
colorbar

```

```

Mdt=min(Ldt,Hdt); %nuovo delta t
figure (136)
plot (NLt,dwrL(:,20),'kx')%traccia con il resampling
hold on
plot (Lt,dwL(:,20),'r')%traccia originale
legend('Resampled trace', 'original trace')
xlabel('Time (ns)')
ylabel('Amplitude')

```

```

display ('resampling done, new dt=min(Ldt,Hdt)')

%%%%%%%%%%%%%%%%%%%%%%%%%%%%%%%%%%%%%%%%%%%%%%%%%%%%%%%%%%%%%%%%%%%%%%%% REMOVE INITIAL DELAY %%%%%%%%%%%%%%%

subav=menu('Remove initial delay?','yes','No');
if subav==1
    dwdlH=delayFX(dwrH);

                    figure (140)

    imagesc(Hx',Ht'*10^9,dwdlH);
    title('High frequency without initial delay')
    xlabel('Distance (m)')
    ylabel('Time (ns)')
    colorbar

    dwdlL=delayFX(dwrL);

                    figure (150)
    imagesc(Lx',Lt'*10^9,dwdlL);
    title('Low frequency without initial delay')
    xlabel('Distance (m)')
    ylabel('Time (ns)')
    colorbar

    display ('initial delay removed')
else
    dwdlH=dwrH;
    dwdlL=dwrL;
    display ('no initial delay removed')
end

%%%%%%%%%%%%%%%%%%%%%%%%%%%%%%%%%%%%%%%%%%%%%%%%%%%%%%%%%%%%%%%%%%%%%%%% EQUAL SIZE%%%%%%%%%%%%%%%%%%%%%%%%%%%%%%%%%%%%%%%%%%%%%%%%%%%%%%%%%%%%%%%%%%%%%%%%

[HrawEqlz,LrawEqlz,Mdx]=EqlzFX(dwdlH,Hdx,dwdlL,Ldx);
[MNosa,MNotr]=size(HrawEqlz);

j=(1:MNotr);
Mx=j*Mdx; %nuovo vettore degli spazi
i=(1:MNosa);
Mt=i*Mdt; %nuovo vettore dei tempi
Mfq=(i/(max(Mt)*10^6));%nuovo vettore delle frequenze

                    figure (180)

    imagesc(Mx',Mt'*10^9,LrawEqlz);
    xlabel('Distance (m)')

```



```

xlabel('frequency (MHz)')
ylabel('Amplitude')

SumFD=fft(HrawNorm)+fft(LrawNorm);
MixFD=ifft(SumFD) ;
MAntF=HAntF;

MAmp=mean(abs(SumFD),2);

figure(209)
plot(Mfq, MAmp)
axis ([0 Mfq(floor(MNosa/2)) 0 inf]);
title ('Mixed signal spectrum')
xlabel('frequency (MHz)')
ylabel('Amplitude')

figure (210)
imagesc (Mx',Mt'*10^9,MixFD)
xlabel('Distance (m)')
ylabel('Time (ns)')
title('Mixing in FREQUENCY domain')
colorbar

display ('Mixing in frequency domain done')

%% %%%%%%%%%%% ENERGY FILTER %%%%%%%%%%%

subav=menu('Energy filter?','yes','No');
if subav==1
[MixFiltFD,Amp2D,Amp2Dfilt]=filtmixfdFX2(HrawNorm,LrawNorm);
Amp2DxGRAF=fftshift(Amp2D);
figure(212)

%imagesc(,-inf inf], Amp2DxGRAF);
image([-1/(max(Mx'/2)) 1/(max(Mx'/2))],[-1/(2*Hdt) (1/(2*Hdt))],Amp2DxGRAF);
xlabel('kx (1/m)')
ylabel('frequency (Hz)')
title('Original Amplitude spectrum')
colorbar

FAmp=mean(abs(fft(MixFiltFD)),2);
% provaF=FAmp/max(max(FAmp));
figure (213)

plot(Mfq,FAmp)
axis ([0 Mfq(floor(MNosa/2)) 0 inf]);
title ('Mixed and filtered spectrum')

```

```

xlabel('frequency (MHz)')
ylabel('Amplitude')

figure(214)
imagesc (Mx',Mt'*10^9,MixFiltFD)
title('Mixed and filtered in frequency domain radargram')
Amp2DfiltxGRAF=fftshift(Amp2Dfilt);
colorbar

figure(215)
image([-1/(max(Mx'/2)) 1/(max(Mx'/2))],[-(1/(2*Hdt))
(1/(2*Hdt))],Amp2DfiltxGRAF);
xlabel('kx (1/m)')
ylabel('Frequency (Hz)')
title('Filtred Amplitude spectrum')

colorbar

display ('Filtering in frequency done')
else
MixFiltFD=MixFD;
display ('No filtering in frequency')
end

%% %%%%%%%%%%%REMOVE MEAN TRACE%%%%%%%%%%

subav=menu('Remove mean trace?','yes','No');
if subav==1
[rdr]=MeanTraceFX(MixFiltFD,MNotr);

display ('Mean trace removed')
else
rdr=MixFiltFD;
display ('Mean trace NOT removed')
end
if subav==1

figure (220)
imagesc(Mx',Mt'*10^9,rdr)
colorbar
title('Mean trace removed ')
xlabel('Distance (m)')
ylabel('Time (ns)')
grid
else
end

figure(230)

plot(MixFiltFD(:,200),'k');%traccia di entrata blu

```

```

hold on
plot(rdr(:,200),'r');%traccia di uscita rossa
legend('original trace', 'mean trace removed')
xlabel('time (ns)')
ylabel('Amplitude')

```

%% %%% %%% %%% %%% %%% SPECTRAL ANALYSIS %%% %%% %%% %%% %%% %%% %%% %%% %%%

```
[asprdr,fr,rdrf]=SpectralAnalysisFX(MAntF, rdr, Mt);
```

figure (440)

```

frfr=repmat(fr',1,length(j));
xxs=repmat(j,length(fr), 1);
contourf(xxs,frfr,asprdr);
title('Trace spectra')
xlabel('n° of traces')
ylabel('freq.[Hz]')
colorbar
grid

```

figure (250)

```

imagesc(Mx',Mt'*10^9,rdrf);
title('Bandpass (5 poles Butterworth) filtered data')
xlabel('Distance (m)')
ylabel('Time (ns)')
colorbar

```

%% %%% %%% %%% %%% %%% DIVERGENCE RECOVERY %%% %%% %%% %%% %%% %%% %%% %%% %%%

```
[rdrg,AMP]=DivRecFX(Mt,Mx,rdrf);
```

figure (260)

```

imagesc(Mx',Mt'*10^9,rdrg);
xlabel('Distance (m)')
ylabel('Time (ns)')
titf5=['Divergence recovered data with exponent ' AMP];
grid
title(titf5)
colorbar
colormapeditor

```

Appendix 2. Functions that conform the code

1) Dewow function

```
function rdrdewow=dewowFX(rdr, n, m, Wn)

    figure
    [bbu,abu] = maxflat(n,m,Wn);
    fvtool(bbu,abu)
    title ('filtro')

    C_dewrdr2=filtfilt(bbu,abu,rdr); %zero-phase lowpass filter
    rdrdewow=rdr-C_dewrdr2; %zero-phase high pass filter -> dewow

end
```

2) Resampling function

```
function [NLt,NHt, dwrL2, dwrH2]=resamp2FX(dwrL,dwrH,Ldt,Hdt)
%La funzione fa il resampling del dt di due radargrammi,
%prendendo il dt piu alto e interpolando per arrivare al dt piu piccolo.

%Dati di entrata:
%i due radargrammi, i due delta t
%Dati di uscita:
%I due radargrammi con lo stesso delta t (pari al minimo tra i due)
%I nuovi vettori dei tempi

[HNosa,HNotr]=size(dwrH);
[LNosa,LNotr]=size(dwrL);
i=(1:HNosa);
j=(1:LNosa);
Ht=i*Hdt;
Lt=j*Ldt;

if Ldt>Hdt
    resfac=floor(Ldt/Hdt);%fattore di sovracampionamento
    fs=1/Ldt; NHt=Ht;
    [dwrL2,tr]=resample(dwrL,Lt,resfac*fs,resfac,1);%RICAMPIONARE TRACCIA
    dwrH2=dwrH;
    [Nosa, Notr]=size(dwrL2);
    i=(1:Nosa);
    NLt=i*Hdt; %Nuovo vettore dei tempi

else
```

```

resfac=floor(Hdt/Ldt);%fattore di sovracampionamento
fs=1/Hdt; NLt=Lt;
[dwrH2,tr]=resample(dwrH,Ht,resfac*fs,resfac,1); %RICAMPIONARE TRACCIA
dwrL2=dwrL;
[Nosa, Notr]=size(dwrH2);
i=(1:Nosa);
NHt=i*Ldt; %Nuovo vettore dei tempi
end
if length(Lt)==length(Ht)
    dwrL2=dwrL;NLt=Lt;
    dwrH2=dwrH;NHt=Ht;
end

```

3) Remove initial delay function

```

function rrdel=delayFX(rdr)

%dati di entrata: numero di samples, matrice radar
%dati di uscita: radargramma senza delay iniziale

[Nosa,Notr]=size(rdr);
display('SELECT ON THE FIGURE THE POINT BEFORE THE MAIN BANG FOR
THE DELAY TO BE REMOVED');

figure
MeanV=mean(rdr,2);
subplot (1,3,3)
plot (MeanV)
view([90 90])
xlim ([0 max(Nosa)])

subplot(1,3,[1,2])
imagesc(rdr);
title('initial radargram')
xlabel('n° of traces')
ylabel('n° of samples')
grid

[spa, tim]=ginput(1);
tim=round(tim);
Nosa=Nosa-tim;
rrdel=rdr(tim:(Nosa+tim-1),:);

end

```

4) Equal size function

```
function [HrawEqz,LrawEqz,dx]=EqzFX(HrawR,Hdx,LrawR,Ldx)
```

```
%dati di entrata: High frequency dx e radargramma
```

```
%Low frequency dx e radargramma
```

```
%Dati di uscita: i due radargrammi low e high di dimensioni uguali, dx
```

```
[HNosa,HNotr]=size(HrawR);
```

```
[LNosa,LNotr]=size(LrawR);
```

```
%%%Cutting: per quello con maggior numero di samples
```

```
% dif=abs(HNosa-LNosa);
```

```
if max(HNosa,LNosa) == LNosa
```

```
    LrawR=LrawR(1:HNosa,1:LNotr);
```

```
else
```

```
    HrawR=HrawR(1:LNosa,1:HNotr);
```

```
end
```

```
%% uguagliare le tracce.
```

```
if HNotr>LNotr && Hdx==Ldx
```

```
    Num= HNotr-LNotr;%Num è la differenza di tracce tra un profilo e l'altro
```

```
    if rem(Num,2)==0 %per vedere se la differenza è pari oppure no
```

```
        rest=(Num/2); a=rest+1; b=HNotr-rest; %rest divide le differenze di tracce per  
        togliere una parte al inizio ed una alla fine
```

```
        HrawEqz=HrawR(:,a:b); LrawEqz=LrawR; dx=Ldx;
```

```
    else
```

```
        rest=floor(Num/2); a=rest+1; b=HNotr-(Num-rest); %se la differenza non è pari
```

```
        HrawEqz=HrawR(:,a:b); LrawEqz=LrawR; dx=Ldx;
```

```
    end
```

```
elseif HNotr<LNotr && Hdx==Ldx
```

```
    Num= LNotr-HNotr;
```

```
    if rem(Num,2)==0
```

```
        rest=(Num/2); a=rest+1 ; b=LNotr-rest;
```

```
        LrawEqz=LrawR(:,a:b); HrawEqz=HrawR; dx=Ldx;
```

```
    else
```

```
        rest=floor(Num/2); a=rest+1 ; b=LNotr-(Num-rest);
```

```
        LrawEqz=LrawR(:,a:b); HrawEqz=HrawR; dx=Ldx;
```

```
    end
```

```
elseif Hdx~=Ldx
```

```
    met=input('ricampionare rispetto al: 1=dx Maggiore , 2=dx Minore');
```

```
    if met==1
```

```
        dx=max(Hdx,Ldx);
```

```
        HrawEqz=imresize(HrawR,[Nosa, dx]);
```

```
        LrawEqz=imresize(LrawR,[Nosa, dx]);
```

```
    else
```

```
        dx=min(Hdx,Ldx);
```

```
        HrawEqz=imresize(HrawR,[Nosa, dx]);
```

```

    LrawEqLz=imresize(LrawR,[Nosa, dx]);
end
end
end

```

5) Energy filter function

```
function[MixFiltFD,Amp2D,Amp2Dfilt]=filtmixfdFX2(Hraw,Lraw)
```

```

%the function does an energy filter in frequency domain
%Dati di entrata: Matrice radar
%Dati di uscita: Matrice filtrata, spettro, spettro filtrato.

```

```

SumFD=fft2(Hraw)+fft2(Lraw);
Amp2D=abs(SumFD);
% Amp2DxGRAF=fftshift(Amp2D);
figure (501)

```

```

HH=histogram(Amp2D);
HH.NumBins=100000; set(gca,'YScale','log');
xlabel('Amplitudes')
ylabel('frequency')
title('Amplitudes histogram')
display ('SELECT THE **LOW** ENERGY LIMITS IN THE HISTOGRAM')

```

```

[ThrLx,ThrLy] = ginput2(1);
%GIMPOT: SI PUO FARE ZOOM AD UNA FINESTRA, PREMENDO TASTO SX E
SCORRENDO
%DOPIO CLICK SX PER TORNARE ALLO ZOOM INIZIALE
%TASTO DESTRO PER SELEZIONARE IL PUNTO
figure (511)

```

```

HH=histogram(Amp2D);
HH.NumBins=1000;set(gca,'YScale','log')
xlabel('Amplitudes')
ylabel('frequency')
title('Amplitudes histogram')
display ('SELECT THE **HIGH** ENERGY LIMITS IN THE HISTOGRAM')
[ThrHx,ThrHy]=ginput2(1);

```

```

ThrH=ThrHx;
ThrL=ThrLx;
if ThrH<ThrL %With this, it doesnt matter if the user selects
    ThrH=ThrLx; ThrL=ThrHx; %first the high energy
else %cut or the low energy cut

```

```

end
THH=ThrH;%*MMM;
THL=ThrL;%*MMM;
[Lx,Ly]=find(Amp2D<THL);
[Hx,Hy]=find(Amp2D>THH);
IndZerL=sub2ind(size(Amp2D),Lx,Ly);
IndZerH=sub2ind(size(Amp2D),Hx,Hy);
ECSumFD=SumFD;
ECSumFD(IndZerL)=0;
ECSumFD(IndZerH)=0;

MixFiltFD=ifft2(ECSumFD);
Amp2Dfilt=abs(ECSumFD);

```

```
end
```

6) Mean trace function

```
function rdr=MeanTraceFX(MatIng,MNotr)
```

```

%dati di entrata: Matrice radar, numero di tracce.
%Dati di uscita: Matrice radar senza la traccia media.

```

```

meanoftr= repmat(mean(MatIng,2),1,MNotr);
radr=MatIng-meanoftr;
rdr=radr;
end

```

7) BandPass filters function

```
function [asprdr,fr,rdrf]=SpectralAnalysisFX(MAntF, rdr, Mt)
```

```

%fa lo spettro e permette selezionare tra 2 tipi di filtro.
%Parametri di entrata:
%rdr: Matrice radar su cui si applichera il filtro
%MAntF:Frequenza della antenna
%Mt: Vettore dei tempi ( i=(1:MNosa); Mt=i*Mdt; )

```

```

%Parametri di uscita:
%asprdr:matrice spettro
%rdrf:matrice filtrata
%fr:vettore massimi (?)

```

```

[MNosa,MNotr]=size(rdr);
i=(1:MNosa);

```

```

j=(1:MNotr);
T=max(Mt);
f0=1/T;
indfr=(1:floor(MNosa/2));
fr=f0*indfr;
asprdr=(abs(fft(rdr)))/MNosa;%-mean(dewrdr(j));
asprdr(2:length(fr))=2*asprdr(2:length(fr)); %true amplitude
asprdr=asprdr((1:floor(MNosa/2)),:);
% filtering options
[Amax, iframax]=max(asprdr);
framax=iframax*f0;
locf=(framax-framax/2)/max(fr);
hicf=(framax+framax/2)/max(fr);
hhicf1=(MAntF*1.5)/max(fr);
hhicf=(ones(MNotr,1)*hhicf1)';
%%%%%%%%%%%%%%%%%%%%%%%%%%%%%%%%%%%%%%%%%%%%%%%%%%%%%%%%%%%%%%%%%%%%%%%%

for j=1:MNotr
    if locf(j)<mean(locf)-2*std(locf)
        locf(j)=mean(locf);%-2*std(locf);
    end
    if locf(j)>mean(locf)+2*std(locf)
        locf(j)=mean(locf);%+2*std(locf);
    end
    if hicf(j)<mean(hicf)-2*std(hicf)
        hicf(j)=mean(hicf);%-2*std(hicf);
    end
    if hicf(j)>mean(hicf)+2*std(hicf)
        hicf(j)=mean(hicf);%+2*std(hicf);
    end
end

%%%%%%%%%%%%%%%%%%%%%%%%%%%%%%%%%%%%%%%%%%%%%%%%%%%%%%%%%%%%%%%%%%%%%%%%

% Band pass filtering
hcf=num2str((MAntF*1.5)*10^-9);
fsn=input(['Filter ? (0=NO ; 1=BP on signal; 2=BP fixed@1.5HFant = ' hcf ' GHz) ->
']);
if fsn==1
    for ii=1:MNotr
        [bb,aa]=butter(5,[locf(ii) hicf(ii)]);
        rdrf(:,ii)=filtfilt(bb,aa,rdr(:,ii));
    end
    display ('Filter BP on signal done')
elseif fsn==2
    for ii=1:MNotr
        [bb,aa]=butter(5,[locf(ii) hhicf(ii)]);
        rdrf(:,ii)=filtfilt(bb,aa,rdr(:,ii));
    end
end

```

```

end
display ('Filter BP fixed at 1.5HFant done')
else
rdrf=rdr;
display ('No filter applied')
end

end

```

8) Energy recovery function

```

function [rdrg,AMP]=DivRecFX(Mt,Mx,rdrf)

%La funzione applica una divergence recovery al radargramma di
%entrata(rdrf)
%rdrf=Matrice radar di entrata
%Mt: Vettore dei tempi ( i=(1:MNosa); Mt=i*Mdt; )

figure (255)
imagesc(Mx',Mt'*10^9,rdrf);
title('Radargram without divergence recovery')
xlabel('Distance (m)')
ylabel('Time (ns)')

[MNosa,MNotr]=size(rdrf);
v=input('Type estimated velocity [m/ns] ');
v=v*10^9;
%domwav=v./framax;
display('SELECT ON THE FIGURE A STARTING POINT FOR DIVERGENCE
RECOVERY');
[spa2, tim2]=ginput(1);
tim2=round(tim2);
ampl=input('Divergence recovery: NO=0;LIN=1;QUAD=2;CUBE=3;SQRT=0.5 ');
%dist1=Mt(1:tim2)*v;
dist2=Mt(tim2+1:MNosa)*v;
dist2=(dist2-dist2(1))+1;
for ii=1:MNotr
rdrg(1:tim2,ii)=rdrf(1:tim2,ii);
rdrg(tim2+1:MNosa,ii)=rdrf(tim2+1:MNosa,ii).*(dist2.^ampl);
end
AMP=num2str(ampl);
end

```